Master's Thesis
Environmental Management (M.Sc.)

Development of a Purge + Trap System for the Quantification of Methane Variability in the Baltic Sea

by Sonja Gindorf

Kiel, August 2020

First Reviewer: Prof. Dr. Hermann W. Bange

Second Reviewer: Dr. Annette Kock

GEOMAR - Helmholtz Centre for Ocean Research Kiel

Marine Biogeochemistry Unit Chemical Oceanography

Faculty of Agricultural and Nutritional Sciences

Faculty of Mathematics and Natural Sciences

Kiel University

Für Sven, Susanne, Antje, Kurt und Tom

Kinder des Windes,
geboren im Meer,
kommt doch zu mir.
Ich begehre euch sehr.

Ihr seid die schönsten,
am längsten gereist.
Mein Herz überschlägt sich.
Mein Atem vereist.

Doch während ich jetzt
eurer Schönheit gelüste,
brecht ihr schon bald
zu Schaum an der Küste.

Sven Gindorf, 2020

Abstract

Methane (CH_4) is the second most important anthropogenic greenhouse gas. Generally, open ocean surface waters are at atmospheric equilibrium or slightly oversaturated. Oceanic emissions play only a minor role in the global CH_4 budget. However, coastal areas account for up to 75 % of the total CH_4 emissions from the marine environment to the atmosphere which is linked to direct CH_4 inputs from sedimental methanogenesis driven by the high organic matter sedimentation, especially in eutrophicated systems, such as the Baltic Sea. Highly accurate CH_4 measurements are necessary to investigate the small-scale variability of CH_4 in the surface water and the related gradients and fluxes. Therefore, the objective of this thesis was to develop a purge and trap (PT) system coupled to a GC-FID to examine the surface and water column CH_4 distribution within Kiel Bight at a high temporal and spatial resolution in two cruises in June and September 2018. This work showed that PT measurements outplay static HeadSpace equilibration (HS) measurements as the latter bear a significantly higher error in calibration and sample measurements.

The CH_4 distribution and fluxes observed during two cruises in June and September 2018 fit well with previous data of the region. The results indicate that the monthly measurements at Boknis Eck time series station are representative for the Kiel Bight. Generally, CH_4 concentrations were found to increase within the water column. The surface water was at all times oversaturated with respect to atmospheric equilibrium. Concentrations were in the range of observations from previous studies. Strong CH_4 gradients occurred in the upper 1 m of the water column leading to significant differences in flux density calculations depending on the surface depth between 0.1 and 1 m raising the question how suitable (continuous) underway measurements are to estimate CH_4 surface dynamics.

Data Availability

The Baltic GasEx data will be available from the PANGAEA database under the following links PDI-25200 (AL 510) and PDI-25201 (AL 516) (https://www.pangaea.de/). The Boknis Eck and Tavastland data was handed to the working group (A. Kock) and will be processed with the rest of the respective data sets.

Zusammenfassung

Methan (CH_4) ist das zweitwichtigste anthropogene Treibhausgas. Im Allgemeinen befindet sich die Oberfläche des offenen Ozeans im atmosphärischen Gleichgewicht oder weist eine leichte Übersättigung auf. Im globalen CH_4-Budget spielen Emissionen der Ozeane nur eine untergeordnete Rolle. Küstengebiete machen jedoch bis zu 75 % der gesamten marinen CH_4 Emissionen in die Atmosphäre aus. Dies hängt mit direkten CH_4 Einträgen aus der sedimentären Methanogenese zusammen, die durch hohe Sedimentationsraten organischer Stoffe angekurbelt werden, insbesondere in eutrophierten Systemen wie der Ostsee. Hochauflösende CH_4 Messungen sind erforderlich, um die kleinskalige Variabilität von CH_4 im Oberflächenwasser und die damit verbundenen Gradienten und Flüsse zu untersuchen. Ziel dieser Arbeit war es daher, ein „Purge-and-Trap“ (PT) System zu entwickeln, das an einen GC-FID gekoppelt ist, um die CH_4 Verteilung in der Oberfläche sowie der Wassersäule in der Kieler Bucht im Rahmen zweier Forschungsfahrten im Juni und September 2018 mit hoher zeitlicher und räumlicher Auflösung zu untersuchen. Diese Arbeit zeigte, dass PT Messungen das statische „Headspace“ Äquilibrationsverfahren übertreffen, da letztere einen signifikant höheren Fehler bei der Kalibration sowie bei Probenmessungen aufweisen.

Die beobachteten CH_4 Verteilungen und Flüsse passen gut zu früheren Daten der Region. Die Ergebnisse zeigen, dass die monatlichen Messungen an der Zeitreihenstation Boknis Eck repräsentativ für die Kieler Bucht sind. Im Allgemeinen wurden im tiefen Wasser hohe CH_4 Konzentrationen gefunden. Im Oberflächenwasser wurden niedrigere, aber zu jeder Zeit übersättigte Konzentrationen (in Bezug auf das atmosphärische Gleichgewicht) beobachtet. Dies unterstützt die Beobachtungen früherer Studien. Der obere 1 m der Wassersäule weist starke CH_4 Gradienten auf, die zu signifikanten Unterschieden bei der Berechnung der Flussdichte in Abhängigkeit von der Oberflächentiefe zwischen 0.1 und 1 m führten. Dies wirft die Frage auf, wie geeignet (kontinuierliche) Oberflächenmessungen zur Abschätzung der CH_4 Oberflächendynamik sind.

Datenverfügbarkeit

Die Baltic GasEx-Daten sind in der PANGAEA Datenbank (https://www.pangaea.de/) unter den folgenden Links PDI-25200 (AL 510) und PDI-25201 verfügbar. Die Boknis Eck und Tavastland Daten wurden der Arbeitsgruppe (A. Kock) übergeben und werden mit den übrigen jeweiligen Datensätzen weiterverarbeitet.

Table of Contents

1. Introduction

1.1 Methane

Methane (CH_4) is the second most important anthropogenic greenhouse gas. The global warming potential of CH_4 is approximately 28-times higher than that of carbon dioxide (CO_2) on a 100-year time scale and with an atmospheric lifetime of 12.4 years (Myhre et al., 2013). According to Antarctic ice core data, the atmospheric dry air mole fraction of CH_4 has varied between approximately 300 and 800 ppb over the past 160k years (Chappellaz et al., 1990). While it was at approximately 720 ppb around 1750 C.E. (Nisbet et al., 2019), it has more than doubled since the beginning of industrialization and exceeds 1800 ppb as of 2020 (Dlugokencky, 2020, Figure 1).

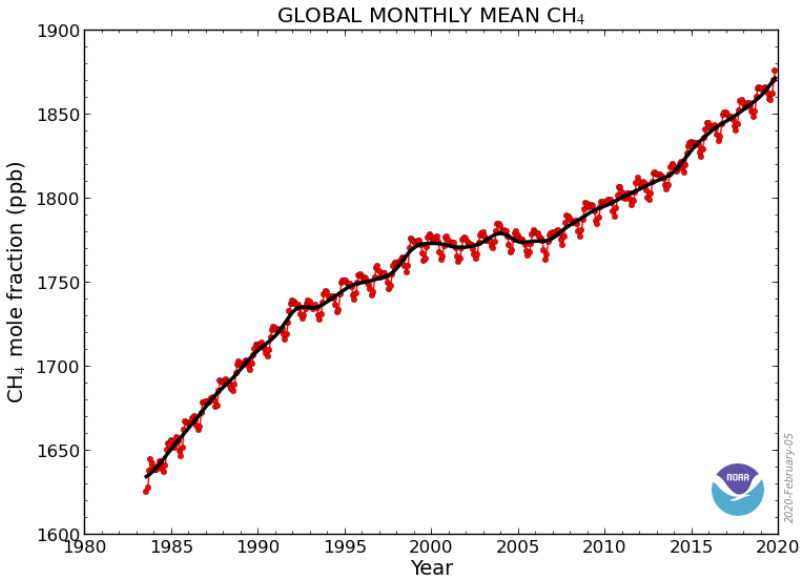

Figure 1: Global monthly mean atmospheric CH_4 since 1984 (Dlugokencky, 2020b).

The large spectrum of CH_4 sources to the atmosphere encompasses biogenic, thermogenic and pyrogenic processes, while atmospheric CH_4 oxidation by hydroxyl radicals (OH) is accounting for approximately 90 % of the global CH_4 sink (Kirschke, 2013). The most important processes releasing CH_4 to the atmosphere are fossil fuel production and biological production (Figure 2). Among the latter different anthropogenic (landfills, waste water treatment, agricultural production systems) and natural sources (wetlands, lakes, oceans, and termites) play an important role (Bodelier et al., 2019). Currently, the total global CH_4 emissions to the atmosphere average at approximately 560 Tg yr^{-1} being approximately 13 Tg yr^{-1} higher than the total sinks (Bižić et al., 2020).

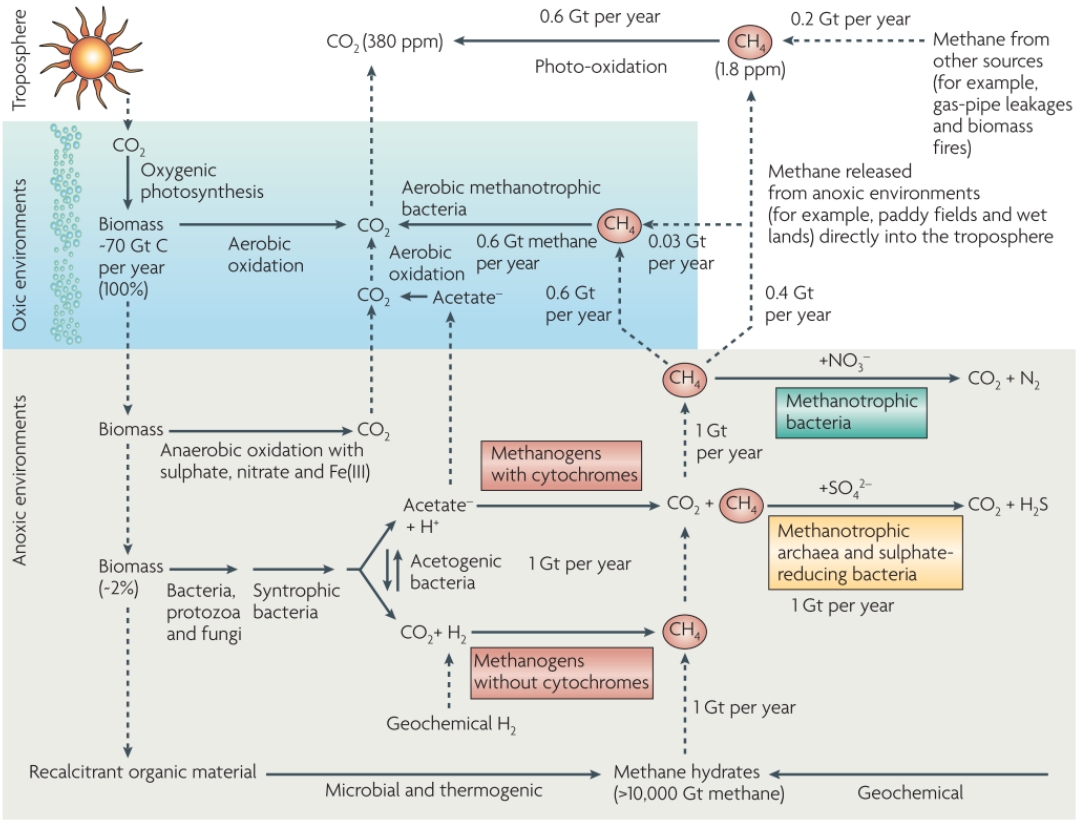

Figure 2: The role of CH_4 in the global carbon cycle. To indicate reactions, continuous arrows are used, dashed arrows indicate diffusion and/or convection (Thauer et al., 2008).

1.1.1. CH_4 in the Ocean

The order of magnitude that oceanic CH_4 plays in the global carbon budget is dependent on the interplay of various environmental factors including biogeochemical, oceanographic and biological factors driving production, consumption and accumulation processes. Oceanic CH_4 can be either of geologic (e.g. Archer et al., 2009; Newman et al., 2008; Rehder et al., 2009) or biologic (e.g. Bodelier et al., 2019; Maltby et al., 2017; Myllykangas et al., 2020; Palacios et al., 2019; Thauer et al., 2008; Valentine, 2011; Zinke et al., 2019) origin. Generally, open ocean surface waters are at atmospheric equilibrium or slightly oversaturated (Bates et al., 1996) and oceanic emissions play only a minor role in the global CH_4 budget (Reeburgh, 2007; Figure 2). The global ocean is a net source of CH_4 to the atmosphere contributing between 6 and 12 Tg yr^{-1} (Weber et al., 2019). However, coastal areas including shelves and estuaries account for up to 75 % of these total CH_4 emissions from the marine environment to the atmosphere (Bange et al., 1994). That such high CH_4 concentrations occur in surface waters of continental shelves is linked to direct CH_4 inputs from estuaries, sedimental methanogenesis driven by high organic matter sedimentation, and natural gas seeps (Borges et al., 2016). Oceanic

CH_4 emissions involve processes such as diffusion, ebullition (Walter et al., 2007), seepage, resuspension (Bussmann, 2005; Bussmann and Suess, 1998) or bioturbation (Bezerra et al., 2020; Oliveira Junior et al., 2019). Microbial methanogenesis in the sediment is contributing the majority of coastal CH_4 (Bakker et al., 2014) but uncertainty remains concerning the magnitude, seasonality, and environmental controls of benthic methanogenesis (Maltby et al., 2017). Moreover, it was recently suggested that in large stratified aquatic systems (surface > 1 km^2) the majority of CH_4 emissions is accounted for CH_4 that was generated under aerobic conditions during stable stratification (Günthel et al., 2019). This drives attention to the production details as marine CH_4 generation was thought to be limited to the anoxic sediments below the suflate reduction zone (Bodelier et al., 2019) as will be described in more detail in the following (Section 1.1.2).

Despite plenty research focusing on marine CH_4, large uncertainties still remain regarding the variability of concentrations and emissions. Especially, the oxidation processes in the sediments and water column leading to nanomolar surface concentrations (Reeburgh, 2007) even though several thousand-fold concentrations are reported to be released from the sediments into the bottom water (e.g. Donis et al., 2017; Reindl and Bolałek, 2014) are not fully understood yet (Reeburgh, 2007).

1.1.2. CH_4 Production

Methanogenesis is the last step of organic matter fermentation, which is carried out predominantly by methanogenic archaea while methylotrophic bacteria can also produce CH_4 as a byproduct (Florez-Leiva et al., 2013). The most common substrates for methanogenesis in marine environments are hydrogen (H_2) and CO_2 (Equation (1)) or acetate (CH_3COOH) (Equation (2)), while some marine methanogens are also able to metabolize formate (HCOOH), or methylamine (CH_3NH_2) to produce CH_4 (Liu and Whitman, 2008).

$$CO_2 + 4\,H_2 \rightarrow\ CH_4 + 2\,H_2O \quad (1)$$

$$CH_3COOH \rightarrow\ CH_4\ +\ CO_2 \quad (2)$$

The major source of methane in marine environments is considered to be anaerobic methane generation in the sediments performed by microbial methanogens. Most of methanogens are found below the sulfate-reducing zone because they are outcompeted by sulfate reducers, for the major substrates H_2 and CH_3COOH, mainly for thermodynamic reasons (Thauer et al., 2008). However, methanogens and sulfate reducers can coexist when methanogens utilize non-competitive substrates, such as methanol or methylated amines (Maltby et al., 2017). Besides substrate availability, environmental factors such as temperature and productivity (especially sedimentation) are determining the magnitude of CH_4 production (Borges et al., 2018).

The super saturation of methane in well-oxygenated surface waters, commonly known as the Oceanic Methane Paradox (OMP), leads to the assumption that in-situ CH_4 production in the aerobic water column takes place (e.g. Repeta et al., 2016), which either occurs in anaerobic microniches or via a so far unidentified CH_4 production pathway. Among other conjectures, it is assumed that such anaerobic microenvironments for methanogenesis may be found in particulate organic matter (POM) (Karl and Tilbrook, 1994) or gastrointestinal tracts of zooplankton (Schmale et al., 2018). Different phytoplankton species were also associated with CH_4 generation (Klintzsch et al., 2019). Bižić et al. (2020) showed that cyanobacteria can convert fixed inorganic carbon into CH_4 under light and dark conditions. Hence, increasing cyanobacteria blooms in the Baltic Sea, due to eutrophication and rising temperatures (Belkin, 2009; Kahru et al., 2020; Meier et al., 2019; Norbäck Ivarsson et al., 2019), may be an important factor considering present and future CH_4 cycle and budget. The increasing amounts of plastic in the environment may provide alternative substrates for CH_4 production in surface water where solar radiation is available (Royer et al., 2018). Moreover, CH_4 may be generated in aerobic surface waters during the microbial cycling of dissolved organic matter (DOM) by the degradation of methylphosphonate (MPn) (Karl et al., 2008; Metcalf et al., 2012) as the microbial catabolism of MPn was demonstrated to be a source of methane in the surface ocean (Taenzer et al., 2020). During microbial transformations of dimethylsulfide (DMS) CH_4 is released as a by-product (Florez-Leiva et al., 2013) and Zindler et al. (2012) conclude in their study in the oligotrophic Pacific Ocean that dimethylsulfoniopropionate (DMSP) and dimethylsulfoxide (DMSO) serve as substrates for CH_4 generation. However, the computations of Weber et al. (2019) suggest that the latter one is not an important pathway at the global scale.

1.1.3. CH_4 Consumption

Methanotrophs are microbial organisms that can utilize environmental CH_4 as their sole carbon and energy source (Ruff et al., 2019). The methane oxidation pathways differ under aerobic and anaerobic conditions and are shown in Figure 3. During both pathways, the amount of yielded CH_4 is dependent on a number of environmental factors including methane supply, oxygen level, temperature, pH, salinity, trace metals and growth-stimulating factors (Rhee et al., 2019).

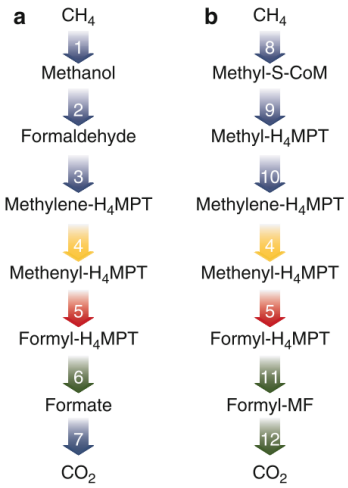

Figure 3: The aerobic (a) and anaerobic (b) methane oxidation pathways. Grey arrows indicate distinct reactions catalyzed by certain enzymes; red arrows indicate the same reactions catalyzed by homologous enzymes; yellow arrows indicate the same reactions catalyzed by non-homologous enzymes; green arrows indicate similar but not the same reactions catalyzed by homologous proteins (Zheng and Chistoserdova, 2019).

Anaerobic oxidation of methane (AOM) is driven by syntrophic interaction between methanotrophs and sulfate-reducing bacteria (Bodelier et al., 2019) as it has been demonstrated to be coupled to the reduction of electron acceptors such as sulfate, nitrate, nitrite, iron, manganese (Rhee et al., 2019). Under aerobic conditions, methanotrophs convert CH_4 into methanol (CH_3OH) (Chan and Lee, 2019).

While aerobic and anaerobic methanotrophy as well as methanogenesis have once been considered to be incompatible processes, Zheng and Chistoserdova (2019) state that they can be present in the very same environmental niches due to symbiotic activities or co-benefits among different bacterial and archaeal species.

1.2. The Baltic Sea

The Baltic Sea is a young semi-enclosed shelf sea with a mean depth of 52 m. Located between 54°and 66°N and 10° and 30°E (IOW, 2018), it is naturally divided into 12 major Basins (Figure 4).

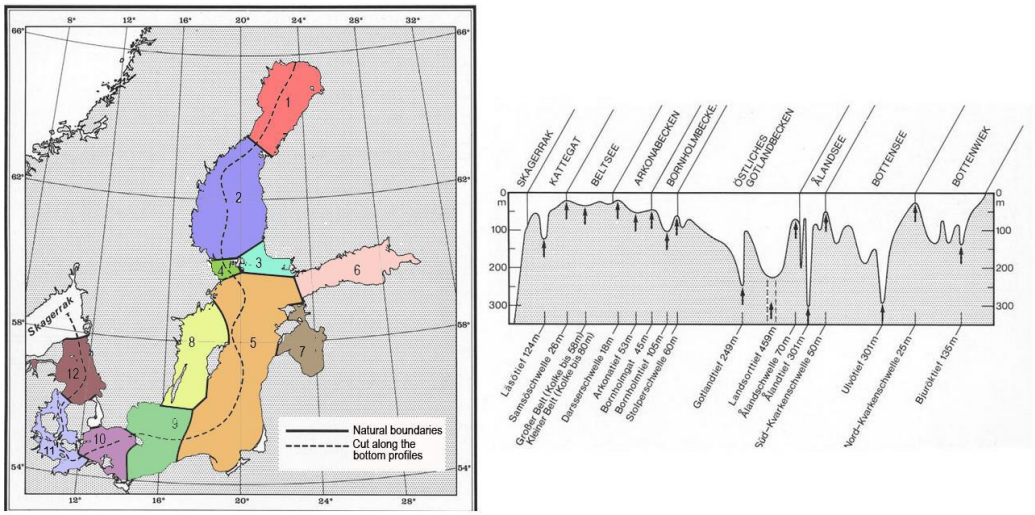

Figure 4: Natural subdivision of the Baltic Sea into 12 Basins (1 Bothnian Bay, 2 Bothnian Sea (1 + 2 = Gulf of Bothnia), 3 Archipelago Sea, 4 Åland Sea, 5 Eastern Gotland Sea, 6 Gulf of Finland, 7 Gulf 10 of Riga, 8 Western Gotland Sea, 9 Bornholm Sea, 10 Arkona Sea, 11 Belt Sea, 12 Kattegat) and a profile cut from south west to north east (Dietrich and Köster, 1974; modified).

The Baltic Sea represents one of the world's largest and most important brackish water ecosystems (WWF, 2019). It is often considered as a large estuary, as a strong salinity gradient from the south west to the north east can be observed. While the Kattegat region is characterized by almost oceanic salinity of up to 35 g kg^{-1} (Müller et al., 2016) it declines throughout the Baltic Sea to a minimum of nearly freshwater conditions of about 2 g kg^{-1} in the Gulf of Bothnia (Reusch et al., 2018). This is mainly caused by the intense influx of fresh water and limited water exchange with the Atlantic Ocean which only occurs through three shallow straits (Figure 5) that leads to an average water residence time of approximately 30 to 40 years (Mohrholz et al., 2015; Norbäck Ivarsson et al., 2019).

Besides the horizontal salinity gradient, the Baltic Sea is also characterized by a strong vertical gradient in salinity (Naumann and Nausch, 2015). In the Kattegat area two diverging flows can be observed. At the surface, brackish water flows northwards while the deep-water masses transport salty North Sea water southward. The pathway of the water circulation in the Baltic Sea is shown in figure 6.

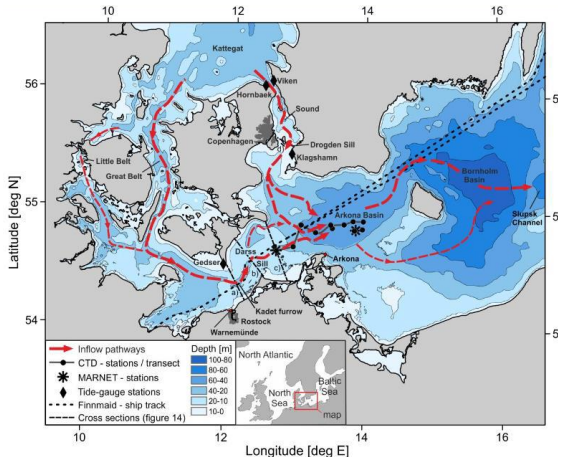

Figure 5: Bathymetric map of the western Baltic Sea that shows the inflow pathways of salty water from the North Sea through the Kattegat (Mohrholz et al., 2015).

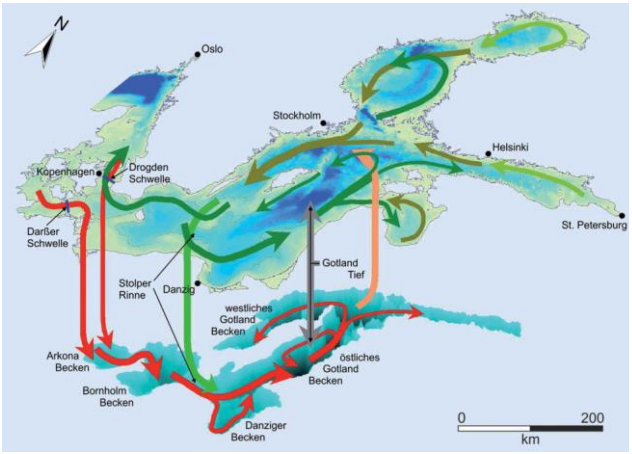

Figure 6: Schematic overview of the water circulation within Baltic displaying the depth beneath 40 m in its lower part. The red arrows demonstrate the inflow of salty North Sea water and its circulation in the deep water (Naumann and Nausch, 2015).

With approximately 85 million people living in its catchment area, the Baltic Sea is one of the most polluted seas in the world (Norbäck Ivarsson et al., 2019). Multiple stressors such as large nutrient inputs, chemical pollution, warming, O_2 depletion, acidification, and invasive species are threatening the ecosystem (Norbäck Ivarsson et al., 2019; Reusch et al., 2018). This leads to ecological as well as economic challenges (Gilek et al., 2016; Hassler, 2017; Hassler et al., 2018; Manzhynski et al., 2016; Reusch et al., 2018; Thureborn et al., 2016). Over the twentieth century these increased pressures have led to altered species composition, more intense cyanobacterial blooms, decreased secchi-depth, and increased hypoxia (Norbäck Ivarsson et al., 2019).

While the Baltic Sea is home to only few endemic species, many populations have locally adapted to enhanced ocean acidification or lower salinity. Due to its young evolutionary age and the challenging brackish water conditions, the species diversity is low. However, the Baltic Sea is a highly productive ecosystem providing important ecosystem goods and services (Reusch et al., 2018) which are vulnerable to being decreased by the high anthropogenic pressure on the environmental system described above. Due to this and the socio-economic dependence of the riparian states, great attention is being paid towards international environmental management and sustainable development measures based on intense scientific research to increase the Baltic Sea water status (e.g., Belkin, 2009; Gilek et al., 2016; Hassler et al., 2018; Myrberg et al., 2019; Reusch et al., 2018).

Due to its proximity to the Arctic, hydrodynamic features and land-locked location (Saraiva et al., 2019), the Baltic Sea has warmed up more than any other large marine ecosystem between 1982 and 2006 (Belkin, 2009). During this period, the observed temperature increase in the Baltic region was more than seven times higher compared to global average. Over the past 30 years an even stronger increase than over the past 50 years was observed (Kniebusch et al., 2019), indicating an acceleration of the warming process.

1.2.1. CH_4 in the Baltic Sea

In the Baltic Proper, deep particulate organic carbon (POC) values are comparable to extremely productive and O_2 depleted areas including the upwelling areas off Peru, South West Africa and the Arabian Sea (Thureborn et al., 2016). Large parts of the Baltic seafloor are covered by organic-rich brackish-water mud (Abegg and Anderson, 1997; Leipe et al., 2011) containing shallow free gas (Flury et al., 2016; Mogollón et al., 2013; Thießen et al., 2006). Predominantly, this free gas is anaerobically produced CH_4 which is most abundant just below the sulphate-methane transition zone in the sediments (Kankaanpää and Virtasalo, 2017).

In stratified marine systems, the CH_4 transport from the seafloor to the atmosphere is prevented through a barrier. This is not given in shallow coastal systems where ebullition from the seafloor can reach the atmosphere. Humborg et al. (2019) have shown that ebullition, upwelling, and strong winds can lead to increased CH_4 fluxes in the coastal areas of the Baltic. Moreover, they claim that the polar amplification effect of global warming can trigger massive CH_4 fluxes to the atmosphere from nearshore sites in the Baltic Sea due to the increasing number of extreme warming events (Humborg et al., 2019).

1.2.2. Boknis Eck

Being located in the entrance of the Eckernförde Bay (54°31’N, 10°02’E) in the southwestern Baltic Sea (Figure 7) with a water depth of approximately 28 m, Boknis Eck is one of the world’s oldest and active marine research time series stations (Bange et al., 2010). While monthly measurements of different physical and chemical parameters have been carried out since April 1957 and CTD (sensor for Conductivity, Temperature, Depth (pressure)), oxygen and nutrient data are available from the 1980s onwards, monthly CH_4 measurements started in 2006 (Ma et al., 2020). Riverine influx into the Eckernförde Bay is neglectable, whereas it is

affected by the inflow of water from the North Sea through the Kattegat and the Great Belt and the outflow of brackish water (Bange et al., 2010, 2011; Lennartz et al., 2014; Steinle et al., 2017) resulting in strong fluctuations in bottom water salinity between 17 and 24 g kg^{-1} (Lennartz et al., 2014).

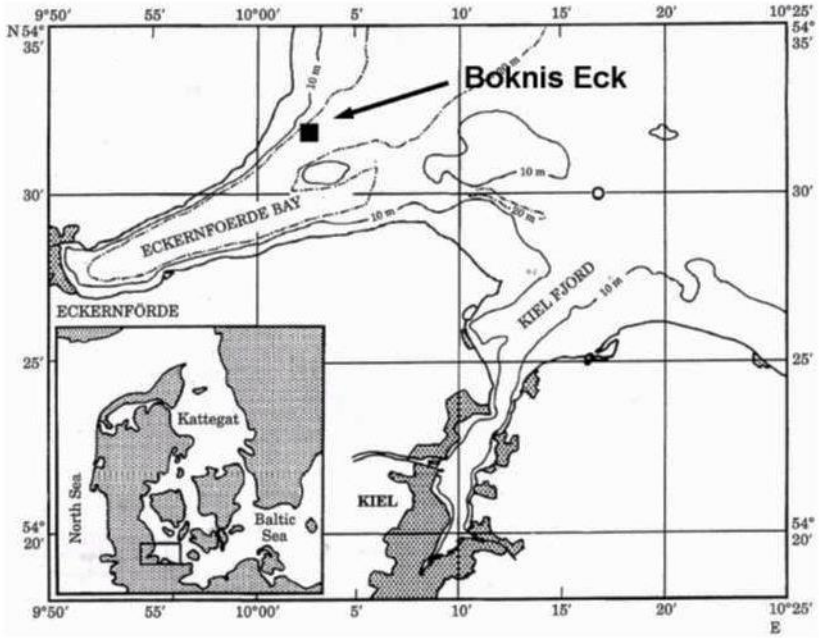

Figure 7: Location of Boknis Eck (Bange et al., 2011).

Vertical mixing is prevented from March to September, as a strong pycnocline develops in the depth of approximately 15 m due to the surface warming and the distinct salinity gradient. During the winter months the whole water column is ventilated due to the onset of autumn storms and surface-water cooling (Bange et al., 2010).

In general, large phytoplankton blooms in spring (February–March) and autumn (September–November) are followed by high rates of organic matter sedimentation and microbial respiration under the consumption of O_2 (Bange et al., 2010; Dale et al., 2011). Consequently, pronounced periods of hypoxia and sporadically anoxia occur in the bottom water during late summer (Bange et al., 2010; Lennartz et al., 2014; Steinle et al., 2017). The occurrence of these events has been continuously increasing in their frequency since the 1970s (Lennartz et al., 2014). These conditions make Boknis Eck an ideal representative of a coastal ecosystem under the impact of distinct variations in salinity, as well as for studying biogeochemical processes that are sensitive to changes in dissolved O_2 (Bange et al., 2011).

Moreover, the high sedimentation rates of organic matter favour methanogenesis in the muddy sediment resulting in high CH_4 concentrations in the overlying water (Bange et al., 2010; Steinle et al., 2017). This coincides with the observation of Steinle et al. (2017) that an increase of chlorophyll a in the water column led to an increase in surface CH_4 concentrations with a 1-month time lag. Year-round CH_4 seepages from the sediments into the water column lead to surface water supersaturation (Bange et al., 2010; Steinle et al., 2017).

A recent analysis of the past ten years of monthly CH_4 measurements at Boknis Eck, showed that concentrations generally increased with depth (Ma et al., 2020). The authors report that Eckernförde Bay is an intense and highly variable source of CH_4 to the atmosphere. Despite environmental changes such as deoxygenation and warming that can be observed at Boknis Eck, no temporal trend in CH_4 concentrations or emissions was found in the respective study. Moreover, on the long term CH_4 concentrations could not be correlated with O_2 or chlorophyll a over the monitoring period which led to the authors conclusion that CH_4 concentrations at Boknis Eck are dependent on a complex interplay of biological and physical parameters.

The sediments of Eckernförde Bay contain large amounts of shallow free gas (Flury et al., 2016) and are characterized by pockmarks as well as groundwater seepage (Bussmann and Suess, 1998). This combination can lead to extremely high CH_4 fluxes in the form of bubbling directly from the sediments to the atmosphere as it was observed in fall 2014 when CH_4 flux densities of up to 1900 µmol m^{-2} d^{-1} occurred (Lohrberg et al., 2020). The authors of that study conclude that large parts of the western Baltic Sea may be subject to such intense CH_4 ebullition events on a regular basis but that individual measurement campaigns are likely to miss these events.

2. Introduction into the Study and Objective

This thesis is part of the BONUS Blue Baltic project "Integrated carboN and TracE Gas monitoRing for the bALtic sea" (INTEGRAL) which comprises eight partners from five nations running from July 2017 to September 2020. One of the main objectives of this project is to improve the ecosystem-based monitoring of the Baltic Sea including high-precision greenhouse gas concentration and flux data (Rehder, 2020).

During the two cruises AL 510 (Booge, 2018) and AL 516 (Booge, 2019) on the R/V Alkor in early summer and autumn 2018 gas exchange experiments (Baltic GasEx) were carried out in Kiel Bight near the Boknis Eck time series station in the southwestern Baltic Sea. During the Baltic GasEx cruises, special emphasis was put on the sampling of the upper water column and within the mixed layer, with high-resolution sampling to determine potential gas gradients within the mixed layer that are not captured with conventional sampling approaches (Fischer et al., 2019).

The objective of this thesis was to develop a purge and trap system coupled to a GC-FID for high accuracy CH_4 measurements for the investigation of the small-scale variability of CH_4 in the surface water and the water column within Kiel Bight.

The Baltic GasEx data are used to assess the representativeness of the data collected at the time series station Boknis Eck for the Belt Sea and complement the basin-scale measurements collected in the framework of the project BONUS INTEGRAL. Comparison samples from the Ship of Opportunity (SOOP) line Tavastland and from the Boknis Eck Time Series station were used to evaluate the inter-comparability of the measurements.

3. Methods

Different methods for quantifying dissolved CH_4 evolved since the first measurements were made in the 1960s (Atkinson and Richards, 1967). Nowadays, the most common ways to measure CH_4 in discrete seawater samples are static HeadSpace equilibration (HS) and dynamic headspace equilibration procedures, such as Purge and Trap (PT) (e.g. Capelle et al., 2015; Magen et al., 2014). The PT technique has been shown to be more sensitive compared to HS (Wilson et al., 2018).

3.1. Sampling

3.1.1. Baltic GasEx

During the two Baltic GasEx cruises with the R/V Alkor AL510 (03.06.2018 – 15.06.2018) and AL516 (12.09.2018 – 22.09.2018), CH_4 samples were taken from 9 and 10 CTD rosette casts, respectively (Figure 8). The cruises covered the coastal waters of the Kiel Bight at a high resolution. To study the vertical CH_4 distribution within the water column, water was taken from mixed layer, within the pycnocline, and the water below the pycnocline at the CTD stations (Booge, 2018, 2019). The CTD was mounted to the rosette water sampler with twelve 10 L Niskin bottles that were closed during the upcast at the requested depths.

To examine potential gradients in the very near surface waters in higher resolution additional samples from a dinghy were taken at selected stations. To avoid turbulence distributions caused by the ship, the sea water samples were taken at some distance from the ship. Using an aquarium pump attached to a swimming board, water from 0.1. 0.5, and 1 m depth was pumped on board of the dinghy as described in detail by Fischer et al. (2019). Moreover, underway (UW) samples were taken from the ship's continuous seawater system from a depth of approximately 4 m.

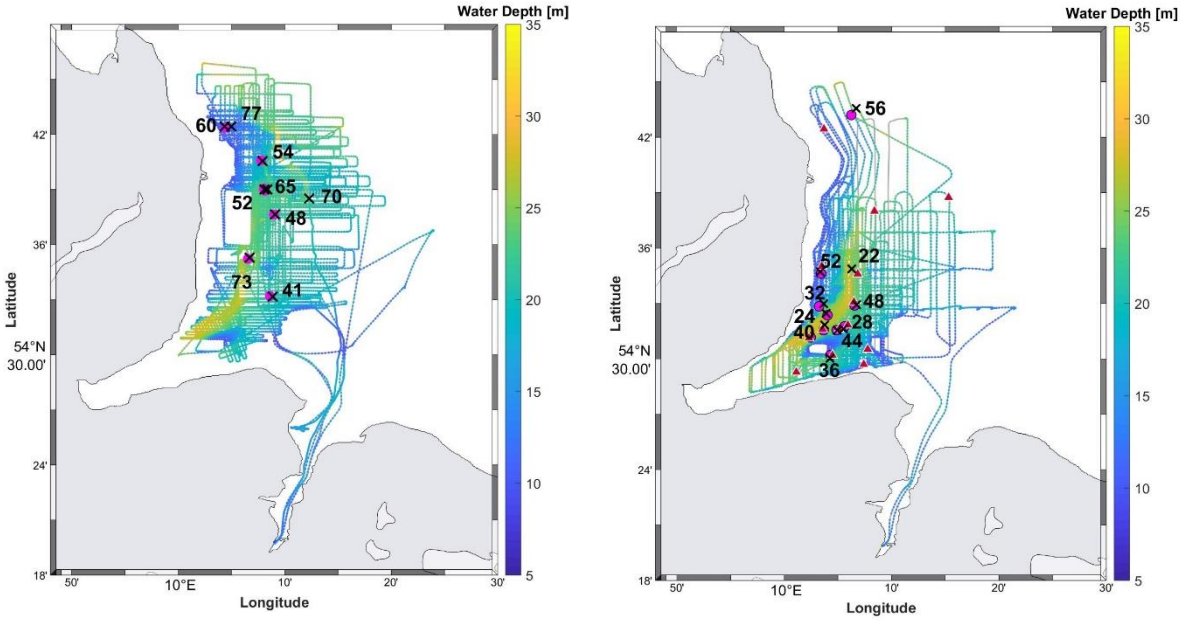

Figure 8: Cruise track of AL510 (left; Booge, 2018) and AL516 (right; Booge, 2019). The black crosses mark CDT stations, pink dots mark dinghy sampling sides and red triangles mark UW sampling sides. All maps that are shown in this thesis were computed using the m_map toolbox in Matlab (Pawlowicz, 2020).

Triplicates were taken through a silicon tube connected to the Niskin bottle (CTD samples), aquarium pump (dinghy samples), or the Alkor's seawater tap (UW samples). At a low flow-rate the 20 mL dark brown glass vials were filled bubble-free by overflowing the approximate threefold volume of seawater. The vials were closed with butyl rubber stoppers and crimp-sealed with aluminium caps (for product details see Table 1). To avoid microbial activity changing the CH_4 concentration within the sample 50 µL of saturated mercury chloride solution ($HgCL_2$ (aq)) were added to each sample using a 1 mL syringe. Due to a misunderstanding, some samples of the June cruise were poisoned adding 500 µL $HgCL_2$ (aq). Using $HgCl_2$ as a preservative for storage of seawater samples is a common standard procedure (e.g. Capelle et al., 2015; Gülzow et al., 2014; Kock, 2007; Wilson et al., 2018). To compensate for the added volume, a 3 mL cannula was inserted into each sample before inserting the poison for the suppressed water to flow out (Figure 9). Due to the higher density of the $HgCL_2$ (aq), the inserting needle should penetrate deeper into the sample than the needle for pressure balancing to avoid suppressing contaminated water. The samples were stored at room temperature in dark conditions until the measurements were carried out.

Figure 9: Sample preservation. Photo of the samples with the syringes for pressure balancing (left) and schematic of the $HgCl_2$ injection (1) into the sample vial (2) with a syringe for pressure balancing (3) (right).

3.1.2. Boknis Eck

For a method intercomparison between PT and HS measurements two sets of triplicates from each of the six standard depths (1, 5, 10, 15, 20, 25 m) were collected during the Boknis Eck cruise in April 2020. A water sampler rosette with six 3.5 L Niskin bottles connected to a CTD was used to take the water from the R/V Littorina. Samples were taken and processed as described above.

One set was measured with the traditionally-used HS method which is described in detail in Kock (2007), the other one with the PT technique that will be described in detail in section 3.2.

3.1.3. Ship of Opportunity line Tavastland

The Swedish cargo vessel M/V Tavastland serves as a Ship of opportunity (SOOP) carrying measurement equipment for continuous surface water observations of different parameters including the greenhouse gases CO_2, CH_4 and N_2O since spring 2019. Going from Lübeck (Germany) to Oulu (Finland), Kemi (Finland), and Husum (Sweden), it provides surface data throughout most basins of the Baltic Sea on a weekly basis. From August 2nd to 9th 2019 and February 22nd to 29th 2020, discrete comparison samples were taken during the roundtrip. The cruise track and discrete sampling locations for both cruises are displayed in Figure 10.

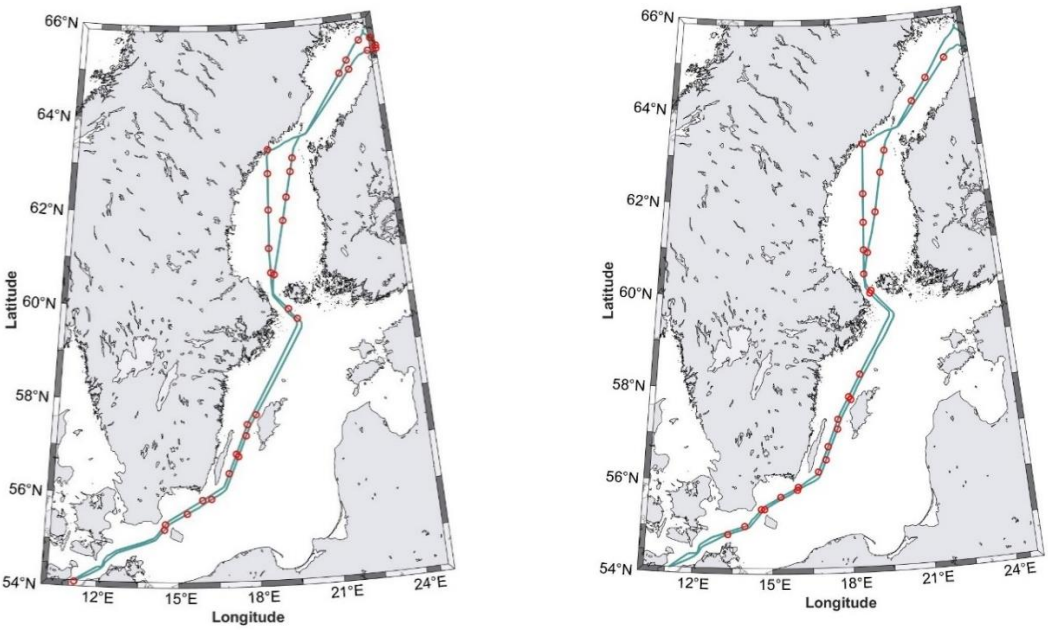

Figure 10: Tavastland cruise track in August 2019 (left) and February 2020 (right). Red circles mark the UW sampling sides of discrete measurements.

The continuous measurement system is set up in the engine room. Surface sea water from approximately 6 m depth is pumped in. After the intake, the water flow is divided into a GO-system (Figure 12) and a ferry box system (Karlson et al., 2016, Figure 13). The greenhouse gas sensors are coupled to the GO-system.

The measurement unit for trace gases consists of three sensors. Two of which are Off-Axis Integrated Cavity Output Spectroscopy (OA-ICOS) sensors, a Methane and Carbon dioxide Analyzer (MCA; Los Gatos Research, San Jose, California, USA; Gülzow et al., 2011) and a Nitrous oxide and Carbon monoxide Analyzer (NCA; Los Gatos Research; Arévalo-Martínez et al., 2013). The third sensor is a Non-Dispersive InfraRed analyzer (NDIR; LI-COR Biosciences, Lincoln, Nebraska, USA; Becker et al., 2012) for additional CO_2 partial pressure detection. The OA-ICOS working principle is that a band laser beam (DFB diode laser) is directed at a slight angle into the measurement cell that is continuously passed by a gas flow (Figure 11). The laser beam passes the cell up to 100k times due to reflection at highly reflective mirrors (reflectivity 0.9999; Hendriks et al., 2007), creating an absorption path length of up to 20000 m. The fractional absorption of light at the CH_4 resonant wavelength of 1600 nm is measured by the detector leading to an absolute measurement of the CH_4 concentration in the cell (Hendriks et al., 2007).

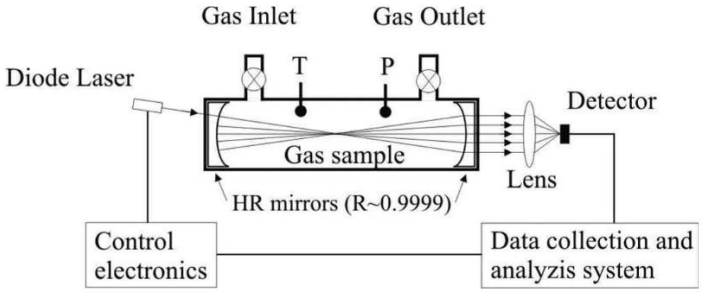

Figure 11: Scheme of the OA-ICOS-MCA measurement cell after Baer et al. (2002). The stainless steel tube is sealed with high-reflectivity mirrors. Temperature (T) and Pressure (P) are monitored (Gülzow et al., 2011).

306 Seawater enters continuously at the top of the spray head equilibrator (Steinhoff, 2010)
307 forming a circular spray (Becker et al., 2012) and leaves through a siphon to regulate a
308 constant water volume and headspace. From the equilibrator, the gas flow passes a cooling
309 trap (5° C) and a water guard to protect the sensors from water (Gülzow et al., 2011).
310 Additionally, a Nafion® drying tube (Perma Pure LLC, Lakewood, New Jersey, USA) with a
311 counter-flow of air is used to further dry the gas stream. Afterwards, the flow is divided to
312 enter the OA-ICOS MCA and NCA simultaneously. Both analysers are equipped with
313 membrane pumps, with the continuous flow of both instruments adding up to 500 mL min^{-1}.
314 The gas streams are merged after leaving the OA-ICOS sensors and pass through a LI-COR
315 sensor for additional CO_2 measurement before the air is pumped back to the equilibrator
316 again. A second equilibration chamber is installed to compensate potential air volume changes
317 that may result from humidity removal, solubility changes due to warming or cooling of the
318 water, or disequilibrium of one of the main dissolved gases. This second equilibrator provides
319 preequilibrated air in such cases to minimize contamination in the main equilibrator (Gülzow
320 et al., 2011).

321 Inside the measuring cell of the MCA a pressure of 184 hPa is created and constantly
322 monitored to achieve a better measuring signal by limiting peak broadening. The water
323 temperature in the main equilibration cell is recorded continuously with a precision of 0.02 °C.
324 Moreover, the average period over which the laser is being reflected in the measurement cell,
325 called mirror ring down time (MRT), is continuously monitored by the MCA. CH_4
326 concentrations ranging from 0.1 - 8 ± 0.002 ppm can be measured with a total uncertainty of
327 < 1 %. (Gülzow et al., 2011). The measurement frequency is set to 0.2 Hz which accounts for a
328 5-second measurement interval. A customized software is used to merge the data with all
329 important parameters and calculations including date, time, position, salinity, in situ

temperature of the seawater and atmospheric pressure, which are stored at a temporal resolution of one minute, to which the different parameters are synchronized. For further processing, a correction, to account for the temporal and temperature offsets from water intake to the measurement cell, is performed.

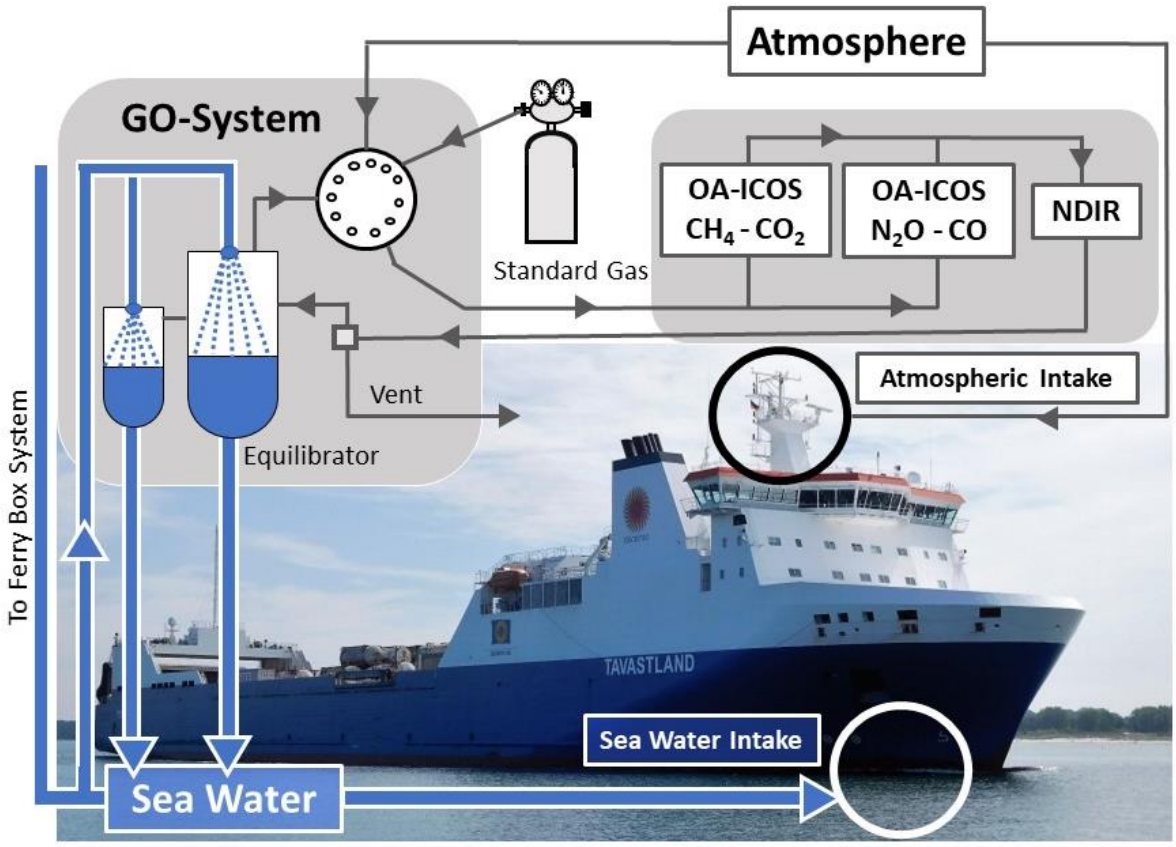

Figure 12: Setup of the continuous measurement system for trace gases inboard the Tavastland (Foto Credit WALLENIUS SOL, n.d.). The systematic scheme was adapted from Becker et al. (2012).

From 2nd to 9th of August 2019 and 21st to 28th February 2020, discrete water samples were taken out of the ferry box water flow via a silicon tube. In August, samples were drawn from the de-bubbler (red circle in Figure 13) and the WET Labs Fluorometer and Turbidity Sensor in February (magenta circle in Figure 13) as there is no water outlet in the GO-system in the current setup. Afterwards, the samples were processed as described above (Section 3.1.1). In total, 31 duplicates for discrete PT measurements were taken in August. In February, 29 triplicates each, for HS and PT measurements, were taken. During both cruises the samples were drawn during daytime at a temporal resolution of approximately every two to three hours.

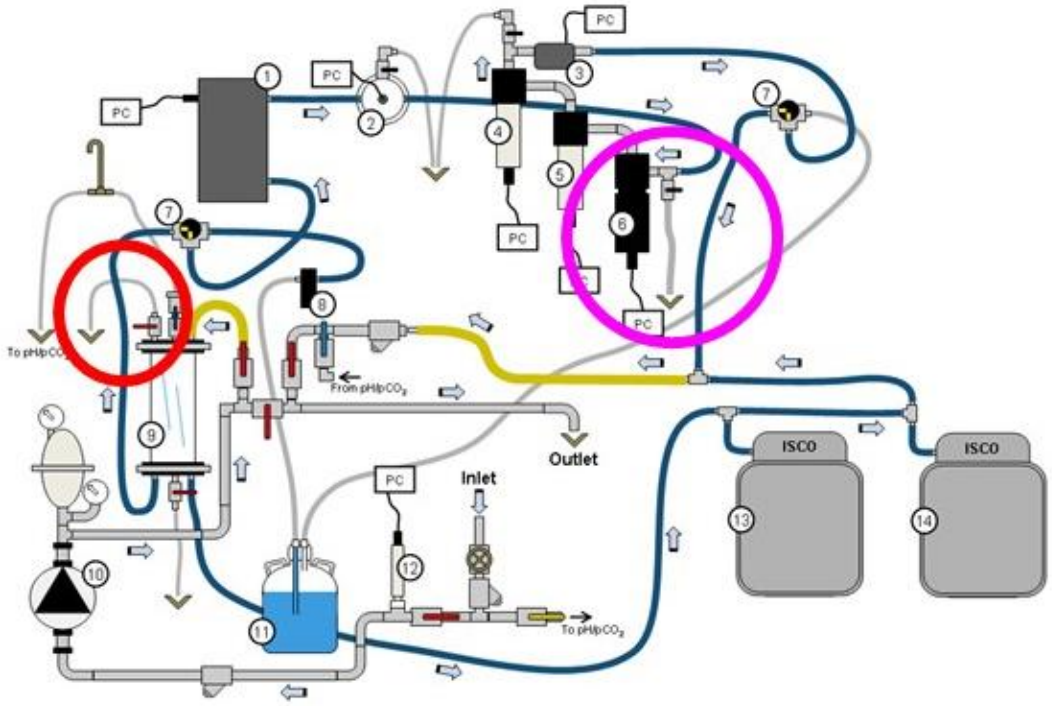

Figure 13: Tavastland ferry box system set up. 1 Sea-Bird Thermosalinograph - SBE 45 MicroTSG; 2 Aanderaa O_2 Sensor - Oxygen Optode 3835; 3 Ultrasonic Flow sensor - UF25B100; 4 TriOS CDOM Sensor - microFlu-CDOM; 5 TriOS Phycocyanin Sensor - microFlu-blue; 6 WET Labs Fluorometer and Turbidity Sensor - ECO FLNTU(RT); 7 Washing programme valves; 8 Washing programme pump; 9 Debubbler; 10 Pulsafeeder Pump - Pulsar Shadow 55BF; 11 Washing solution container – 0,01% Triton X 100; 12 Sea-Bird Digital Thermometer - SBE 38; 13 ISCO Refrigerated Sampler - 6712FR; 14 ISCO Refrigerated Sampler - 6712FR; 15 Pump; 16 pH System; 17 pH Wastewater tank; 18 pCO_2 System; 19 Pump; 20 Wastewater tank (A. Willstrand Wranne, personal communication).

3.2. Purge and Trap System

The final set up of the PT measurement system (Figures 14 & 15) and the operation principle will be described divided into the purge, the trapping, and the GC-FID unit of the system. In the following descriptions, all numbers used in brackets refer to the numbers displayed in the scheme. The materials that were used are listed in Table 1.

All tubes that are used in the setup are 1/8” stainless steel or nylon tubes. For those tubes that need to be changed regularly, plastic tubes with Luer Lock connectors were chosen. These are made of polypropylene (PP), polycarbonate (PC), high density polyethylene (HDPE), styrol-acrylnitril-copolymere (SAN) and silicone. The plastic products are primarily intended for medical use and not for chemical laboratory analysis. However, no contamination, leakage or inconsistency in standard gas and blank (pre-purged) sea water measurements could be observed. These products were chosen due to being easy in handling, especially regarding the changing of needles and connections as well as for the standard gas injections. Helium (He)

(1) is used as the purging agent and as the carrier gas for the gas chromatograph (GC) (19). Therefore, a ball valve and a needle valve (3) are installed after the gas stream is divided and before He enters the purging unit (4) to enable flow regulation for the PT system without changing the carrier flowrate through the GC. A digital thermometer (5) is installed next to the system for temperature measurements (Figure 14). To avoid spilling of poisoned water in case of a leakage, plastic zipper bags were used to cover the sample vial and purge chamber (Figure 15).

Table 1: List of materials and manufacturers.

Component	Product Specification; Manufacturer
4-port valve	SS-43YFS2-1466; Swagelok®, Solon, Ohio, USA
6-port Valco valve	6UWE, 1/8", med. temp. range; VICI™, Valco Instruments, Houston, Texas, USA
12-port Valco valve	12UWE, 1/8", med. temp. range; VICI™, Valco Instruments, Houston, Texas, USA
Aluminium Caps	15 R20-oA, 772013; Chromatographie Handel Müller, Fridolfing, Germany
Butyl rubber stoppers	4451283; Chromatographie Handel Müller, Fridolfing, Germany
CH_4 Trap	1/8" stainless steel column; Spherocarb 100-200 mesh; Phase Separations Limeted, London, United Kingdom
Column	Stainless steel, 1.83 m length, 3.2 mm OD, 2.2 mm ID; packed with washed molsieve 5A (mesh 80/100); Alltech GmbH, Germany
Drying agent	Sicapent®; phosphorus pentoxide (P_2O_5); E. Merck, Darmstadt, Germany
Flowmeter	VAF-G2; Swagelok®, Solon, Ohio, USA
Gas chromatograph	Hewlett Packard 5890 Series II; Hewlett Packard, Palo Alto, California, USA
Gas-tight glass syringe	VICI Precision Sampling, Baton Rouge, LA, USA
Helium	5.0; Air Liquide GmbH, Düsseldorf, Germany
Luer Lock 3-way valve	30600-04; Cole Parmer, Vernon Hills, Illinois, USA
Luer Lock check valve	With silicone diaphragm; 30505-92; Cole Parmer, Vernon Hills, Illinois, USA
Luer Lock tubes	Flexible PVC tubing with Female/Male Luer Ends, 30600-65; Cole Parmer
Nafion® drying tube	MD-050-72P-2; Perma Pure™, Halma, Amersham, United Kingdom
Needles	Sterican® B.Braun, Melsungen, Germany
Plastic syringes 20 mL	BD Plastipak™ Luer Lock; Becton, Dickinson and Company, Franklin Lakes, New Jersy, Vereinigte Staaten
Plastic syringes 3 mL	SOFT-JECT Luer Lock; Henke Sass Wolf, Tuttlingen, Germany
Safeflow® infusion valve	409100H; B.Braun, Melsungen, Germany
Sample vials	R20-20br HS, 75.5 x 23 mm, 4451254; Chr. Handel Müller, Fridolfing, Germany
Screw connections	Swagelok®, Solon, Ohio, USA
Standard gases	DEUSTE-Steininger GmbH, Mühlheim, Germany
Thermometer	Checktemp; Hanna Instruments, Woonsocket, Rhode Island, USA
Water filter	Gelman Acro 50 45µm PTFE Lot no 2591; Pall, Port Washington, New York, USA

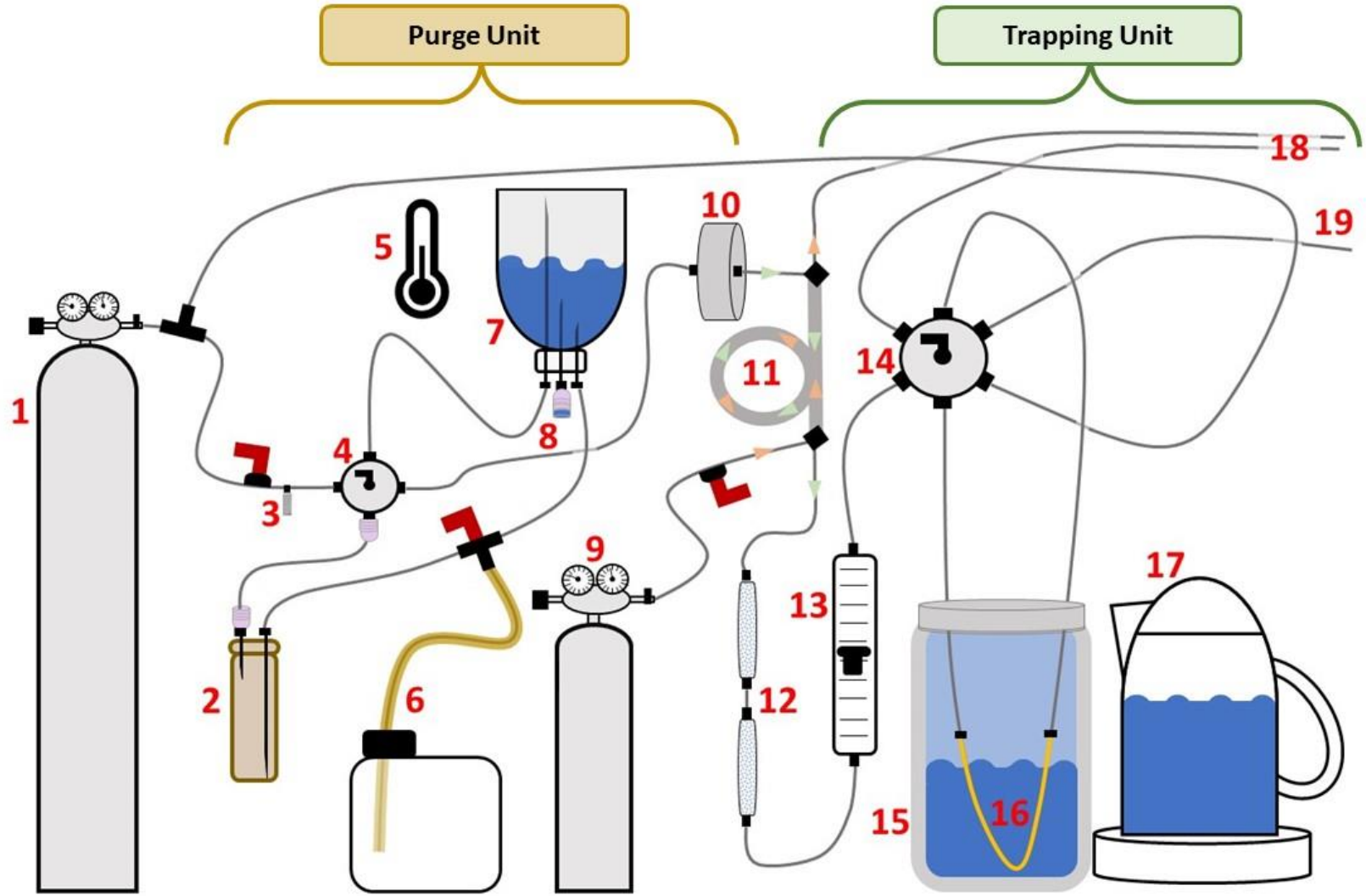

Figure 14: Schematic illustration of the PT system set up. 1 He gas bottle with pressure regulator; 2 sample vial; 3 needle valve; 4 four-port valve; 5 thermometer; 6 double-walled wastewater pipe and wastewater canister; 7 purge chamber; 8 Luer Lock injection port with check valve and Safeflow® infusion valve; 9 compressed air with pressure regulator; 10 liquid filter; 11: Nafion® counterflow drying tube; 12 two glass dry traps filled with P_2O_5; 13 flowmeter; 14 six-port valve; 15 Dewar tank filled with liquid nitrogen; 16 CH_4 trap filled with molecular sieve; 17 water boiler; 18 vent; 19 connection to GC-FID.

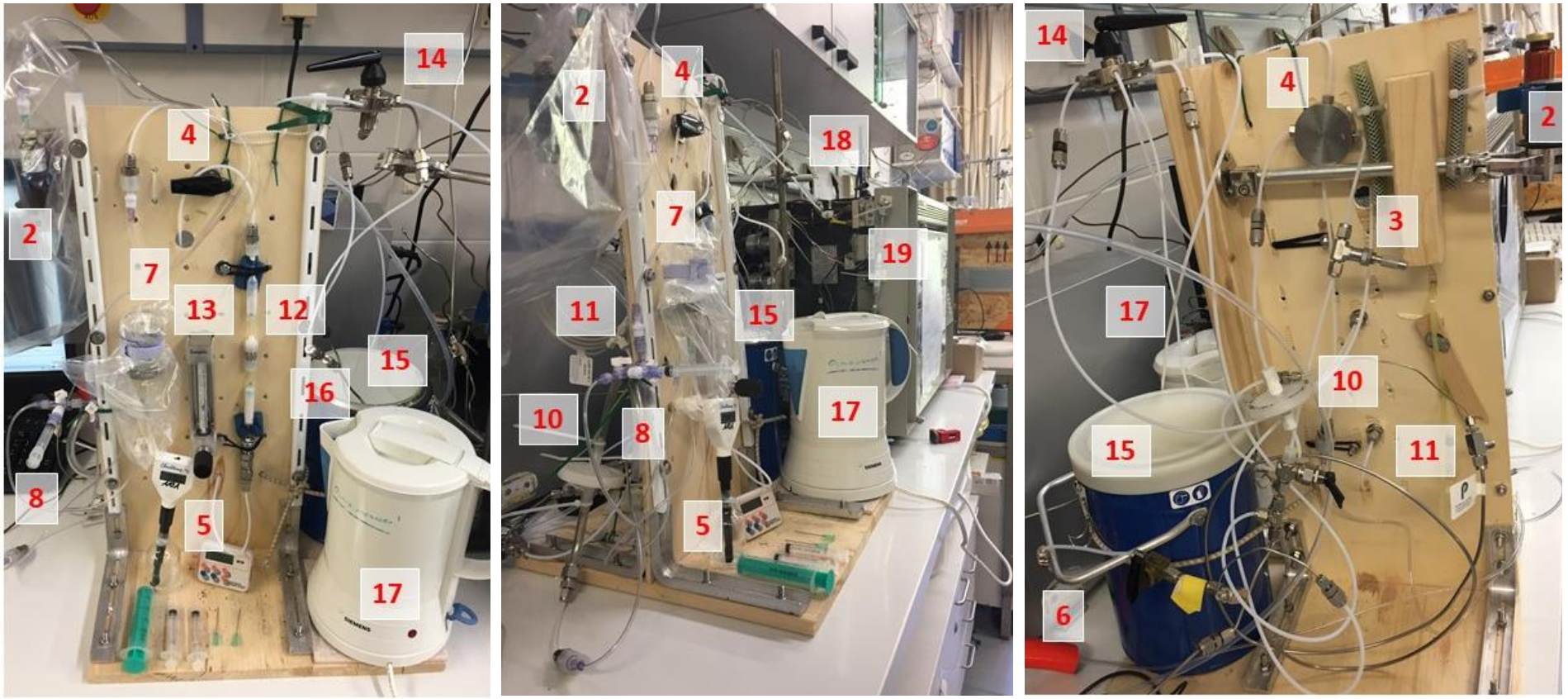

Figure 15: Photographic illustration of the PT system set up showing the front view (left), side view (middle), and back view (right). The labels equal those of the schematic (Figure 14).

3.2.1. Purge Unit

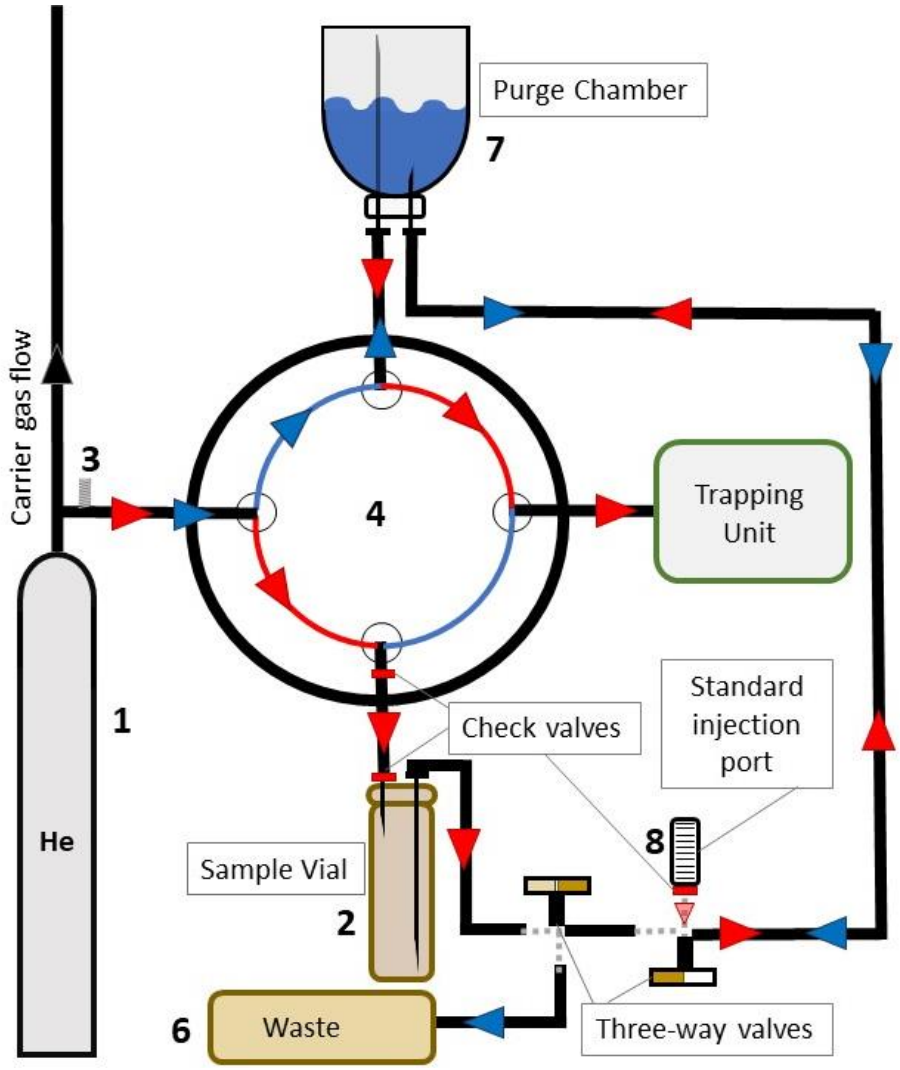

Figure 16: Purge unit of the PT system. How the gas flow is directed in two different valve positions is color-coded. Red arrows represent the gas flow direction during purging ("Purge" position). Blue arrows show the gas flow direction when emptying the purge chamber into waste ("Waste" position). Red check valves indicate backflow barriers. Three-way alves are used to direct the gas flow into the desired components. 1 He gas bottle with pressure regulator; 2 sample vial; 3 needle valve; 4 four-port valve; 6 wastewater canister; 7 purge chamber; 8 Luer Lock injection port with check valve and Safeflow® infusion valve.

For the measurements, a short (0.4 x 12 mm) and a long (0.8 x 120 mm) needle are inserted into the sample vial (2) through the butyl rubber stopper. The short needle is connected via a plastic tube to the four-way valve (4). The long needle is connected to the purge chamber (7) via plastic tubes and two three-way valves. To avoid water going into the valve (4), two check valves are used to restrict the backflush at both ends of the tube between valve and sample. When the sample is being purged, the valve (4) is in the "Purge" position (red flow direction in Figure 16).

When the He flow through the system is turned on, it enters the sample vial through the short needle and the water sample is pushed through the long needle which touches the ground of the vial to ensure that the whole sample volume is purged (if drops remained in the vial, this was noted in the measurement protocol). The three-way valves between sample vial and purge chamber are positioned to allow for the water sample to be inserted into the purge chamber through a short needle that stays in the purge chamber which is a 50 mL glass vial that is crimp-sealed with a butyl rubber stopper and an aluminium cap. As it is turned upside-down, gas leakages through the rubber stopper are inhibited through the water barrier and it can be used for several measurements before it needs to be changed.

When the He is bubbling through the sample all dissolved gases are stripped from the water phase. Due to its low solubility in seawater at room temperature and normal pressure (Duan et al., 1992), CH_4 goes into the gaseous phase comparably fast. From the purge chamber the gas stream is pushed through a long needle and a plastic tube to the four-port valve (4). From there the gas passes a water filter (10) that blocks when getting in contact with water (H_2O (aq.)) while water vapor can pass. To dry the gas stream, it continues through a Nafion™ tubing (11) using a counterflow of compressed air (9) at a flow rate of approximately 200 mL min^{-1} to avoid water vapor reaching the CH_4 trap as frozen water would disturb the He flow through the trap. Inside the Nafion™ tube, the two gas streams are separated by a membrane that is only passable for H_2O. The drying gas goes into the exhaust after the Nafion™ tube and can be turned on/off through a switch. Additionally, two glass tubes filled with phosphorus pentoxide (Sicapent®; P_2O_5) are used as back-up dry traps (12). A benefit of Sicapent® is that it functions as an indicator by changing its colour from white to green to blue to purple when in contact with H_2O making the drying efficiency easily visible. When the first trap had turned blue, it was exchanged before the second started changing its colour. Afterwards the gas stream passes a flowmeter (13) to ensure a continuous and uniform flow rate during the measurements. The flow was set to approximately 0.03 NL min^{-1} during the purging. From the flowmeter the gas stream continues into the six-port valve (14) which will be described in section 3.2.2.

To avoid contact with the $HgCl_2$-poisoned waste, a wastewater pipe was integrated into the set up. The He flow through the system is switched off before switching the three-way-valve between sample vial, purge chamber and waste water pipe so that the purge chamber and

the waste water canister (6) are connected. Afterwards, the four-way-valve is switched to the "Waste" position (blue flow direction in Figure 16). When the He flow is switched on again, the He flows from the valve (4) into the purge chamber through the long needle and the water is pushed through the short needle. To secure leakage contaminations, the plastic wastewater tube is surrounded by a thick hose and the canister is standing in a catch basin.

When the purge chamber is empty, the He flow is turned off and both valves are switched back into the "Purge" position before putting the next sample.

3.2.2. Trapping-Unit

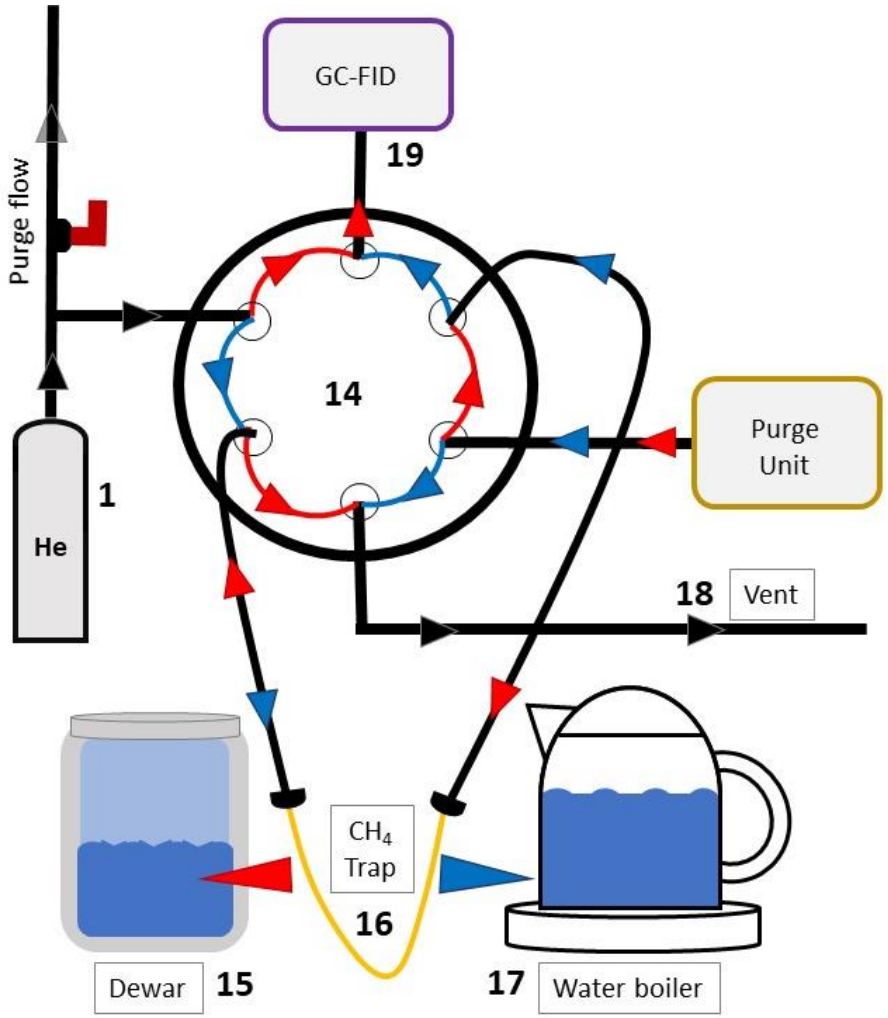

Figure 17: Trapping unit of the PT system. How the gas flow is directed in the two different valve positions is color-coded. Red arrows represent the gas flow direction during purging ("Trap" position). Blue arrows show the gas flow direction when the trapped CH_4 is injected into the GC-FID ("GC" position). 1 He bottle; 14 six-port valve; 15 Dewar tank filled with N_2 (aq.); 16 CH_4 trap; 17 water boiler; 18 vent; 19 connection to GC-FID. The trap is put into the Dewar bin when the valve (14) is in "Trap" position and into the water boiler when the valve (14) is switched to "GC" position as indicated by the arrows in the according colors. Black arrows are used when only one flow direction is possible.

The gas stream enters the six-port valve (14) from the flowmeter (13). During the purge process, the valve (14) is set in the "Trap" position (red flow direction in Figure 17). During this setting, the gas flow continues through the CH_4 trap (16). While purging, the trap is put into a Dewar bin (15) filled with liquid nitrogen (N_2 (aq.)) the whole time at a temperature of approximately 77 K (-196 °C). As the melting point of CH_4 is 91 K (-182 °C), CH_4 sublimates into the solid aggregate phase and is trapped on the mesh inside the column, whereas the small He molecules are not limited in their mobility with a melting point of 4.21 K (-268.9 °C). Hence, the He streams into the exhaust.

To bring the trapped CH_4 onto the column inside the GC and quantify it with the flame ionisation detector (FID), the six-port valve position needs to be changed to the "GC" position (blue flow direction in Figure 17). In this position the gas stream from the purge unit goes directly into the exhaust (and should be turned off), the He from the T-connection (He bottle) goes through the trap and leaves the trap to continue to the GC. To mobilize the CH_4 from the trap, the trap is put into hot water (17) at approximately 90 °C right after switching the valve (14). It takes approximately four minutes until the CH_4 peak has passed the FID detector.

3.2.3. GC-FID

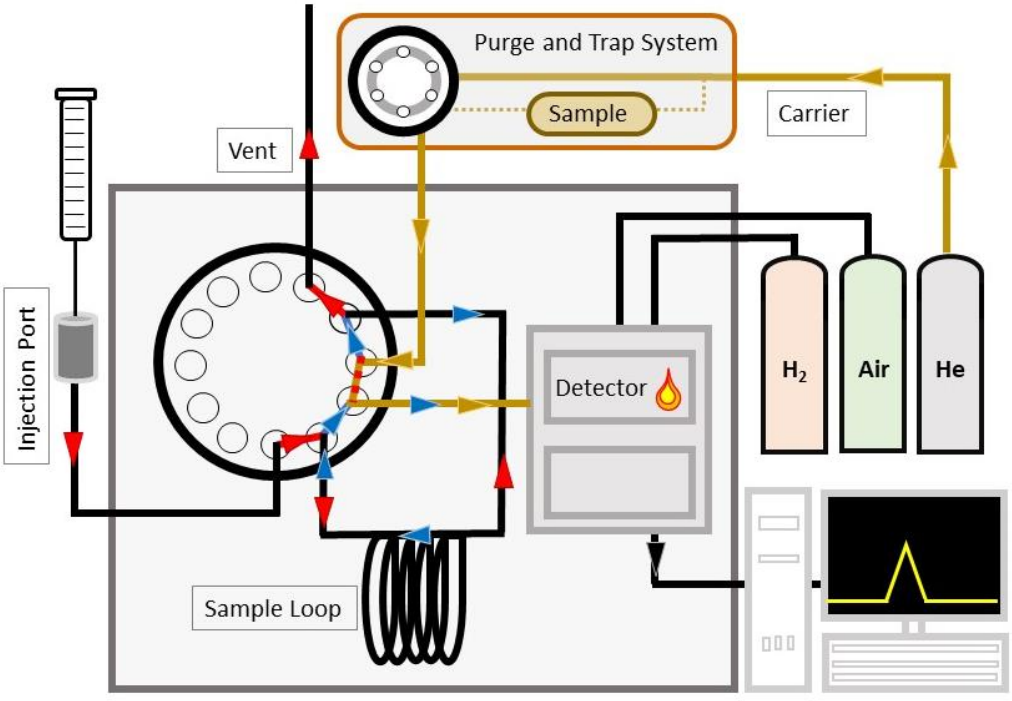

Figure 18: Schematic of the GC-FID for HS and PT measurements. Red arrows indicate the flow direction when the valve inside the GC is in the "Load" position. Blue arrows indicate the flow direction when it is in the "Inject" position. For PT measurements the valve stays in load position.

The third important component is the GC-FID (Figure 18). Inside the GC, a 12-port Valco valve is used to enable either measurements with the FID or an Electron Capture Detector (ECD). However, the ECD is not relevant for this thesis and therefore will not be further explained. The valve can either be set to the "Load" or to the "Inject" position. The direction of the gas flows in the respective positions is indicated by red ("Load") and blue ("Inject") arrows (Figure 18). For HS measurements, 9 mL samples are inserted into the injection port that is sealed with a 12.5 mm septum using a 10 mL gas-tight VICI Valco® glass syringe. Prior to each sample injection, 9 mL of He are injected similarly to flush the sample loop and avoid atmospheric contamination from the vent. The valve is switched to the "Load" position right before the injections. After the manual injection, the valve is switched to the "Inject" position. Hence, the carrier gas flows through the sample loop and carries the sample to the column and detector. Further details about the HS measurement technique are described in Kock (2007).

For PT measurements, the valve inside the GC stays in the "Load" position. The carrier gas flows through the valve to the detector. For sample injection the six-port valve in the trapping unit is switched to the "GC" position as described previously (Section 3.2.2). The flow rate of the carrier He as well as of the PT sample injection are set to 30 mL min^{-1}. A similar flow rate avoids baseline shifts when switching the valve of the trapping unit.

The functioning principal of the FID is that a flame of synthetic air (flow rate approximately 120 mL min^{-1}) and hydrogen (flow rate approximately 170 mL min^{-1}) burns at a temperature of approximately 2000 °C to ionize the hydrocarbon compounds in the inserted sample. The oven temperature was set to 60 °C and the temperature of the detector was set to 250 °C. The CH_4 content of the sample is detected as an electric current by electrodes next to the flame which is displayed in the size of the unitless peak area in the gas chromatogram (Figure 20 in section 3.3.1). Details about further settings and the procedure of the gas detection inside the chromatograph is described in Kock (2007).

3.2.4. Purge Time Adjustment

To find the ideal purge time to quantitatively strip all CH_4 contained in a sample, different standard gases with different sample volumes were purged for different times. In Table 2, an exemplary comparison of different purge times for 20 mL of a standard (2025.2973 ppb) are displayed. The unitless peak area was chosen for CH_4 concentration calculations as it shows a

much better reproducibility compared to the unitless peak height. Especially, slight differences of the water temperature inside the water boiler lead to variations in the peak height and shape while peak areas were still reproducible. Due to the long column the system operates under high pressure of approximately 3 bar. A higher signal for longer purge times was observed (Table 2) which makes it important to adjust the purge time of the standard gases and samples. Therefore, the timer for the calibration measurements was started when the He flow was turned on, whereas for the sample measurements it was started when all sample water had been purged to the purge chamber.

Table 2: Chromatographic peak report of 20 mL injections of Standard A (Table 4 in Section 3.2.5) for different purge times.

Peak Area	Peak Height	Purge Time [minutes]
204070	23.268	4.0
203067	22.688	4.0
202539	21.583	4.0
200991	22.409	4.0
201707	22.652	4.0
218092	24.481	5.0
221175	25.311	5.0
222843	25.156	5.0
227162	26.010	5.0
244008	27.549	6.0
244590	27.032	6.0

To adjust the ideal purge time for sea water CH_4 concentration measurements, Baltic Sea samples from the Boknis Eck cruise on the 3rd of March 2020 from 15 m depth were purged for different times (Table 3). Due to the length of the trap (approximately 40 cm) and the spherocarb filling, CH_4 is effectively trapped for long purge times of over 30 minutes. However, as the deviation for such long purge times was found to be higher compared to shorter times and as CH_4 gases out quickly, shorter purge times were found to be more efficient. When purging for less than three minutes a larger variability among resulting peaks was observed. From four minutes onward, the variability among the different purge times was comparable to that within the same time. To make sure that also for higher concentrations all CH_4 will be captured the purge time was set to 4 minutes and 30 seconds.

Table 3: CH_4 concentrations for HS PT measurements with different purge times of Boknis Eck samples from 15 m depth in March 2020. Standards were purged for the same time.

Purge Time [minutes]	Number of samples	Mean CH_4 [nmol L^{-1}]	Std. Deviation [nmol L^{-1}]	Deviation [%]
15.0	5	4.85	0.13	2.71
4.0	6	4.99	0.14	2.72
5.0	3	5.06	0.09	1.82
30.0	6	5.11	0.53	10.46
2.0	7	4.21	0.75	17.69
Headspace	3	5.06	0.32	6.41

3.2.5. Calibration

On every measurement day, a set of standard gases with a known dry mole fraction of CH_4 was measured prior to sample measurements (Table 4). To verify the exact CH_4 content in the standard gases, they were measured against two National Oceanic and Atmospheric Administration (NOAA) primary standards that were provided from an international initiative for CH_4 and N_2O intercomparison (Wilson et al., 2018).

To avoid dead volume, a Safeflow® infusion valve was attached to the check valve at the standard injection port. For the standard injection, 20 mL plastic syringes were used. After each standard injection, 3 mL of He were injected with a 3 mL plastic syringe through the port to ensure that all injected volume of the standard was measured. To avoid overpressure the He flow through the purge unit is switched off during the standard injection.

Prior to standard measurements, one sea water sample was purged on every measurement day. This water was not pushed to the wastewater canister after purging but left inside the purge chamber and used for the blank and standard measurements. Blanks were always measured before standards. The reproducibility of the blanks was used as an indicator to assure the efficiency of the purge time. If any CH_4 would have been left in the sample vial after purging, this would have led to a larger peak area of the first blank which was not the case. Three blanks without injection were measured to adjust for the background noise so that this could be subtracted from the sample peak areas of the respective day for concentration calculations.

Table 4: Standard gas CH_4 dry mole fractions.

Standard	CH_4 dry mole fraction [ppb]	Inserted volume [mL]
A	2025.2973	20
A	2025.2973	15
B	110.4659	20

The amount of substance n [nmol] of the inserted standards was calculated using the ideal gas law (Equation (3)) in order to produce a linear calibration fit of it in dependence of the unitless peak area (Figure 19).

$$n = \frac{V * x * p}{R * T} * 1000^{-1} \quad (3)$$

Where V is the volume inserted into the purge chamber in L,

x is the dry mole fraction of CH_4 in ppb in the inserted standard sample,

p is the air pressure that was set to 101325 pa,

R is the universal gas constant 8,3145 J mol^{-1} K,

and T is the temperature in K.

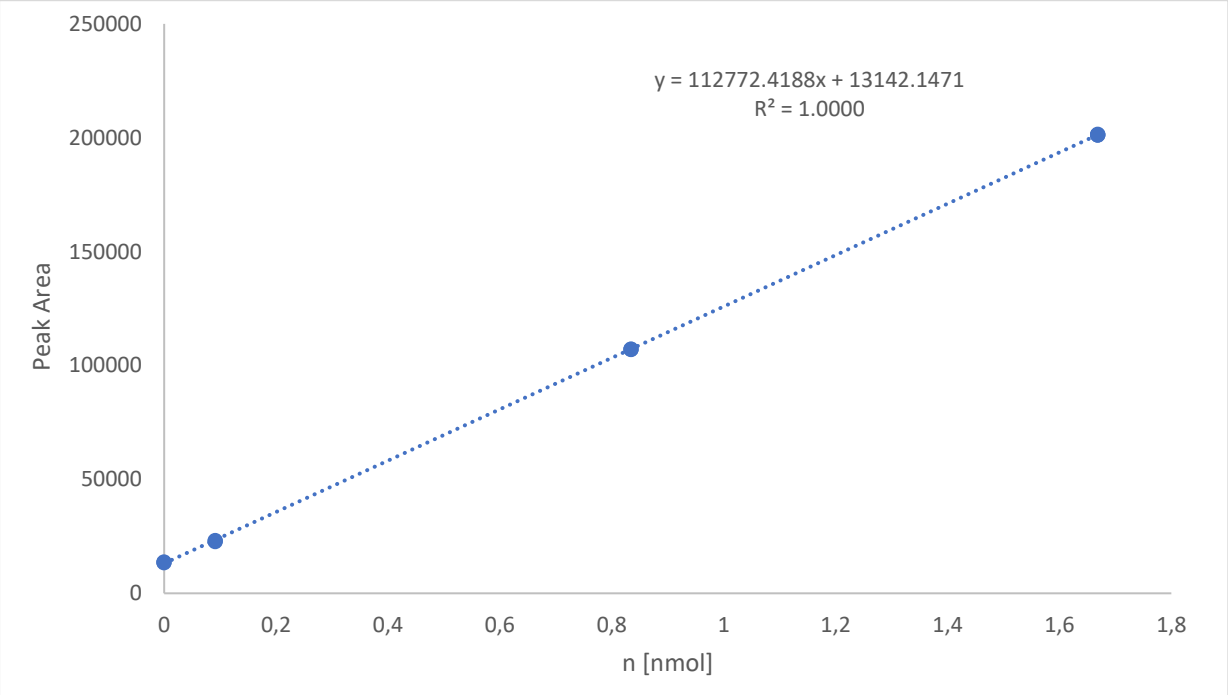

Figure 19: Linear calibration fit of the amount of substance n against the peak area.

3.3. Data Processing

3.3.1. Peak Integration

The chromatography software Chromstar 6.3 (SCPA GmbH, Weyhe-Leeste, Germany) was used for data acquisition. Afterwards, we used the same program to manually integrate the CH_4 peaks (Figure 20). In the beginning, each peak was integrated several times to ensure that the integration process is reproduceable and all peaks were integrated the same way.

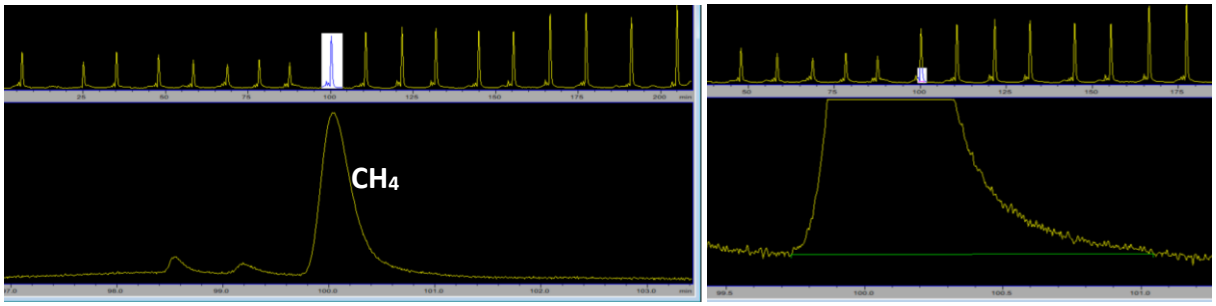

Figure 20: CH_4 chromatogram showing the overall shape of the CH_4 peak (left) and the manual baseline integration (right).

3.3.2. Calculation of CH_4 Concentrations

The CH_4 concentration in the PT sample was calculated using Equation (4). Due to the linear correlation of the FID's signal intensity and the CH_4 content in the sample, the slope of the calibration is used to calculate the CH_4 concentration in the sample. The mean area of the measured blanks was subtracted from the sample peak area to account for the background noise of the system.

$$n = \frac{PA_{sample} - PA_{blank}}{\delta} \quad (4)$$

Where n is the amount of CH_4 [nmol] in the sample,

PA_{Sample} is the peak area of the measured sample,

PA_{Blank} is the mean peak area of the measured blanks,

δ is the slope of the calibration curve [$nmol^{-1}$].

By dividing n by the injected volume, the CH_4 concentration c [nmol L^{-1}] in the sample was calculated afterwards applying equation (5).

$$c = \frac{n}{V} \quad (5)$$

Where n is the amount of CH_4 in nmol,

V is the sample volume [L] inserted into the purge chamber (0.0203 L).

The mean sample vial volume was calculated with Equation (6). 10 sample vials with butyl rubber stoppers and aluminium caps were weighed empty and filled bubble-free with deionized water.

$$V = \frac{(G_{filled} - G_{empty})}{\varrho} \quad (6)$$

Where G_{filled} is the weight of the filled vial in g,

G_{empty} is the weight of the empty vial in g,

ϱ is the water density of 1 g cm^{-3}.

The HS CH_4 concentrations were calculated with the solubility equation for CH_4 in seawater (Wiesenburg and Guinasso, 1979, Equation (7)) according to the routine described in Kock (2007).

3.3.3. Saturation and Flow Rate Calculations

For saturation [%] estimations, the temperature and salinity that were measured with the thermosalinograph are used. First the solubility equation for CH_4 in seawater (Wiesenburg and Guinasso, 1979, Equation (7)) was applied to calculate the concentration in atmospheric equilibrium based on the atmospheric mixing ratio. These were taken from Mace Head observatory in Ireland which is with approximately 1350 km distance the closest measurement station to the study area. Monthly means of 1918.24 ppb for June and 1925.83 ppb for September 2018 (Dlugokencky, 2020a) were used for the calculations.

543 $$c = e^{\left(A_1+A_2\left(\frac{100}{T_{eq}}\right)+A_3\left(ln\left(\frac{T}{100}\right)\right)+A_4\left(\frac{T}{100}\right)+S\left(B_1+B_2\left(\frac{T}{100}\right)+B_3\left(\frac{T}{100}\right)^2\right)\right)} * x_{atm} * 10^{-9}\, p_{atm} \quad (7)$$

544 Where c is the CH_4 concentration in nmol L^{-1},

545 T is the temperature in K,

546 S is the salinity in g kg^{-1},

547 A_1-A_4 & B_1-B_4 are the solubility coefficients for CH_4 (see table 5),

548 x_{atm} is the atmospheric dry mole fraction of CH_4 in ppb.

549 p_{atm} is the atmospheric air pressure in Pa.

Table 5: Solubility coefficients of CH_4 (Wiesenburg and Guinasso, 1979).

Coefficient	A_1	A_2	A_3	A_4	B_1	B_2	B_3
Value	-415.2807	596.8104	379.2599	-62.0757	-0.059160	0.032174	-0.0048198

550 The saturation was obtained using Equation 8.

551 $$Sat\ [\%] = 100 * \frac{c}{c_{eq}} \quad (8)$$

552 The CH_4 flux density F in µmol m^{-2} d^{-1} is determined according to Liss and Slater (1974) by the
553 application of Equation (9).

554 $$F = k * \left(C - C_{eq}\right) \quad (9)$$

555 Where k is the gas transfer velocity in m s^{-1} which was calculated by applying Equation (10)
556 (Sarmiento and Gruber, 2006). The parameterization provided by Nightingale et al. (2000) was
557 used as it is commonly applied for the respective study area and environmental conditions
558 including the influences of wind and breaking waves (for example Ma et al., 2020 & Ma et al.,
559 2019).

560 $$k = k_a * 10^{-7} * u_{10} + 6.17 * 10^{-7} * {u_{10}}^2 * \left(\frac{Sc}{600}\right)^{-0.5} \quad (10)$$

561 Where k_a is the parameter 9.23 m s^{-1} (Nightingale et al., 2000).

562 u_{10} is the wind speed in m s^{-1} in 10 m above the sea surface,

563 Sc is the Schmidt number.

As the anemometer on the R/V Alkor was installed 23 m above the water line, Equation (11) was used to calculate u_{10} (Justus et al., 1978; Panofsky, H. and Dutton, 1984).

$$u_{10} = u * \left(\frac{z_{10}}{z}\right)^{s} \quad (11)$$

Where u is the measured wind speed,

z_{10} is the height of 10 m,

z is the measurement height of 23 m,

s is a function of the atmospheric stability in the determined layer and the characteristics of the underlying surface.

For the calculations represented here, s was set to 0.11 as this was proved to be valid for most at sea conditions (Hsu et al., 1994).

The Schmidt number was calculated with Equation (12) (Sarmiento and Gruber, 2006).

$$Sc = \frac{v}{D} \quad (12)$$

Where v is the kinematic viscosity in $m^2\ s^{-1}$,

D is the molecular diffusivity in $m^2\ s^{-1}$ that was calculated using the diffusion coefficients of CH_4 in water (Jähne et al., 1987) applying Equation (13).

$$D = (3{,}047 * 10^{-6})^{\frac{-18360*8{,}314^{-1}}{T}} \quad (13)$$

Where T is the temperature in K.

The kinematic viscosity v was calculated using the empirical equations of Siedler and Peters (1986) by applying Equation (14).

$$v = \frac{\varrho}{\mu} \quad (14)$$

Where ϱ is the density of the seawater that was measured with a thermosalinograph in $kg\ m^{-3}$,

μ is the molecular viscosity that was calculated with Equations (15 - 21).

$$\mu = \mu_s * \mu_T \quad (15)$$

Where

$$\mu_s = 1 + A * Cl^{0.5} + B * Cl \quad (16)$$

Where

$$A = 5{,}185 * 10^{-5} * T + 1{,}0675 * 10^{-4} \quad (17)$$

$$B = 3{,}3 * 10^{-5} * T + 2{,}591 * 10^{-3} \quad (18)$$

Where *T* is the temperature in °C,

S is the salinity in g kg^{-1},

Cl is the volume chlorinity which was calculated with Equation (19).

$$Cl = \frac{\varrho * S}{1806.55} \quad (19)$$

$$\mu_T = 10^a * \frac{1{,}002}{1000} \quad (20)$$

Where

$$a = \frac{1.1709 * (20 - T) - \frac{1.827}{1000} * (T - 20)}{(T + 89{,}93)} \quad (21)$$

Where *T* is the temperature in °C.

On June 15th, 2018 data for wind speed, sea surface salinity (SSS), sea surface temperature (SST), and air pressure were only measured until noon. For the calculations the atmospheric pressure was assumed to be to 101325 pa, salinity was set to the average 10.942 g kg^{-1} of all measured SSS on that day. The range was 10.59 to 11.489 g kg^{-1}. Wind speed was set to 3 m s^{-1} as a great range between 0.4 and 8 m s^{-1} was measured earlier on that day with lower values at noon than in the morning. Density was set to 1005 kg m^{-3}.

3.4. Uncertainty Estimate

Various error sources may contribute to the statistical uncertainty of both discrete measurement techniques. For PT measurements, gas pressure or flow variations between the purge processes, gas leakages, or variations in the purge time can play a role. Moreover, underpressure when switching the valve of the trapping unit may lead to air contamination. This was tested with a flowmeter that measures positive and negative flows. However, the

flowmeter is too inaccurate below 30 mL min^{-1} to be absolutely sure. The compressed air used for drying in the Nafion™ tube may be another contamination source due to CH_4 transfer from the compressed air that was used for drying into the sample gas flow. The purged volume is an important determinant for PT concentration calculations. As such, the precision of this volume can hold an error source. For the calculations of this thesis a mean volume of 0.0203 L that had been determined previously (Equation (6) in Section 3.3.2) was applied. To identify the approximate error related to the volume, ten sample vials were filled bubble-free with tap water and closed with butyl rubber stoppers and crimp sealed with aluminium caps. These were weighed before and after purging. The calculation was performed using Equation (6). A density of 1 g cm^{-3} was assumed. Only minor volume variations of < 1 % were observed (Table 6). This uncertainty is in the same order as that of the previous volume determination initiative. However, to increase the accuracy of future measurements samples could be weighed before and after measurement to use the exact volume of each sample for concentration calculations.

Table 6: Purged volume determination for 10 vials filled with tap water.

Weight full [g]	Weight empty [g]	Weight water [g]	Volume Vials [cm^3 or ml]	Standard Deviation [cm^3 or ml]	Deviation [%]
37.66	17.27	20.39	20.39	0.17	0.83

For HS measurements the accuracy of the added headspace as well as the injection and extraction procedures can play an important role as volume variations or contamination with air can confound the concentration estimation. Moreover, the equilibration time is relevant (Gindorf, 2020). As the sample loop in the GC is open towards the exhaust, contamination with air is possible when the valve inside the GC is in the “Load” position. A bias of this is avoided by flushing the system with He (Section 3.2.3). The sample loop has a volume of 2 mL. However, due to the connection tubes, a large dead volume occurs, and the inserted volume of 9 mL is not sufficient. When larger volumes are inserted, the occurring peaks increase. Nonetheless, this error is assumed to be neglectable due to the high reproducibility when inserting 9 mL. Temporal variations of switching the GC valve may also have a minor impact on the peak area.

According to the statistical analysis of David (1951), an estimate of the standard deviation σ for each triplicate's CH_4 concentration was calculated by dividing the substrate of maximum and minimum measured concentration by the factor f = 1.91 for triplicates and by the factor f = 1.52 for duplicates (Equation 22).

$$\sigma = (max_c - min_c) * f^{-1} \quad (22)$$

To make the errors of the different measurement campaigns comparable, percentual means were calculated (Table 7).

Table 7: Mean errors of AL 510, AL 516, Tavastland August 2019 (TVL AUG), Tavastland February 2020 (TVL FEB) PT and HS, Bocknis Eck April 2020 (BE APR) PT and HS.

Campaign	AL 510	AL 516	TVL AUG	TVL FEB PT	TVL FEB HS	BE APR PT	BE APR HS
Mean Error [%]	5.7	3.1	6.2	6.2	22.2	1.2	5.3

A variety of systematic errors may impact the discrete measurements. This includes the assumption of normal air pressure for the calculations as this is not measured in the laboratory. Temperature is measured with an accuracy of only 0.1 °C which may lead to minor divergences. Moreover, contamination with air during sample collection as well as during poisoning may bias the measurements. In general, samples with small CH_4 content are most vulnerable towards biases due to air contamination which leads to too high estimations in this case (Wilson et al., 2018). The manual peak integration may also bear an error source.

Moreover, Niemann et al. (2015) discussed that butyl rubber stoppers can lead to adulterations in CH_4 measurements and the usage of $HgCl_2$ as a preservative is subject to international discussions as recent studies indicate that some methanotrophs can reduce $HgCl_2$ to elemental Hg (Bussmann et al., 2015) and produce a chalkophore called Methanobactin that can bind Hg from the environment (Baral, 2017; Chang et al., 2018; DiSpirito et al., 2016; Lu et al., 2017) which could lead to fraud measurements when contained in a sample. Different other preservatives have been suggested and tested, such as potassium hydroxide (KOH), sodium chloride (NaCl) (Magen et al., 2014), sulfuric acid (H_2SO_4), and sodiumhydroxide solution (NaOH) (Bussmann et al., 2015). Moreover, first measurements of samples preserved with hydrochloric acid (HCL) indicate that this may be a suitable alternative (D. L. Arévalo-Martínez, personal communication).

The calibration procedure may furthermore be a source for systematic errors. The accuracy of the injected volume is an important factor for the CH_4 concentration calculation. This plays an especially important role for HS calibrations as standard gases are manually diluted with He to gain different CH_4 dry mole fractions while injecting the same volume leading to two manual extractions for one standard measurement. The calculation of the sample CH_4 concentration depending on the slope and intercept of the calibration curve may bear another error source. However, for PT measurements the calculations of the same sample (15 m Boknis Eck March 2020) with different calibrations indicates a high reproducibility (Table 2, Section 3.2.4). Moreover, the comparison of the mean errors in slope and intercept of the calibrations indicate a clear advantage of the PT calibration over the HS calibration (Table 8). For both parameters, the minimum error of HS is higher than the maximum error of PT.

Table 8: Comparison of calibration errors [%] for PT and HS calibrations.

	Slope			Intercept			Number of
	Mean Error	**Min. Error**	**Max. Error**	**Mean Error**	**Min. Error**	**Max. Error**	**Calibrations**
HS	1.7	1.3	1.9	12.3	9.2	15.6	4
PT	0.5	0.1	0.9	3.1	0.6	5.2	16

Another possible error source during the calibration process may be related to the syringes. The gas tight glass syringes used for HS measurements are used several times and might lose their accuracy over time. However, this is tested on a regular basis. The needles are also reused and sometimes problems with plugging are observed. On the other hand, the single-use plastic syringes and needles used for PT are not gas tight and may be less accurate. No evidence for this assumption or for a possible contamination from the plastic components that were used in the PT setup was found during the measurements that were carried out during this thesis.

The Limit Of Detection (LOD) and Limit Of Quantification (LOQ) of the PT system were estimated to 0.4772 nmol L^{-1} with Equations (23) and 1.2464 nmol L^{-1} (24) respectively.

$$LOD = y_B + 3 * d_B \quad (23)$$

$$LOQ = y_B + 10 * d_B \quad (24)$$

Where y_B is the average blank peak area,

d_B is the standard deviation of the blank peak areas.

These variables were derived from ten blank measurements of five different measurement days. The amount of substance was calculated with Equation (4) (Section 3.2.2) with slope and intercept of the five according calibrations being averaged. The calibrations and blanks of different measurement days were used for this estimation as the flows of H_2 and synthetic air are subject to minor variations from one measurement day to another.

The MCA can measure CH_4 with an uncertainty < 1 %. However, due to the equilibration other uncertainty factors, such as temporal shifts or flow and pressure variations in the equilibration cell may play a role. Generally, it is known that the gas exchange between the water phase and the gas phase is approximately three times slower for CH_4 than for CO_2 (Gülzow et al., 2011). UW measurements may thus not capture sharp CH_4 gradients, but produce a temporally integrated, smoothed CH_4 signal.

One very important point for the comparison of UW and discrete samples is that small air bubbles in the water flow of the seawater supply would lead to a small underestimation of the actual CH_4 concentration in the continuous data, whereas the same error may lead to strongly enhanced overestimation in the discrete measurements due to the low solubility of CH_4 in water and different measurement principles as described above. To give a quantification estimate of the error that may occur due to air bubble contamination in the discrete samples Equations (3) and (5) were applied to calculate the contribution of different bubble sizes assuming a dry mole fraction of 2000 ppb, air pressure of 1013.25 hpa, a sample vial volume of 20.3 mL and a temperature of 22.5 °C (Table 9).

Table 9: Error estimation of air bubble contamination in discrete samples.

Air bubble volume [mL]	n CH_4 [nmol]	c CH_4 [nmol L^{-1}]
0.1	0.0824	0.4061
0.01	0.0082	0.0406
0.001	0.0008	0.0041

4. Results and Discussion

4.1. Comparison of Static Headspace Equilibrium and Purge and Trap

To compare PT with HS measurements, triplicates of seawater samples from the six standard depths were taken each, for PT and HS during the Boknis Eck cruise on 28th of April 2020. Unfortunately, one of the three HS samples for 20 m broke so that the mean concentration was obtained from duplicate measurements. The CH_4 concentrations ranged from 5 to 222 nmol L^{-1} allowing a comparison over a broad concentration range. Both profiles show a similar trend with lowest CH_4 concentrations in the surface that are constantly increasing from 1 to 15 m depth, while a strong gradient can be observed between 15 and 20 m and highest values in the bottom water (Figure 21).

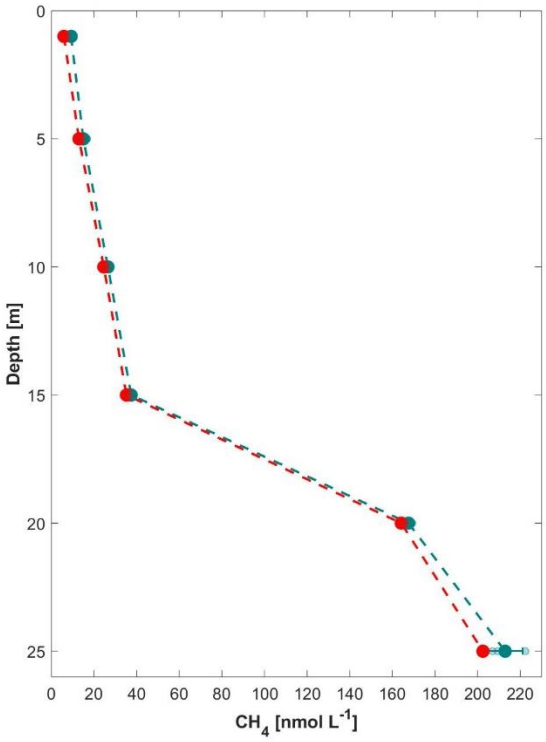

Figure 21: Boknis Eck depth profile of CH_4 measured with PT (red) and HS (green) for April 2020. Means are shown as filled dots and dashed line, discrete measurements are shown as transparent dots and standard deviation is displayed as error bars.

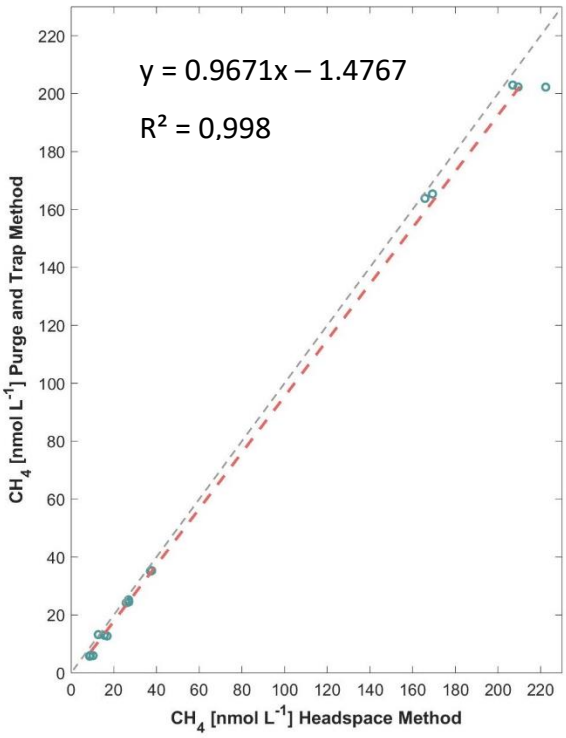

Figure 22: Linear regression of CH_4 concentrations measured with PT against HS for samples from Boknis Eck in April 2020. The grey dashed line indicates the 1-1 relation.

Over all depths, the PT measured concentrations were slightly lower and showed significantly less variation among the triplicates, thereby reflecting a better precision of the PT measurements over the HS method (Table 10). The direct comparison of both techniques shows that the measurements agree well with the HS measurements (Figure 22). Other

720 studies have proven higher precision and sensitivity as well as handling benefits of PT over HS
721 (e.g. Capelle et al., 2015).

Table 10: Boknis Eck April concentrations and deviations measured with PT and HS.

	Purge and Trap			Headspace		
Depth [m]	Mean CH_4 [nmol L^{-1}]	Deviation [nmol L^{-1}]	Deviation [%]	Mean CH_4 [nmol L^{-1}]	Deviation [nmol L^{-1}]	Deviation [%]
1	5.89	0.12	1.99	9.26	0.84	9.06
5	12.97	0.25	1.89	14.99	2.16	14.42
10	24.61	0.56	2.27	26.55	0.63	2.36
15	35.24	0.09	0.25	37.46	0.30	0.80
20	164.17	1.08	0.66	167.57	2.34	1.11
25	202.50	0.37	0.18	212.93	8.91	3.80

722 The difference between HS and PT measurement could reflect small systematic differences
723 between the two methods as discussed in Section 3.4. Moreover, it is possible that a gradient
724 in the Niskin bottle occurred if the bottle was closed in a depth with a strong gradient due to
725 the bottle height (S. Schmidtko, personal communication). It might furthermore be possible
726 that during the sample collection a systematic error appeared. When one triplicate was taken
727 first, a headspace was created inside the Niskin bottle allowing gas exchange of the remaining
728 water with the surrounding air.

729 ## 4.2. Tavastland

730 ### 4.2.1. August 2019

731 The continuous measurements of the surface water showed CH_4 values between 2.8 and 3.5
732 nmol L^{-1} close to atmospheric equilibrium for most parts of the cruise track, particularly in the
733 open waters of the Baltic Sea (Figure 23). Very high concentrations were found in the coastal
734 area of the Bothnian Bay and especially in the areas close to the ports of Oulu, Kemi and
735 Husum where surface CH_4 concentrations exceed 60 nmol L^{-1}. In the harbours of Lübeck, Kemi,
736 and Oulu the continuous measurement system was turned off. On the 7th of August reduced
737 pressure in the ICOS sensors occurred. The respective data is displayed in green in Figure 23.
738 It is very likely that the CH_4 concentration is comparable to that in the beginning of the cruise
739 (A. Kock, personal communication, e.g. Figure 24). The variability of the CH_4 surface
740 concentration in the open water is low and a gradient from lowest values in the southwest to

highest values in the northeast seems to reflect the temperature and salinity dependence of the solubility of CH_4 (Wiesenburg and Guinasso, 1979).

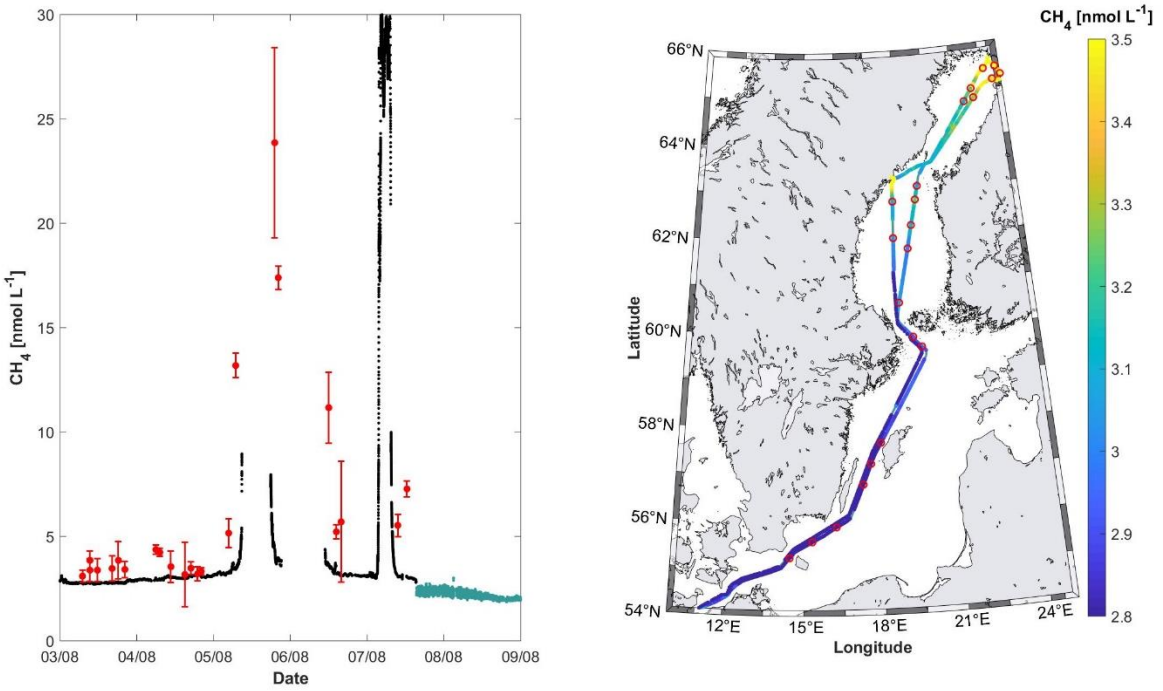

Figure 23: Comparison of continuous (black) and discrete CH_4 measurements including error bars (red) over time (right). During the last part of the cruise the pump did not work appropriately (green). Surface CH_4 concentration along the cruise track and discrete sample locations (left).

The discrete samples estimate higher CH_4 concentrations along the whole cruise track (Figure 23). For the first part of the cruise an averaged difference between discrete and continuous samples of 1.57 nmol L^{-1} was be observed that increased during the cruise. Other measurement campaigns in the open Baltic Sea (e.g. Gülzow et al., 2013) show surface CH_4 concentrations close to atmospheric equilibrium as reflected by the UW measurements (A. Kock, personal communication). Combined with the high consistency in the UW measurements and the high variabilities and errors in the PT measurements it is assumed that the highly consistent UW measurements are more reliable. The comparably large variabilities and errors in the PT measurements support this assumption.

When considering the samples on the 6th of August after the high surface CH_4 concentrations in the northernmost parts, it seems like a drift can be observed. The continuous measurements are back to the baseline quickly, whereas, the discrete samples show much higher values between 5 and 10 nmol L^{-1}. For the last part continuous measurements estimate most likely too low CH_4 concentrations discrete samples suggest even higher CH_4 concentrations than in the beginning of the cruise.

The difference might be caused by divergences related to the sample collection. As the water was not directly sampled from the GO system but from the ferry box system, the comparison of continuous and discrete measurements may be compromised by (I) different water residence times in the two systems, (II) potential accumulation of CH_4 in the "debubbler" of the ferrybox system, an approximately 10 L water tank that is continuously flushed by the system and allows the removal of air bubbles from the water stream, (III) potential CH_4 production in seawater lines of the ferrybox system . A small (approximately 1 %) headspace was always present in the upper part of the of the debubbler and the water passes it before sampling, contamination with atmospheric air is possible.

4.2.2. February 2020

Similar observations were made in the February data. The continuous measurements of CH_4 in the open waters have a higher range in CH_4 concentrations of 3.5 to 4.5 nmol L^{-1}, which reflects the higher solubility of CH_4 in cold winter waters (Figure 24). When comparing the discrete measurements carried out with PT (red) and HS (green) to the continuous measurements (black) in the left panel of Figure 24, large differences between the two discrete measurements and the UW derived CH_4 concentrations are obvious. For most stations, HS measurements show a larger variation coefficient than the PT measurements. It has to be mentioned that triplicates were measured for HS while duplicates were measured for PT. After leaving the extremely high concentrations found in the harbour of Husum, both discrete measurements showed slowly decreasing values between the 26th and 27th of February, while the continuous measurements rapidly decreased to concentrations close to equilibrium with the atmosphere. Except for the last two days of the cruise, PT measurements show lower values, whereas, HS shows much better agreement with the UW data for the last two days. The PT measurements between the 27th and 28th of February were carried out in one measurement day.

No significant correlation between the measurement techniques can be observed (Figure 25). Overall, as for the August 2019 cruise, it is most likely that contamination during the sample collection and treatment led to the higher concentrations. Therefore, it would be good to take the water from the GO system right before it enters the CH_4 analyser and rinse the tubes even longer next time.

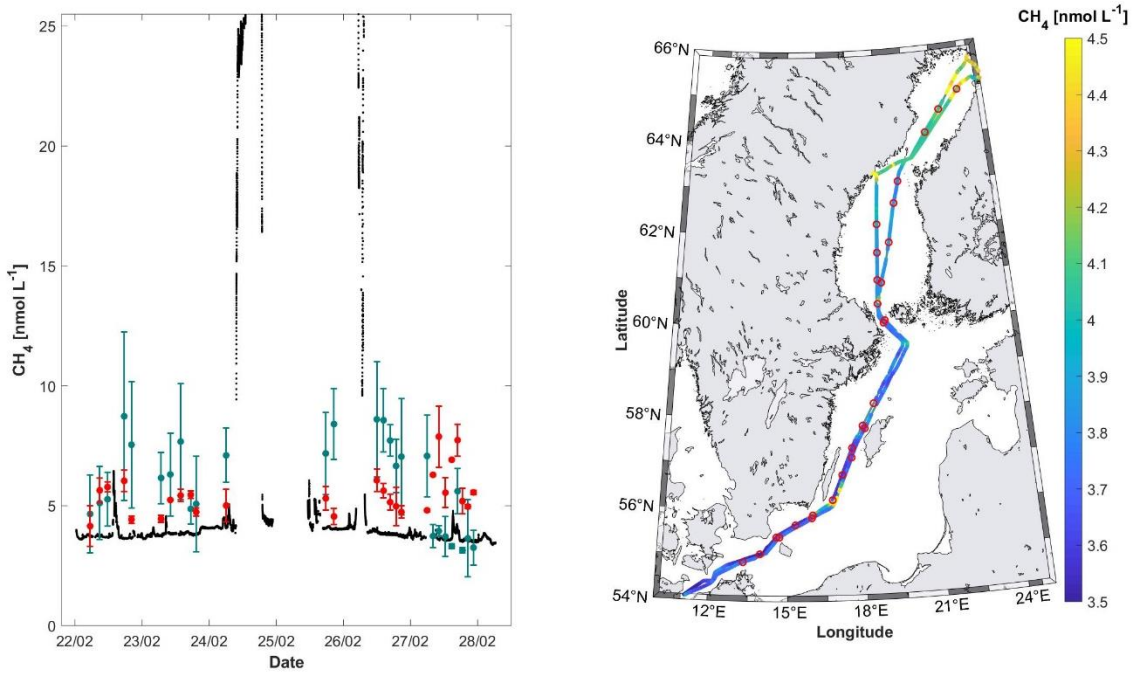

Figure 24: Surface CH_4 concentration along the cruise track and discrete sample locations (left) and comparison of continuous (black) and discrete CH_4 measurements including error bars (red) over time (right). During the last part of the cruise the pump did not work appropriately (green).

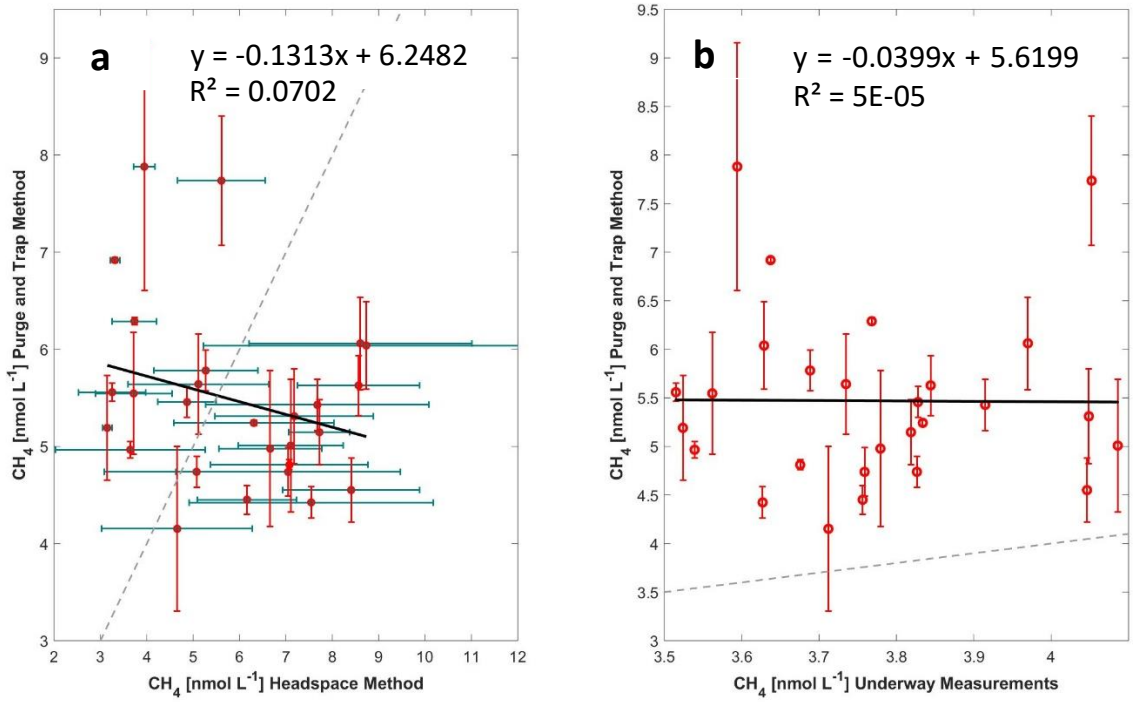

Figure 25: Linear regressions of CH_4 concentrations during 21st to 28th of February 2020 measured with PT against (a) HS and (b) UW. The grey lines indicate the 1-1 relation.

788 Ships of opportunity provide a great monitoring tool for surface water greenhouse gas
789 concentrations and fluxes to the atmosphere, especially when combined with vertical profiling
790 in the respective area (Gülzow et al., 2011; Schneider et al., 2014). Therefore, the comparison

791 measurements should be repeated with a different setup as the Boknis Eck comparison
792 showed a high agreement of PT and HS. Karlson et al. (2016) also observed deviations between
793 ferry box and traditional sampling from research vessels that may be associated with the
794 different sample collection and treatment. However, UW and discrete gaschromatographic
795 measurements have agreed very well in previous studies (e.g. Gülzow et al., 2011).

796 The whole process of sample collection, preservation and storage should be reconsidered to
797 optimize the measurement accuracy according to the potential errors discussed in Section 3.4.
798 An international intercomparison experiment has shown that PT measurements tend to be
799 more accurate for CH_4 measurements and less susceptible for contamination errors (Wilson
800 et al., 2018). This supports the suggestion to repeat the method intercomparison under
801 optimized conditions. Additionally, water samples with a known CH_4 concentration should be
802 used to assure the calibration with the standard gases is working well.

803 ## 4.3. Baltic GasEx Cruises

804 ### 4.3.1. AL 510

805 Due to the multiple overlap of the cruise track (Figure 26) it is difficult to distinguish between
806 temporal and spatial influences on the small-scaled CH_4 distribution and variability. When
807 comparing SSS and SST with position data, topography, and time, the temporal dependence
808 seems to have the strongest impact in these parameters in the surface water. Gradients from
809 shallow coastal to deeper, more open waters seem to be rather negligible, whereas in the
810 same areas high and low values can be found for both parameters at different points of time.
811 Strong temporal variability, short-term as well as long-term, have been observed in other
812 studies as well (Gülzow et al., 2014; Kniebusch et al., 2019). Overall, SSS varied between 9.58
813 and 12.53 g kg^{-1} with a mean of 10.97 g kg^{-1} and SST between 14.4 and 24.4 °C with an average
814 of 18.29 °C. The highest SSS values were recorded in the very beginning of the cruise in the
815 southwestern part of the study area. During the mid-part of the cruise SSS values were lower
816 and increased in the very end of the cruise. Highest SST values were observed during the mid-
817 part of the cruise. In the beginning and end, lower SST values were observed. The co-
818 occurrence of high SSS and low SST can be an indicator for upwelling (Humborg et al., 2019)
819 which can have an impact on other parameters throughout the water column. Moreover, this
820 signal might be linked to an inflow of North Sea water.

When considering salinity, temperature and O_2 in the whole water column along the cruise time, stratification can be observed in the different parameters (Figure 27). A strong salinity gradient from low values in the surface with a minimum of 11.08 g kg^{-1} and high values in the bottom water with a maximum of 19.46 g kg^{-1} can be found. A halocline can be observed between 15 and 20 m depth along the 1013 kg m^{-3} density line which agrees well with former studies in the respective area (e.g. Bange et al., 2010; Dale et al., 2011; Lennartz et al., 2014; Ma et al., 2019, 2020).

Some of the highest temperatures were measured in the surface water with a maximum of 20.11 °C, which is very high for this respective area (Lennartz et al., 2014). In contrast, lowest values were found in the bottom water with a minimum of 5.97 °C. The strongest gradient was found between 10 and 15 m depth changing by approximately 10 °C between the 1009 kg m^{-3} to the 1010 kg m^{-3} density lines. Over the whole cruise, the vertical extension of this boundary layer depth had a maximum of approximately 6 m in the beginning of the cruise and decreased to just about 2 m towards the end as the surface temperature increased especially on the 10th and 11th of June and the mixed layer extended further down.

Highest O_2 concentrations of up to 363.70 µmol L^{-1} were measured between approximately 7 m and 18 m depth and between the 1009 and the 1012 kg m^{-3} density lines. In the beginning this O_2 maximum had the greatest vertical extension of more than 10 m which decreased continuously in its thickness and intensity until it vanished after the 15th of June. Lowest O_2 values were found in the bottom water with a minimum of 127.44 µmol L^{-1}. As such, the whole water column was oxygenated throughout the whole cruise. In this time of the year, the oxygen depletion in the deep water starts to evolve in the respective area (Lennartz et al., 2014). In combination with the change in salinity this indicates an advection of other water masses that may be induced by the inflow of North Sea water.

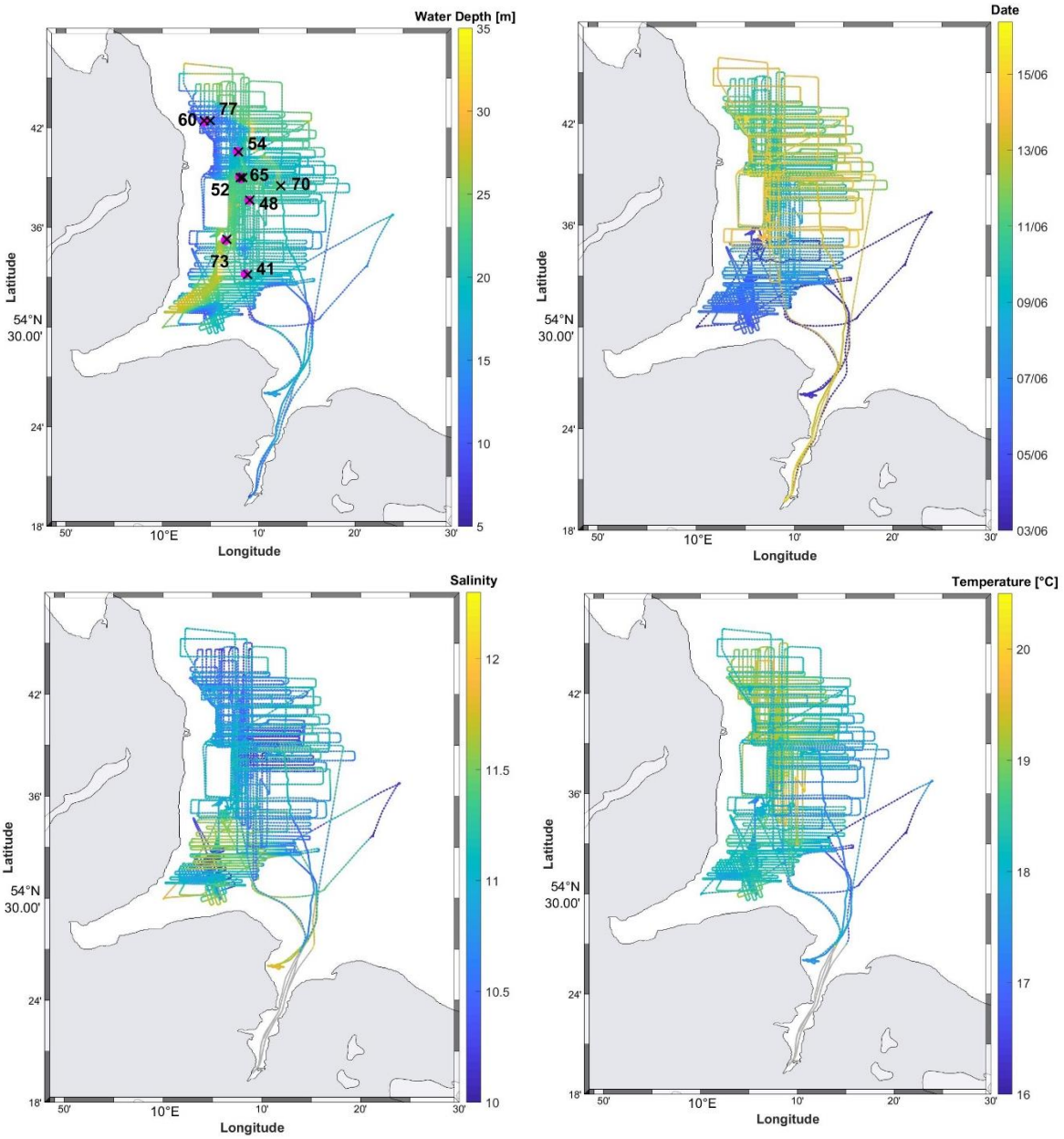

Figure 26: Water depth and CH_4 CTD stations (black crosses and numbers) and dinghy sample sites (pink dots) (a), chronology (b), SSS (c) and SST (d) along the cruise track.

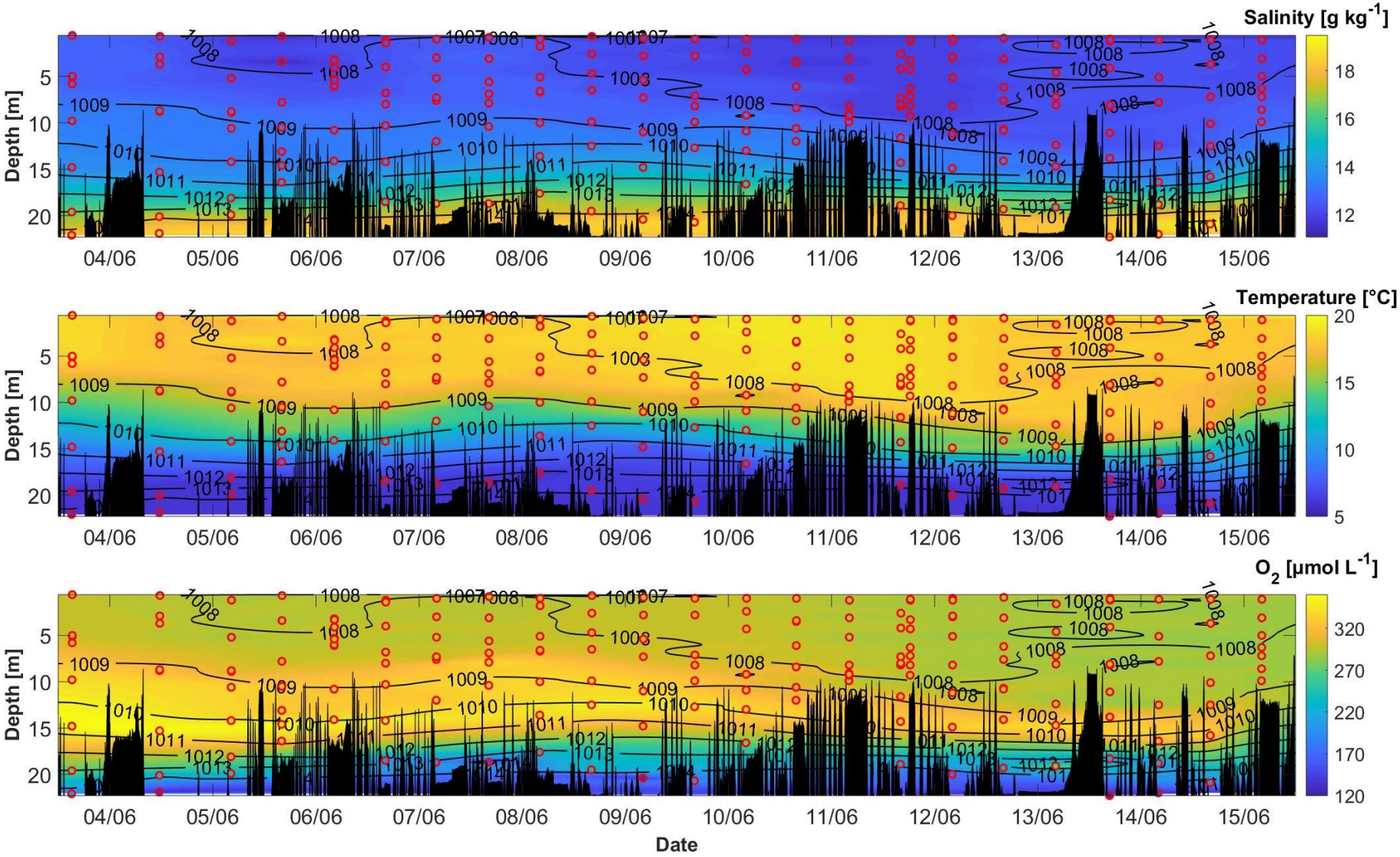

Figure 27: Contour plots of salinity (upper panel), temperature (middle panel), and O_2 (lower panel) during AL 510. Red circles mark a scatter plot of the discrete measurements. Black peaks show the topography along the cruise track.

The water column CH_4 distribution along the cruise track ranges from 2.76 nmol L^{-1} in the surface waters to 28.27 nmol L^{-1} in the bottom waters (Figure 28). Outliers did exist, for example at stations 41 and 52, where the CH_4 concentrations were higher in the mid-layer depth than in the bottom water. This could potentially be caused by lateral water dynamics since station 41 is the southernmost CH_4 station and located at the mouth of the Eckernförde Bay while station 52 is located close to the Schlei estuary (Figure 26). In contrast, station 65 is almost at the same location as station 52 and does not show this inversed trend three days later. Another possible explanation for the high CH_4 concentrations in the mid-layer depth could be high abundances of zooplankton which were shown to be involved in direct and indirect CH_4 production lately (Schmale et al., 2018; Stawiarski et al., 2019). Primary production could also explain this phenomenon as Klintzsch et al. (2019) found that also widespread marine phytoplankton species mediate CH_4 contributing to CH_4 oversaturation in well-oxygenated surface waters. A combination of primary and secondary production is most likely as Klintzsch et al. (2019) and Schmale et al. (2018) both found that neither primary nor secondary production was the sole source of the high CH_4 concentrations observed in oxygen rich waters. Moreover, it has recently been shown that cyanobacterial blooms might involve CH_4 generation (Bižić et al., 2020; Yan et al., 2019).

It appears that the temporal variability plays a more important role for this data set than the spatial variability. The importance of temporal variability is especially apparent at stations 52 and 65 as well as 60 and 77 (Figure 29) which were in close proximity to one another (Figure 26) but sampled at different days. The mid-layer O_2 maximum was much stronger in the earlier part of the cruise (stations 52 and 60) and less pronounced in the later stations (65 and 77).

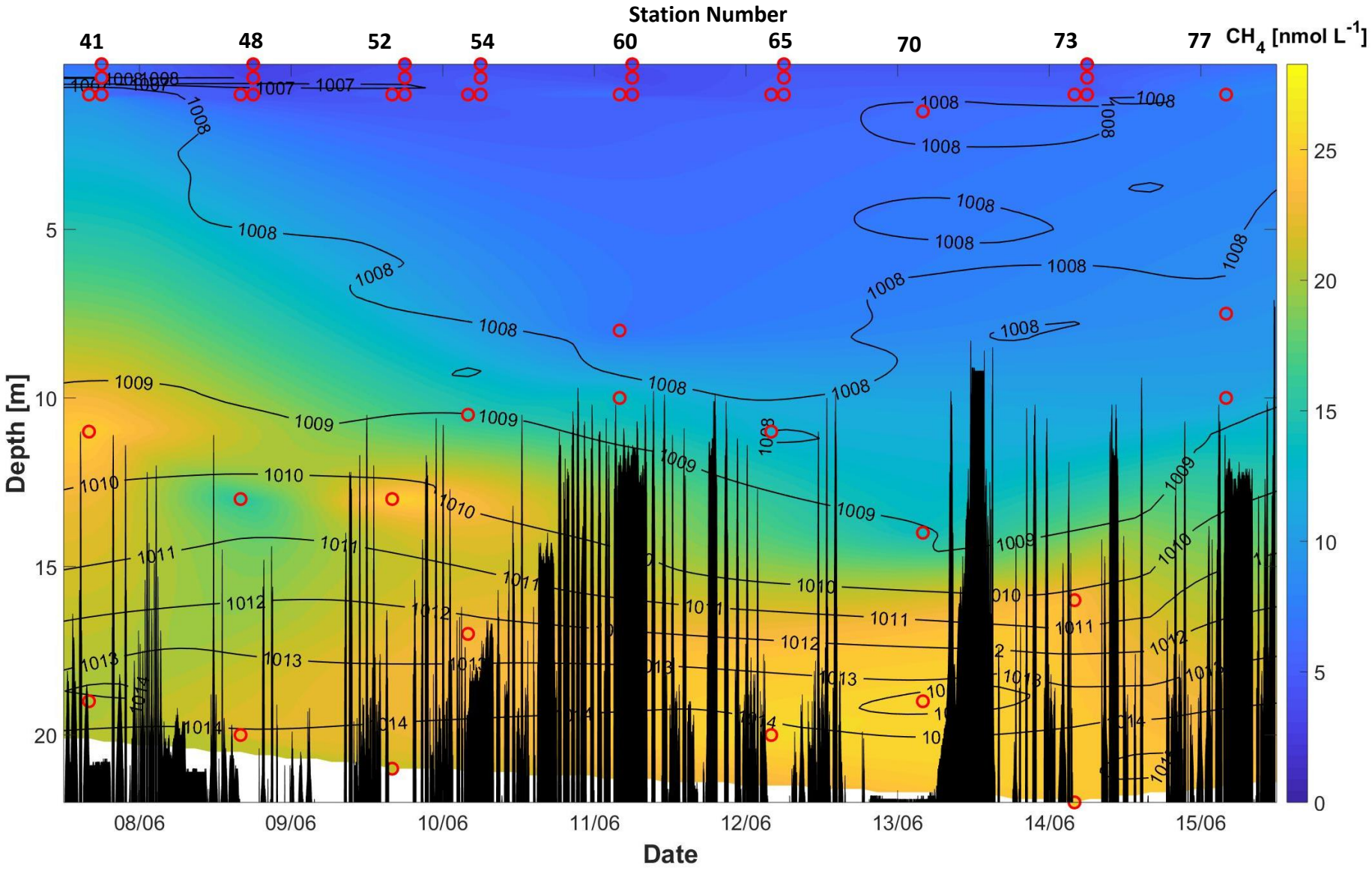

Figure 28: Contour plot of CH_4 during AL 510. Red circles mark a scatter plot of the discrete measurements. Black peaks show the topography along the cruise track.

At station 52, the O_2 maximum co-occurred with a strong CH_4 maximum that was at 25.46 nmol L^{-1} among the highest concentrations that were measured during this cruise. The highest mean concentration was found at station 65 in the depth of 20 m. At station 60, the vertical O_2 distribution was very constant throughout the water column with a small increase in the depth of approximately 9 m. Being constant in the mixed layer, the CH_4 concentration also showed a strong increase in the mid-layer depth coinciding with the high O_2 concentration. At stations 48 and 54, the CH_4 distribution showed a linear trend from the surface to the bottom water. At station 48, the surface water had a concentration of 5.21 nmol L^{-1} and the bottom waters had a more than four-fold higher concentration at 22.21 nmol L^{-1}. It must be taken into consideration that the CH_4 profiles are derived from three observation points only while O_2 was measured at seven depths which leads to a higher resolution for O_2.

Compared to O_2, the variability of CH_4 concentrations was higher for the surface and intermediate water depths (Figure 31). Surface CH_4 varied from 2.76 nmol L^{-1} to 10.29 nmol L^{-1}. In the mid-layer depth, intermediate CH_4 values were found ranging from 6.36 nmol L^{-1} to 25.81 nmol L^{-1}. The variability of O_2 increases in this depth ranging from 283.87 µmol L^{-1} to 363.70 µmol L^{-1} representing approximately a third of the scale. While the variability of CH_4 concentrations in the surface is comparably as low as in the bottom water, highest variabilities for O_2 are found in this depth ranging from 127.44 µmol L^{-1} to 329.89 µmol L^{-1}. The CH_4 concentrations reported in the scope of this study support the hypothesis that aerobic methane generation may occurred between 10 and 20 m, possibly due to biological activity, which can result in a co-occurrence of high O_2 and high CH_4 concentrations (Bižić et al., 2020; Emerson et al., 2008; Günthel et al., 2019; Klintzsch et al., 2019; Schmale et al., 2018; Stawiarski et al., 2019).

Salinity increased throughout the water column, whereas, temperature followed the reverse trend (Figure 30). Salinities ranged from 11.08 g kg^{-1} at the surface to 19.46 g kg^{-1} at depth. In contrast, highest temperatures of 20.11 °C were measured in the surface decreasing towards the bottom water at 5.97 °C. Strongest gradients in the two parameters appear around the depth of 15 m (Figure 32) which is in good agreement with the CH_4 and O_2 data showing that a change in the characteristics of the water masses occurs in this depth (Lennartz et al., 2014).

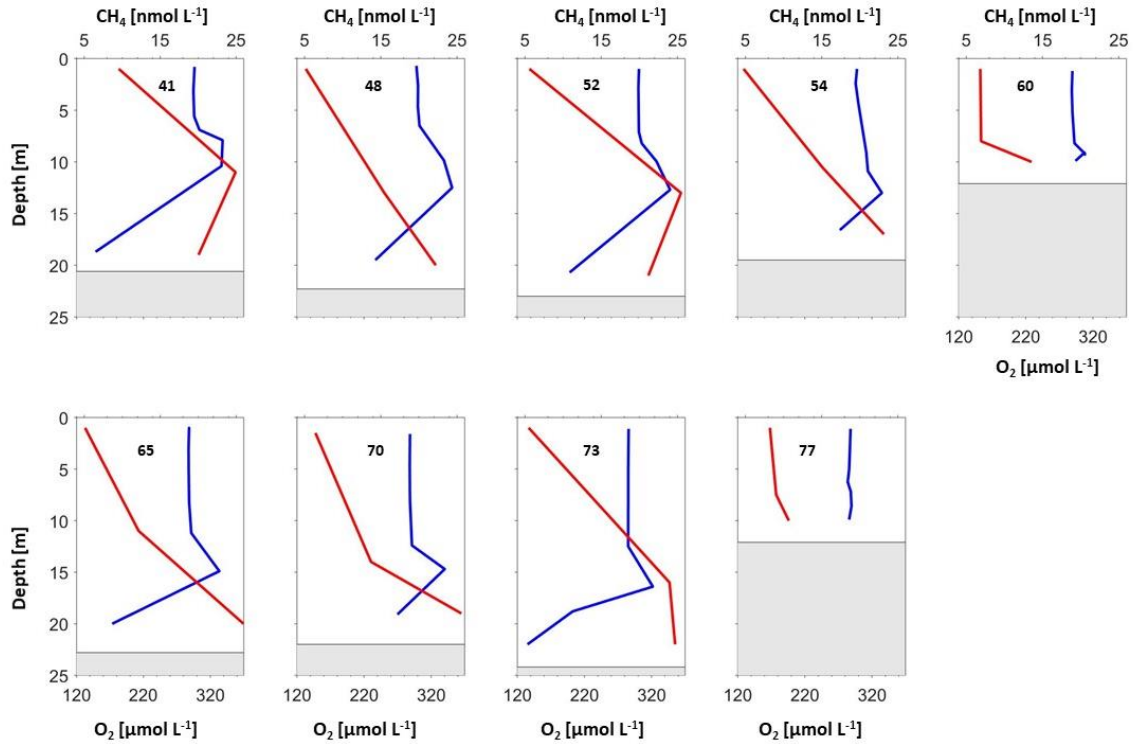

Figure 29: Profiles of CH_4 (red) and O_2 (blue) during AL 510. The bottom water depth at each station is indicated by the grey area.

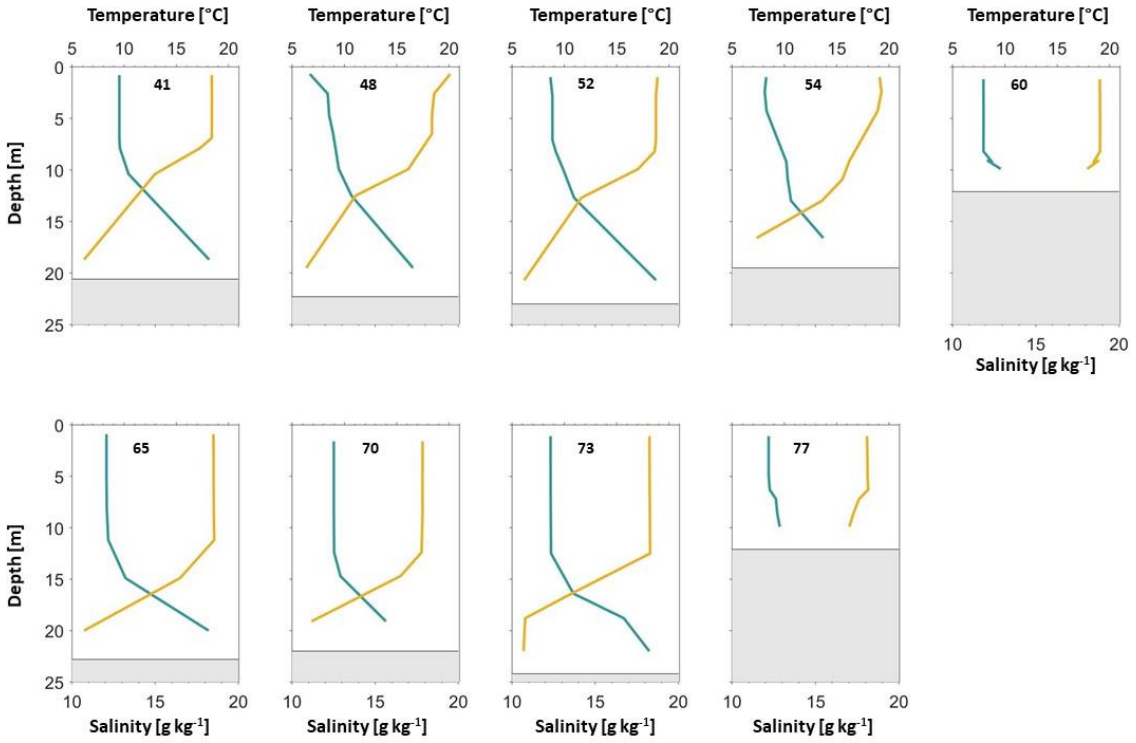

Figure 30: Profiles of Temperature (orange) and Salinity (green) during AL 510. The bottom water depth at each station is indicated by the grey area.

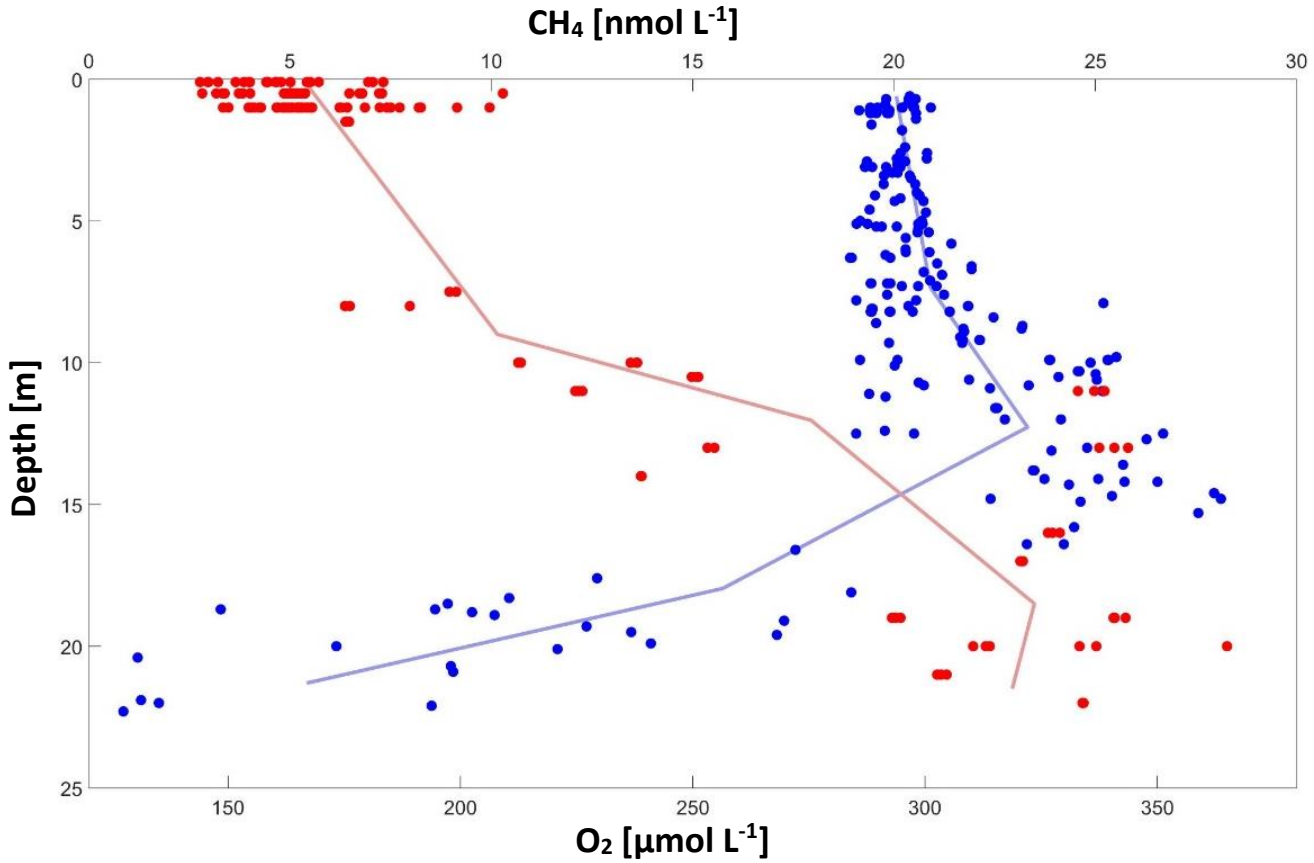

Figure 31: Mean profiles of CH_4 (red) and O_2 (blue) during AL 510 are displayed as lines. All discrete measurements are shown as dots.

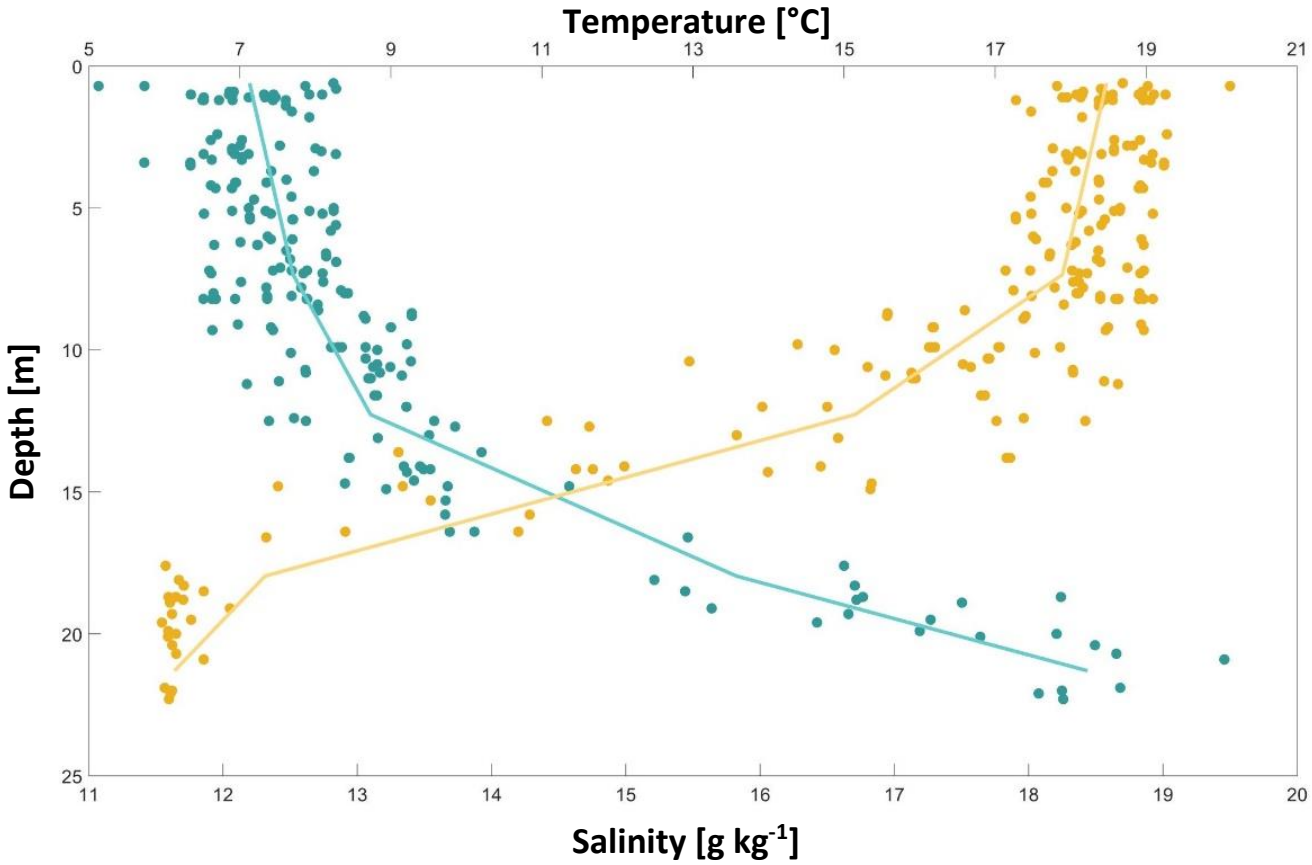

Figure 32: Mean profiles of temperature (orange) and salinity (green) during AL 510 are displayed as lines. All discrete measurements are shown as dots.

Surface CH_4

When considering the surface CH_4 concentration that was measured from the samples collected from a dinghy, small gradients can be observed (Figure 33). In most stations, highest values are found in the depth of 1 m while lowest values are most likely to be found in the depth of 0.1 m.

Surface CH_4 concentrations were highest in the first and last dinghy sample collections of the cruise (Figure 33) coinciding with the upwelling signal observed in SSS and SST (Figure 26). According to Humborg et al. (2019), coastal upwelling is an important driver for enhanced CH_4 emissions from the Baltic Sea. This is caused by the circumstance that CH_4-enriched bottom water is brought to the surface (Schneider et al., 2014). Very low surface concentration in all three depths were found on the following day (June 8th).

In some samplings, very high variation among the triplicates of up to 4 nmol L^{-1} were observed. This might reflect the challenging sampling conditions in the dinghy, making these samples more susceptible to contamination with air. Moreover, this can indicate very high surface variability due to wind or turbulence related to the dinghy.

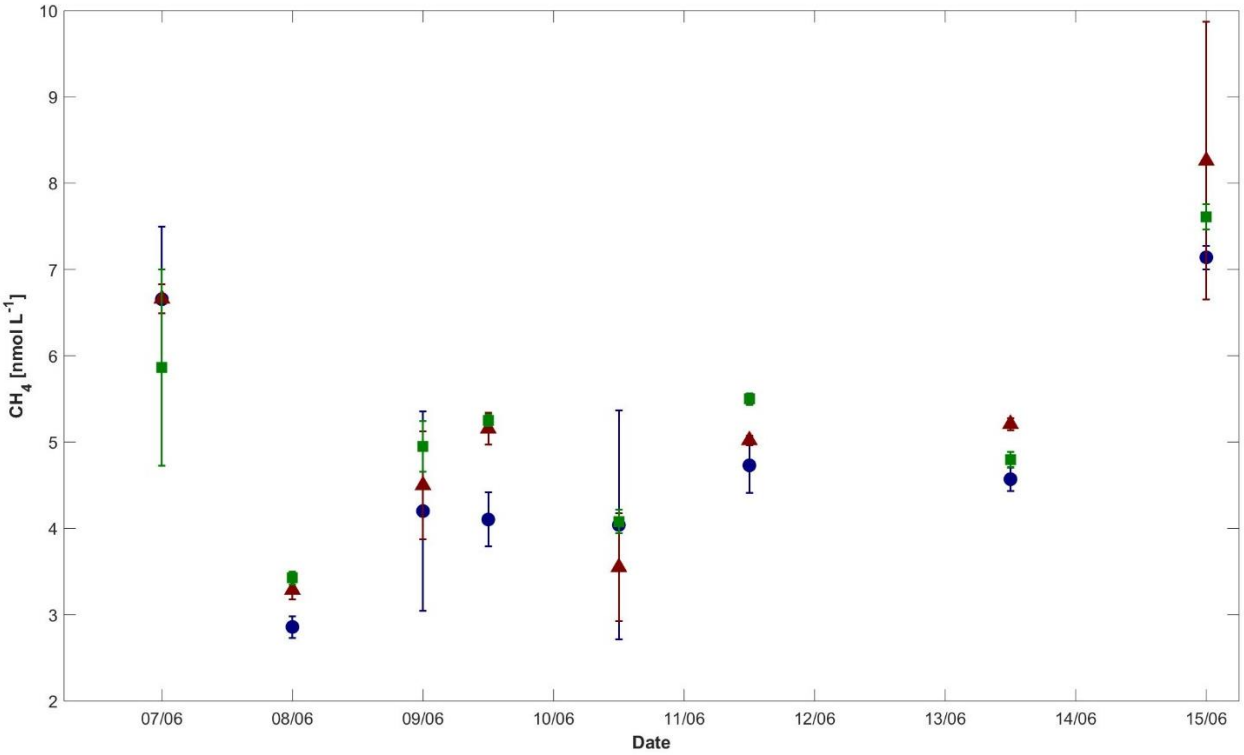

Figure 33: Changes in surface concentration of CH_4 over the cruise time derived from the dinghy samples during AL 510 differentiated for 0.1 m depth (blue dots), 0.5 m depth (red triangles), and 1 m depth (green squares). Error bars are displayed in the according colours.

4.3.2. AL 516

Similar to AL 510, temporal aspects seem to have the strongest impact on SSS and SST variability, while spatial impacts and topography seem to be of minor relevance (Figure 34). SSS showed much higher values and variability compared to the observations in June, ranging from 14.91 to 20.52 g kg^{-1} averaging at 17.82 g kg^{-1}, whereas SST values were more constant throughout the cruise ranging from 15.90 to 18.00 °C with a mean of 17.17 °C. In the beginning of the cruise, highest SST values co-occurred with lowest SSS values. In contrast, lowest SST and highest SSS values were measured in the end of the cruise. The co-occurrence of highest SSS and lowest SST can point out an upwelling event (Humborg et al., 2019) on the 21st of September.

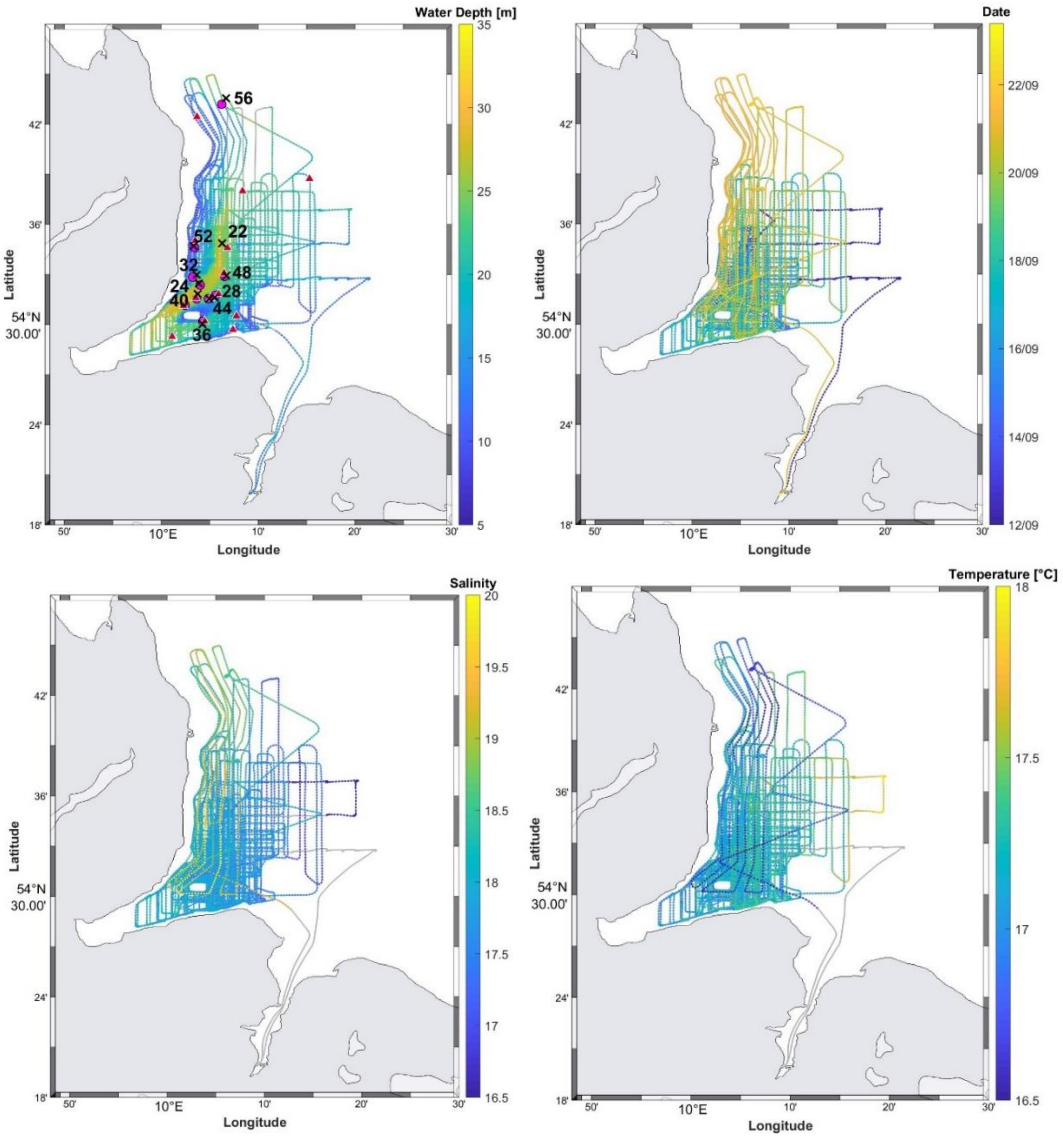

Figure 34: Water depth and CH_4 CTD stations (black crosses and numbers), dinghy sample sites (pink dots), and UW measurement locations (red triangles) (a), chronology (b), SSS (c) and SST (d) along the cruise track of AL 516.

In the beginning of the cruise, a stronger stratification can be observed in salinity, temperature and O_2 that is decreasing and moving further upward towards the end of the cruise, which is especially visible in the 1013 to 1016 kg m^{-3} density lines (Figure 35) indicating upwelling. Within the water column lowest salinities down to 15.90 g kg^{-1} are found in the surface water above the 1013 kg m^{-3} density line which varies in depth between 0 and 12 m. The density lines of 1014, 1015, and 1016 kg m^{-3} are located close to each other, reflecting the strongest density gradients in 15 to 20 m. The water in-between these lines is characterized by intermediate salinities. Highest salinities up to 24.23 g kg^{-1} were measured in the bottom water.

Bottom water salinity maxima are lower in the beginning than in the end of the cruise and the high values extend further upward into the water column throughout the cruise in agreement with the upshift of the density line of 1016 kg m^{-3} (Figure 35). This signal could be related to an inflow of saline North Sea water.

A similar stratification throughout the cruise can be observed in the temperature data. The surface water shows a homogeneous distribution of about 17 °C downward to the 1014 kg m^{-3} density line in the depth of approximately 15 m. Below that, a smooth gradient agreeing well with the density lines can be observed. The temperature decreases to lowest values of 12 °C in the bottom water. The inversions that are displayed between the 15th and 16th of September are likely to be artefacts produced through the interpolation.

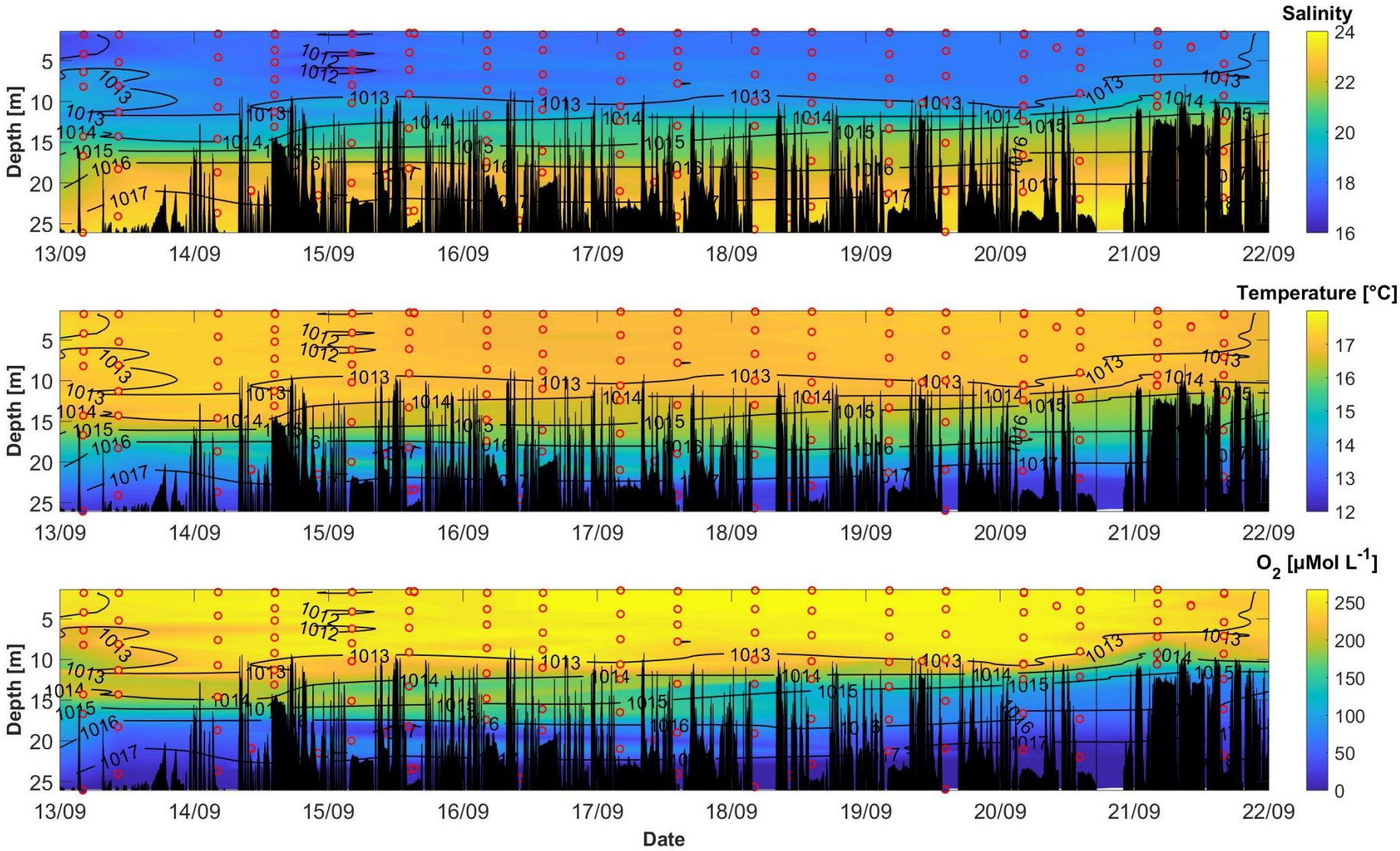

Figure 35: Contour plots of salinity (upper panel), temperature (middle panel), and O_2 (lower panel) during AL 516. Red circles mark a scatter plot of the discrete measurements. Black peaks show the topography along the cruise track.

During the whole cruise, highest O_2 concentrations of up to 267.50 µmol L^{-1} were measured in the surface water above the 1013 kg m^{-3} density line. Between the 1014 and 1015 kg m^{-3} density lines a strong oxycline could be observed as O_2 decreased by approximately 100 µmol L^{-1} within a few meters. With increasing depth, the O_2 concentration decreased to suboxic (O_2 < 5 µmol L^{-1} (Deutsch et al., 2011)) and almost anoxic (O_2 = 0 µmol L^{-1} (Bange, 2008)) conditions in the bottom water where O_2 went down to 0.59 µmol L^{-1}. The oxygen sensors were calibrated against Winkler measurements (Winkler, 1888) which might not be sensitive enough to distinguish suboxic from anoxic conditions as indicated from highly sensitive STOX (Switchable Trace amount Oxygen) sensors for oxygen measurements (Thamdrup et al., 2012). An indicator for anoxia is the occurrence of hydrogen sulphide (H_2S). However, during AL 516 no sulfidic conditions could be observed (D. Booge, personal communication). Along with the upward shifting density lines, hypoxia (O_2 < 60 µmol L^{-1} (Liss and Johnson, 2014)) characterized almost half of the water column in the end of the cruise. Intense hypoxic and even anoxic conditions in the bottom water of Boknis Eck are common between late summer and autumn (e.g. Bange et al., 2010; Dale et al., 2011; Lennartz et al., 2014; Ma et al., 2019, 2020). With the 1013 kg m^{-3} density line reaching the water surface, the lowest surface O_2 concentration of 233.49 µmol L^{-1} was measured, which is another indication for upwelling that occurred on the 21st of September.

The distribution of the three parameters helps to identify the different water masses. The surface water and mixed layer covers the upper part of the water column until the 1014 kg m^{-3} density line. The boundary layer is characterized by strong gradients and lies between the 1014 and 1016 kg m^{-3} density lines. Below that, the bottom water is found.

A contour plot of the CH_4 concentration during AL 516 over depth and time is shown in Figure 36. Red circles mark the observations on which the nearest neighbour interpolation is based. Due to the limited number of measurements, this plot is only used to get a general overview. It can be observed that lowest concentrations were measured in the surface water, intermediate values were found in the boundary layer, and highest values occurred in the bottom water. The rather intermediate values that are displayed in the bottom water after the 18th of September are not based on observations and should therefore not be trusted.

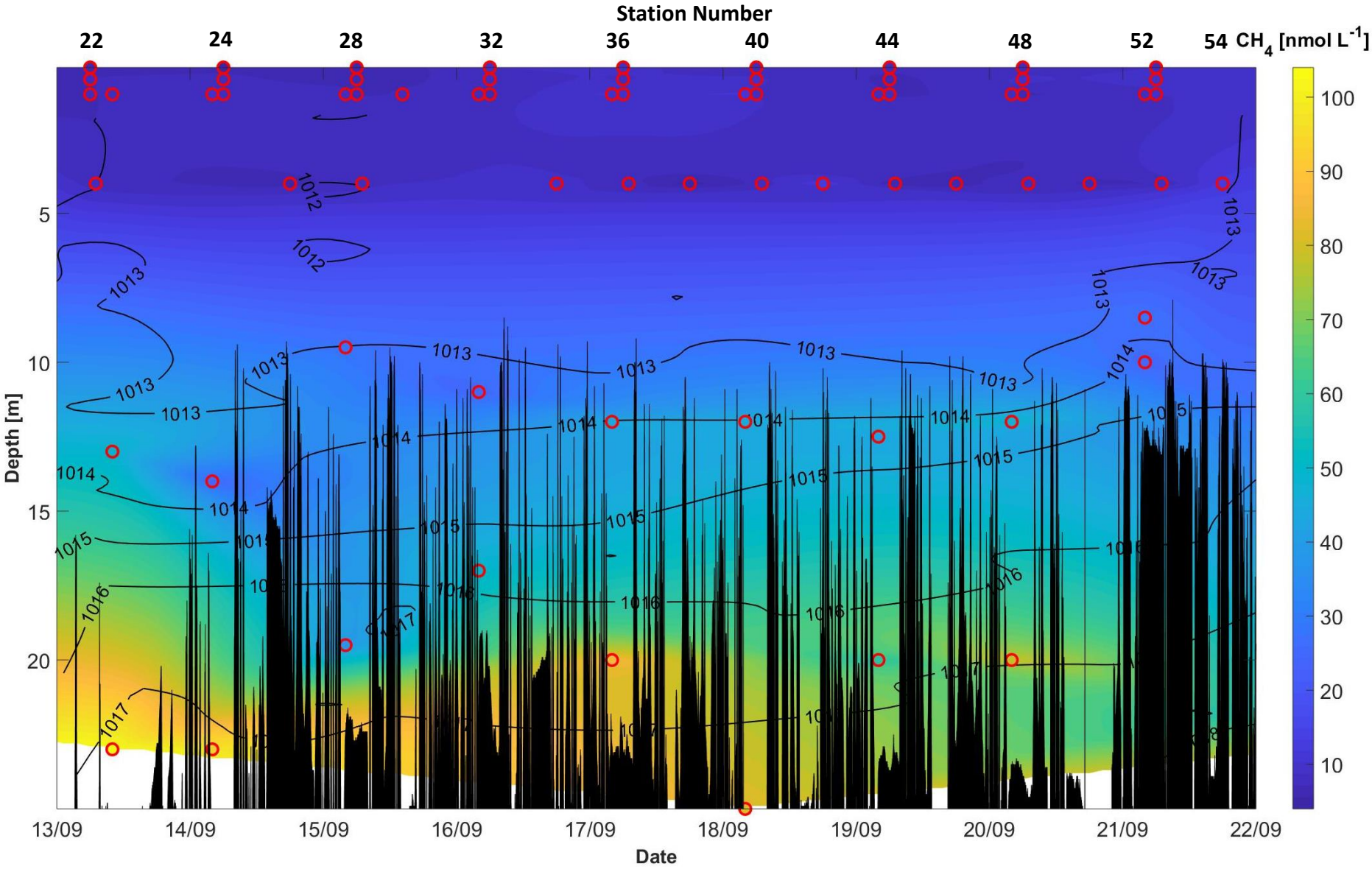

Figure 36: Contour plot of CH_4 during AL 516. Red circles mark a scatter plot of the discrete measurements. Black peaks show the topography along the cruise track.

CH_4 concentrations ranged from 4.72 nmol L^{-1} in the surface to 103.97 nmol L^{-1}in the bottom waters. The rather intermediate values that are displayed in the bottom water after September 18th are not based on observations and should therefore not be trusted. The strong agreement of the parameter distribution and density lines that was observed for salinity, temperature, and O_2 is less prominent in the CH_4 distribution. The strong agreement of the parameter distribution and density lines that was observed for salinity, temperature, and O_2 is less prominent in the CH_4 distribution.

At most stations, O_2 concentrations decreased while CH_4 concentrations increased with depth (Figure 37). However, at the shallowest station 52, O_2 slightly increased while CH_4 slightly decreased in the bottom water. At station 28 an O_2 maximum at approximately 7 m depth can be observed. At six out of ten stations (stations: 22, 24, 40, 44, 48, 56) hypoxic or suboxic conditions in the bottom water occurred. At these stations bottom, water CH_4 concentrations exceeded 50 nmol L^{-1}. It is commonly observed that the combination of low O_2 concentrations and high organic matter sedimentation rates leads to enhanced microbial CH_4 production in the sediments (Bange et al., 2010). The CH_4 rich sediments in the southwestern Baltic Sea are known to be an important source of CH_4 to the water column (e.g. Bange et al., 1998; Ma et al., 2020; Maltby et al., 2017). Reindl and Bolałek (2014) found that CH_4 fluxes of up to almost 50 mmol m^{-2} d^{-1} from the sediments into the water column occurred during warm periods. Another study in the south western Baltic Sea linked high CH_4 fluxes (30 mmol m^{-2} d^{-1}) to the water column to groundwater seepages (Donis et al., 2017) which are present in Eckernförde Bay, too (Bussmann and Suess, 1998). However, the high salinities and the rather homogeneous CH_4 distribution in the bottom water of this study does not support the assumption of a large contribution of groundwater seepage to the CH_4 distribution (compare Figures 37 & 38). The Eckernförde Bay area is known for free CH_4 content in the sediments which can lead to high concentrations in the bottom water varying dependent on production, consumption and accumulation processes (Abegg and Anderson, 1997).

Different processes can drive marine CH_4 emissions to the atmosphere in the respective area including vertical gas transport of dissolved CH_4. However, diapycnal mixing of the water is strongly reduced under density stratified conditions (Gülzow et al., 2013). Another important process might be ebullition. Here, CH_4 bubbles dissolve easily in the water column but due to the shallow conditions in the study area they can reach the mixed layer and can lead to

extreme fluxes to the atmosphere under certain weather conditions (Lohrberg et al., 2020). As mentioned before, upwelling can also lead to increased CH_4 fluxes to the atmosphere as CH_4 enriched bottom water may be brought to the surface (Humborg et al., 2019). Another very important process in the Kiel Bay area is water column intermixing. With the onset of autumn and winter storms the stratification breaks and CH_4 fluxes from the sediments may reach the water (Ma et al., 2020).

At Landsort Deep, Thureborn et al. (2016) have shown that methanogens and methane oxidizers co-occur in the anoxic sediments. However, with increasing sediment accumulation and anoxic conditions, the slow-growing methanotrophs fail in building up enough biomass to consume the CH_4 efficiently which can lead to enhanced CH_4 accumulation in the water column (Egger et al., 2016). The CH_4 supply at the redox zone influences the activity of the CH_4 oxidizing community (Jakobs et al., 2014). Sedimentary methanogenesis is a well-known and important source of high CH_4 concentrations to the water column and can lead to high fluxes to the atmosphere in eutrophicated ecosystems (Myllykangas et al., 2020). Anaerobic CH_4 oxidation rates have been shown to increase at higher CH_4 concentrations (Bowles et al., 2019), while it has been shown that highest aerobic CH_4 oxidation rates occur at Boknis Eck under micromolar O_2 concentrations (Steinle et al., 2017). The mean profiles show that throughout the AL 516 cruise O_2 and temperature decrease from surface to bottom while CH_4 and salinity increase with depth. For all parameters strong gradients can be observed associated with the boundary layer (Figures 39 & 40).

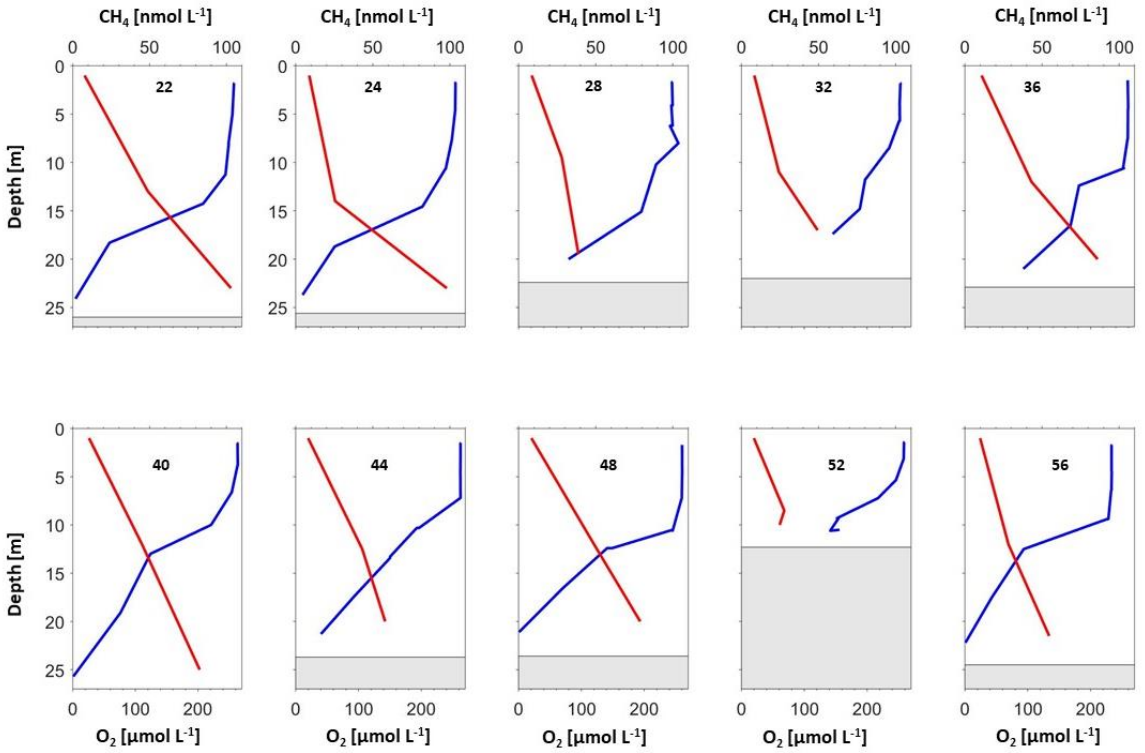

Figure 37: Profiles of CH_4 (red) and O_2 (blue) during AL 516. The bottom water depth at each station is indicated by the grey area.

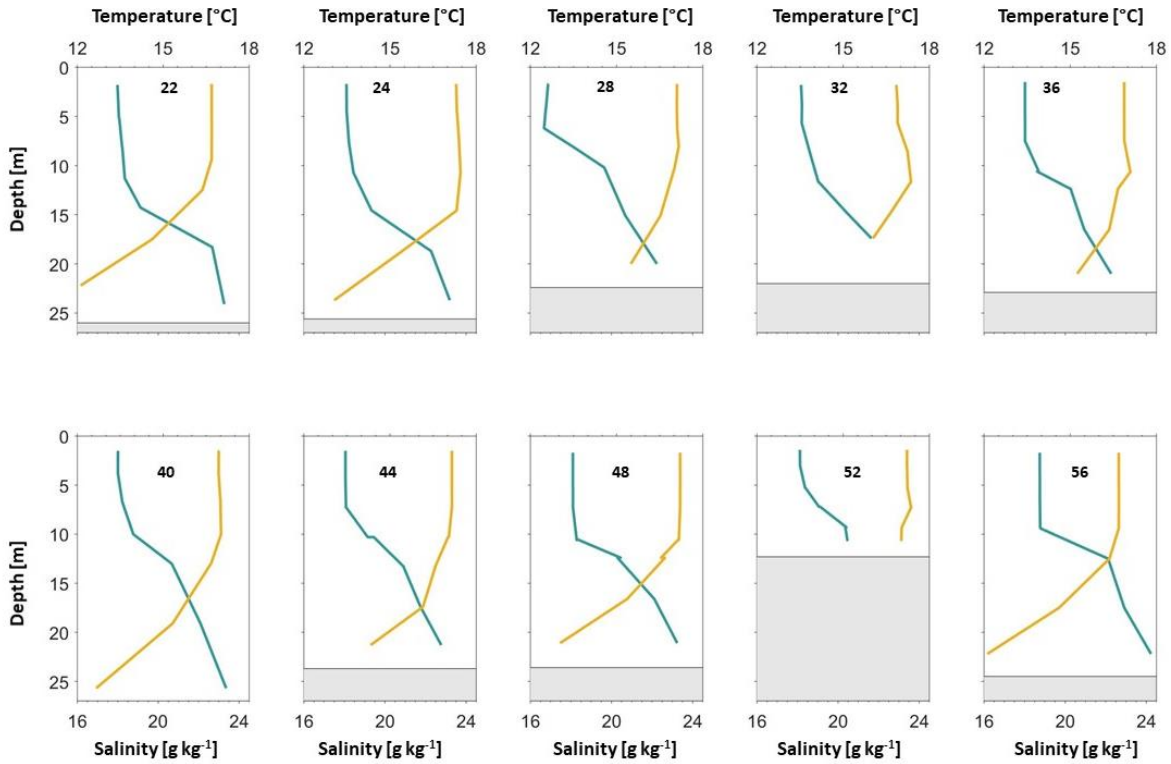

Figure 38: Profiles of Temperature (orange) and Salinity (green) during AL 516. The bottom water depth at each station is indicated by the grey area.

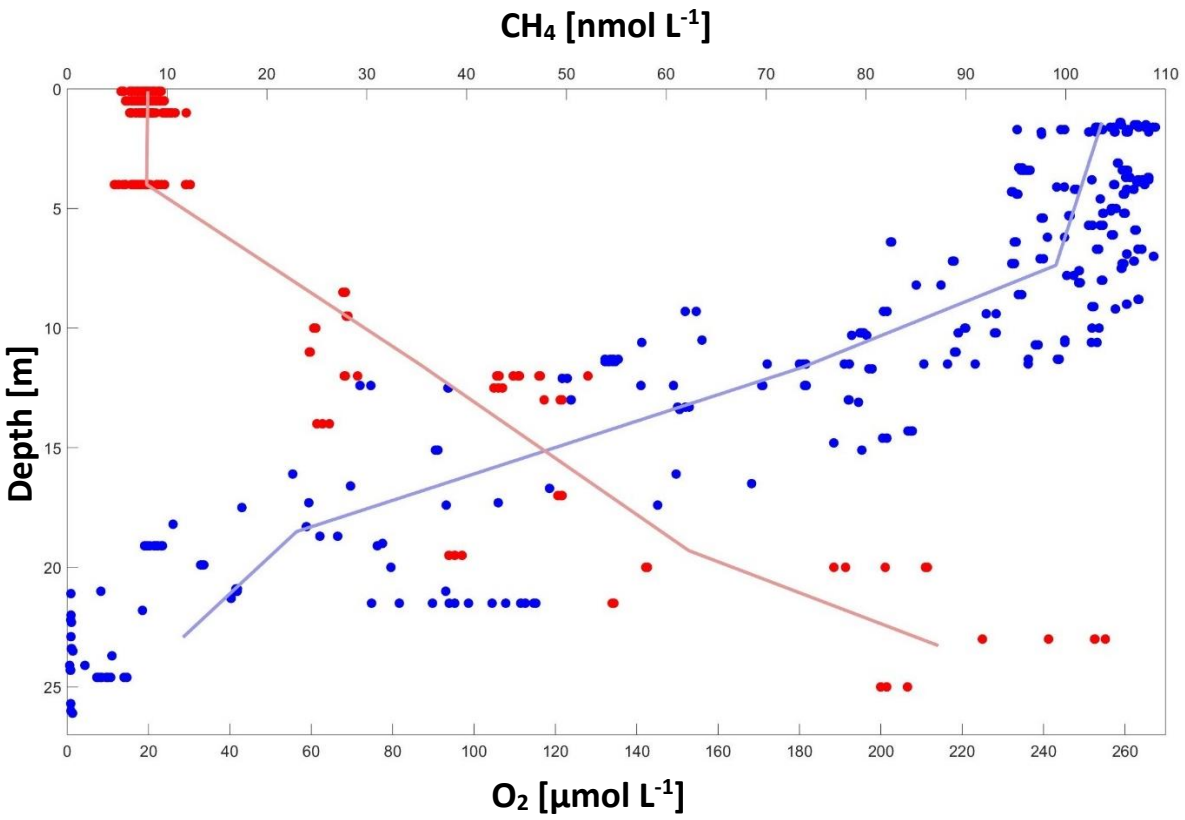

Figure 39: Mean profiles of CH4 (red) and O2 (blue) during AL 516 are displayed as lines. All discrete measurements are shown as dots.

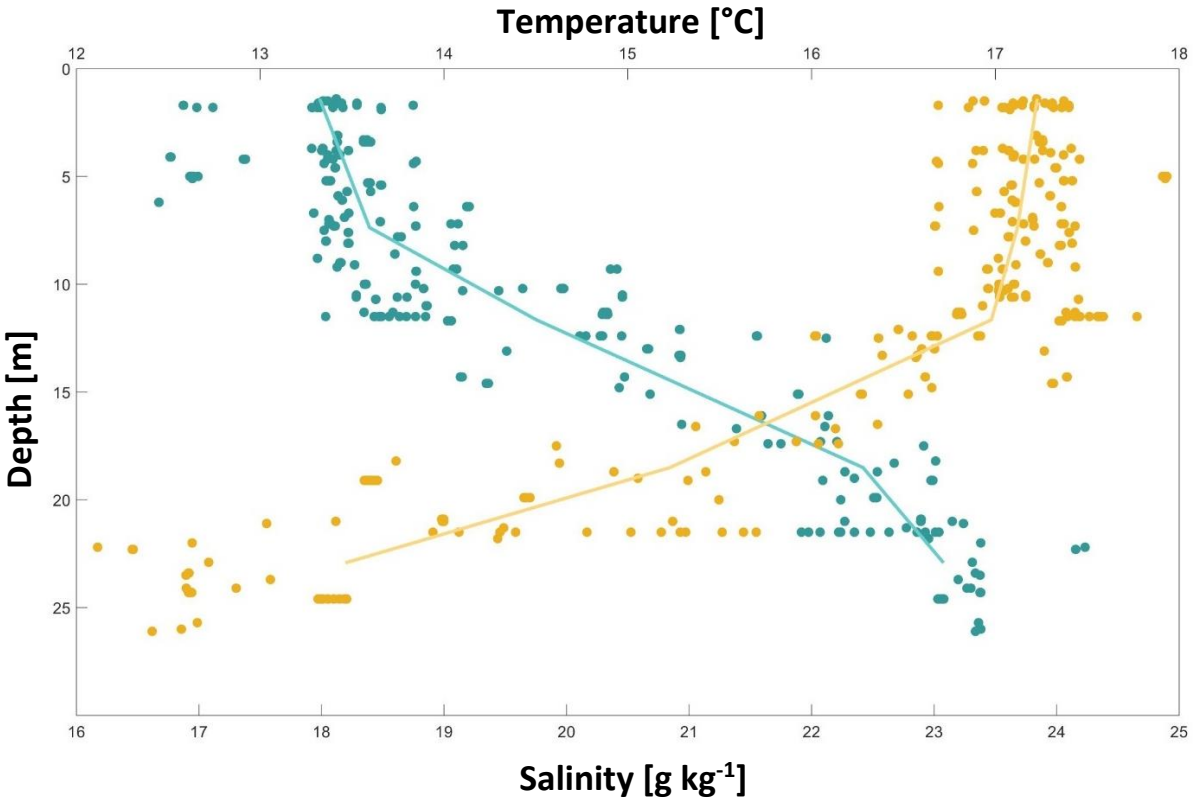

Figure 40: Mean profiles of temperature (orange) and salinity (green) during AL 516 are displayed as lines. All discrete measurements are shown as dots.

Surface CH_4

The surface CH_4 concentration ranged from 5.39 to 11.92 nmol L^{-1} (Figure 41) which is in a similar range to what was measured during AL 510 (Figure 33). No constant gradient within the upper 1 m of the water column was observed. On half of the samplings the intermediate depth of 0.5 m (red triangles) showed the highest concentration. At three stations highest values were observed in the shallowest depth of 0.1 m. Higher concentrations in the shallower surface waters could either indicate local production processes or limitation of CH_4 oxidation processes. A possible explanation would be a local CH_4 production in the surface microlayer in the respective depth. Especially the high values on June 18th and 20th support this hypothesis. Moreover, in September 2018 some smaller phytoplankton blooms were found in the southwestern Baltic Sea. The chlorophyll a maximum observed at Heiligendamm coincides with the respective date range (Wasmund et al., 2019). This could indicate local CH_4 production related to phytoplankton (Capelle et al., 2019; Klintzsch et al., 2019). Only at two stations highest surface CH_4 concentrations were measured at the depth of 1 m. Mean values range between 7.65 and 10.77 nmol L^{-1} co-occurring with a high variability in the errors that range between 0.04 and 0.95 nmol L^{-1} (0.59 and 12.83 %), respectively. The lowest value was measured in the depth of 0.10 m on the 15th when all three depths show the lowest mean values of the whole cruise. The highest concentration was measured on the 17th in the depth of 1 m. The consideration of this data implies that it is difficult to deduce how well the monthly measurements of one surface depth can represent the small-scale variability in this area and season. High small-scaled temporal variations ranging by up to more than 5 nmol L^{-1} within the June cruise (compare 8th and 15th of June in Figure 33) imply that a higher temporal resolution would be more reliable than one data point per month. It is moreover difficult to distinguish whether the high variations in errors result from the measurement technique or from the sampling.

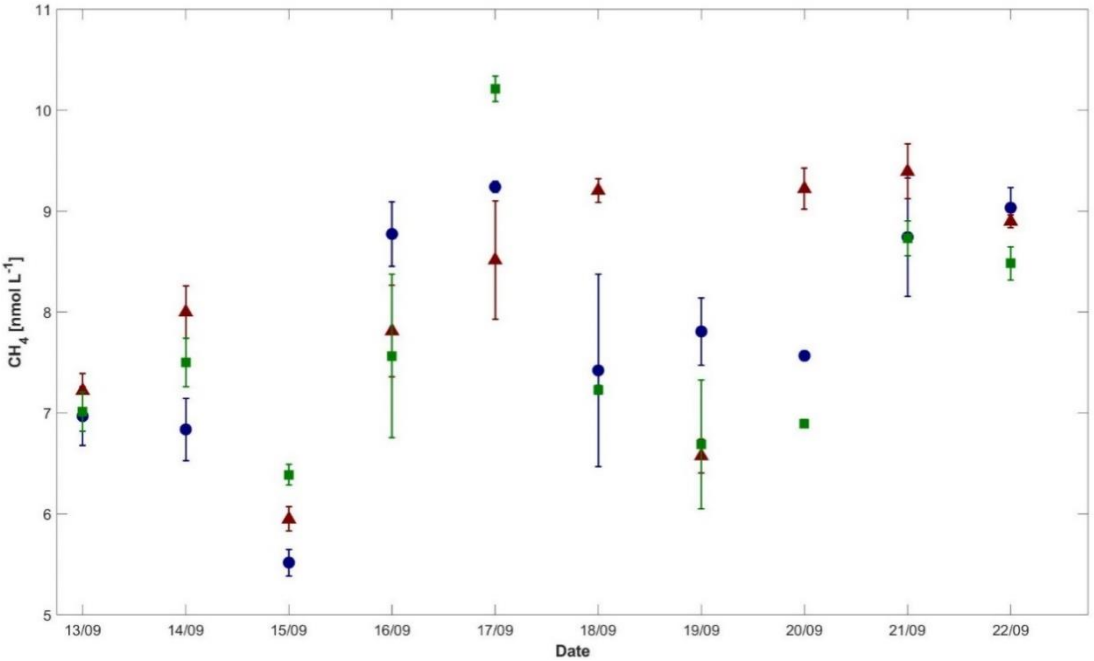

Figure 41: Changes in surface concentration of CH_4 over the cruise time derived from the dinghy samples during AL 516 differentiated for 0.1 m depth (blue dots), 0.5 m depth (red triangles), and 1 m depth (green squares). Error bars are displayed in the according colours.

4.3.3. Seasonal Intercomparison of the Two Cruises

The water masses changed from June to September which can be interpreted based on the relationship of temperature and salinity (Figure 42). Seawater density was calculated using the Gibbs Sea Water toolbox in Matlab (McDougall and Barker, 2011). In June, the surface water had a very low surface salinity at all stations raging between 11.07 and 12.84 kg^{-1} while a large gradient ranging from 11.85 to 18.24 g kg^{-1} characterized the mid-water depths. In the bottom water salinities between 17.64 and 19.46 g kg^{-1} were measured. Exceptionally high temperatures of up to 20.11 °C occurred in the surface water and showed a drop down to 5.97 °C in the bottom waters, where the deep water is subject to a large salinity range. In June, temperature was the most important determinant for the development of stratification in the upper water column down to 15 m depth. Between the density lines of 1008 and 1012 kg m^{-3} a change of more than 10 °C was observed, indicating a strong thermocline. Salinity was the main determinant for stratification in the bottom water (20 to 25 m).

In September, surface temperatures ranged between 16.69 and 17.40 °C and decreased to a minimum of 12.12 °C in the bottom waters. The salinity gradient, however, ranged from 16.67 to 24.23 g kg^{-1} and was the main driver for stratification in September.

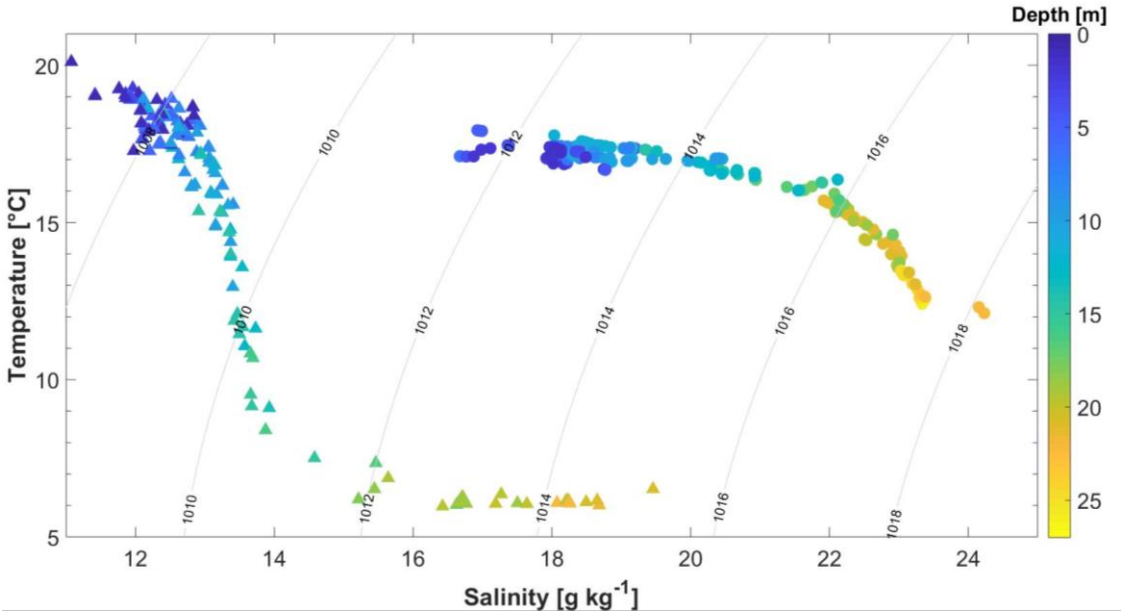

Figure 42: Comparison of the changes in the temperature-salinity dependence from June (triangles) and September (dots).

With the change of the water masses, a clear shift in the CH_4-O_2 relation from June to September can be observed (Figure 43). As discussed in detail above, with upcoming hypoxia and even suboxic conditions much higher CH_4 concentrations were observed in September which leads to a much steeper regression between the two parameters during that time. The development of oxygen depleted and CH_4 enriched bottom water agrees well with what is observed in other studies for the respective area (e.g. Bange et al., 2010; Steinle et al., 2017).

As previously described, the high CH_4 concentration in the bottom water results from methanogenesis in the anoxic sediments which is increasing when the bottom water is O_2 depleted (Bange et al., 2010) yielding enormous amounts of CH_4 that is partly released into the water column (Donis et al., 2017; Reindl and Bolałek, 2014). The summer stratification inhibits the sedimentary CH_4 from reaching the surface and CH_4 accumulates under the pycnocline. The CH_4 oxidation in the water column is very efficient and compared to the CH_4 released from the sediments only small amounts reach the surface water (Steinle et al., 2017).

The much higher salinity throughout the water column in September indicates that the high CH_4 concentration in the bottom water in September can not result from ongoing accumulation since June but represents a more recent signal. It may demonstrate the increased local CH_4 production in the sediments. Another explanation could be that the inflowing salty North Sea water passed a CH_4 rich region and transported CH_4 enriched water to the respective area. However, the data resolution is too poor for distinct conclusions.

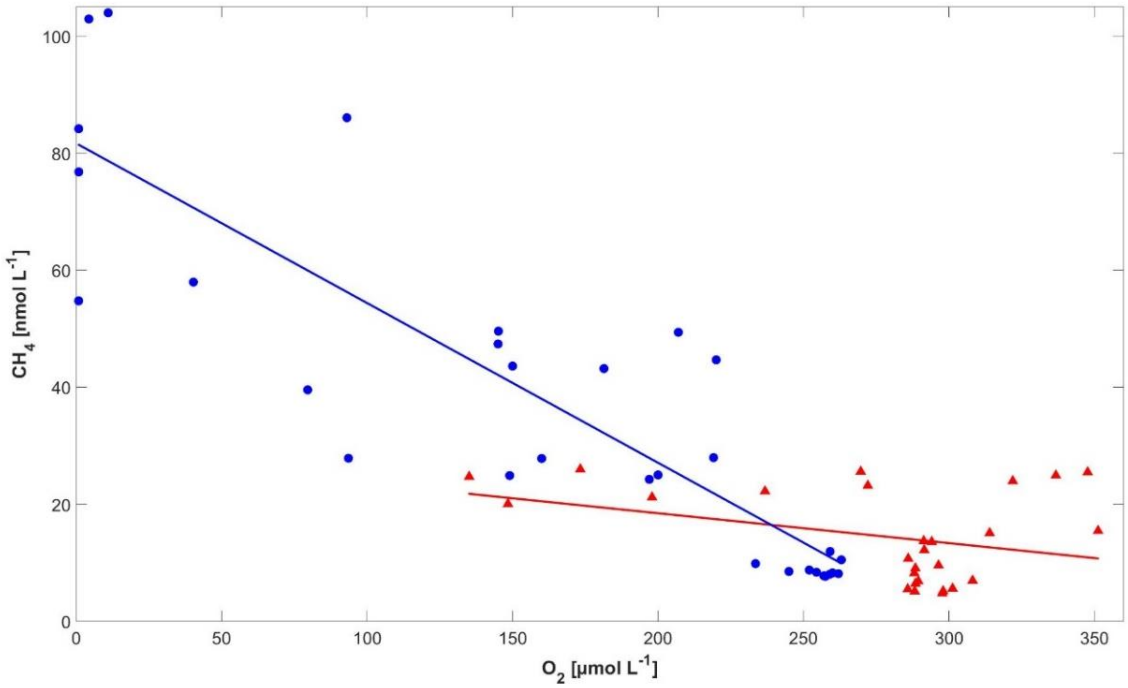

Figure 43: Comparison of the changes in the CH_4-O_2 dependence from June (red triangles) and September (blue dots).

4.3.4. Surface Saturation and CH_4 Flux

For the saturation and flux calculations the surface CH_4 measurements of the dinghy sampling were used. At all times, CH_4 oversaturation was observed during both cruises (Figures 44 & 46). During AL 510, saturations between 100 and 300 % were observed (Figure 44). For the majority of the cruise, values ranged between 150 and 200 %. The highest saturations were observed in the first and last measurement days where upwelling might have taken place. Upwelling events occur regularly in the Baltic Sea coastal areas (Humborg et al., 2019; Kniebusch et al., 2019; Myrberg et al., 2019; Schneider et al., 2014) and have been documented for the respective area (Ma et al., 2019). The lowest CH_4 saturation in all three surface depths was found one day after the first possible upwelling. Large differences of up to 40 % occurred between the three different depths. On most days, lowest saturations were found in the depth of 0.1 m.

The mean flux density during AL 510 was 4.24 µmol m^{-2} d^{-1}. Flux densities varied between 0.08 and 10.06 µmol m^{-2} d^{-1} (Figure 45). The lowest flux rate was observed on the 8th of June where saturations were close to atmospheric equilibrium with a flux of 0 to 1 µmol m^{-2} d^{-1}. The highest flux rates were observed on the 12th and 14th of June ranging between 6 and 11 µmol m^{-2} d^{-1}. The sampling depth for surface water is not uniformly defined. While for open

ocean CTD sampling depths down to 10 m are recognised as surface samples, for coastal areas are usually 1 m (e.g. Ma et al., 2020). For UW measurements the sampling depth depends on the vessel's hull and water intake depth which may range between approximately 4 and 6 m depth. The results of this study imply that this can lead to misinterpretation.

In September, CH_4 surface saturation varied between 200 and 370 % (Figure 46). Overall, very high variability of up to 100 % between the different surface depths on September 15th and 16th occurred. The lowest saturation was found on September 14th in 1 m depth and the highest saturation was found on September 16th as well in 1 m depth. The mean flux density in September was 13.43 µmol m^{-2} d^{-1}. Averaged over the whole cruises, flux densities were 9.19 µmol m^{-2} d^{-1} higher in comparison to June (Figures 45 & 47). While on most days, flux densities ranged between 5 and 20 µmol m^{-2} d^{-1} they went up to a maximum of 36.98 µmol m^{-2} d^{-1} on the 21st of September and down to a minimum of 2.87 µmol m^{-2} d^{-1} on the 18th of September. This is caused by the co-occurrence of higher saturations representing a higher gradient from sea to air and marginal higher wind speed. The wind speed normalized to 10 m ranged between 2.6 and 7.9 with a mean of 5.2 m s^{-1} in June and between 3.2 and 10.2 with a mean of 6.2 m s^{-1} in September.

The permanent emission linked to constant oversaturation agrees well with what was found in other studies. Ma et al. (2020) have shown in their decadal study that large variabilities of CH_4 saturation and flux density occur at Boknis Eck time series station. High variabilities were observed but oversaturation and high CH_4 fluxes were common. Additionally, Ma et al. (2020) showed that surface CH_4 saturations ranged between 129% and > 5500 % with sea-to-air CH_4 flux densities varying between 0.3 and 746.3 µmol m^{-2} d^{-1}. Both, saturation and flux densities, presented in this work are in the lower range of these findings but agree well with the finding that this area is a highly variable source of CH_4 to the atmosphere. Moreover, the extremely high saturations and fluxes occur in autumn and winter. During, summer when the water column is stratified common observations resemble the observations made in this study.

While also other Boknis Eck studies found higher saturations averaging rather between 500 and 700 % (e.g. Bange et al., 2010), the saturations presented in this study rather agree with saturations observed in the coastal south western Baltic Sea where CH_4 saturations varied between 113 and 395 % (Bange et al., 1994). Recent studies showed that the shallow western parts of the Baltic Sea show much higher surface CH_4 saturations compared to the whole Baltic

Sea (Gülzow et al., 2013; Schmale et al., 2010). These high CH_4 fluxes to the atmosphere agree well with the work of Weber et al. (2019) indicating that the majority of oceanic emissions comes from shallow coastal areas with water depths below 50 m.

During both cruises presented in this thesis the water column was stratified. While high CH_4 concentrations could be observed in the bottom water only a minor part of the CH_4 reached the surface and was emitted to the atmosphere. Even though, more than threefold higher bottom water concentrations were observed in September compared to June, surface concentrations were in a similar range during both cruises emphasizing the efficiency of water column CH_4 oxidation. As such it is important to keep in mind that even though the ocean is only a minor source of CH_4 to the atmosphere, it plays an important role in the budget by inhibiting the CH_4 from the sediments to enter the atmosphere.

Considering long-term variations, the CH_4 emissions from the sea were found to be strongest determined by the concentration difference of air and sea surface (Gutiérrez-Loza et al., 2019). Maltby et al. (2017) showed in their study that methanogenesis in the sediments of Eckernförde Bay increased throughout the summer months leading to CH_4 accumulation in the deep water. CH_4 oxidation rates are known to increase with a temporal shift when CH_4 becomes more abundant. However, a temporal shift is observed from increasing methanogenesis to increasing CH_4 oxidation as the oxidizing community takes time for building enough biomass to consume the CH_4 efficiently which can lead to enhanced CH_4 accumulation in the water column (Egger et al., 2016). In large (surface > 1 km^2) stratified aquatic systems the majority of CH_4 emissions is accounted to CH_4 that was generated under aerobic conditions as long as the stratification is stable (Günthel et al., 2019).

To identify the CH_4 dynamics including production consumption and accumulation processes as well as to differentiate biogenic and geological CH_4 sources and seasonal variations in these, it would be interesting to add measurements of the isotopic composition of CH_4 (Jakobs et al., 2014; Schmale et al., 2018) to the monthly Boknis Eck initiative.

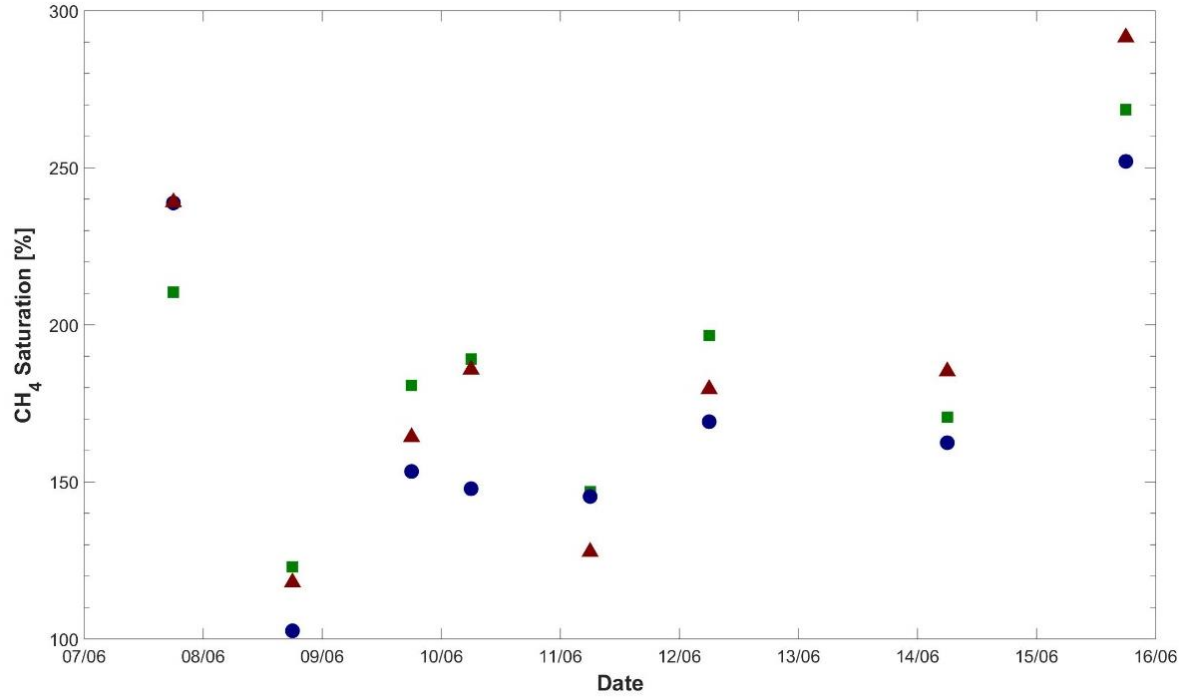

Figure 44: Mean CH_4 Saturation during AL510 differentiated for 0.1 m depth (blue dots), 0.5 m depth (red triangles), and 1 m depth (green squares).

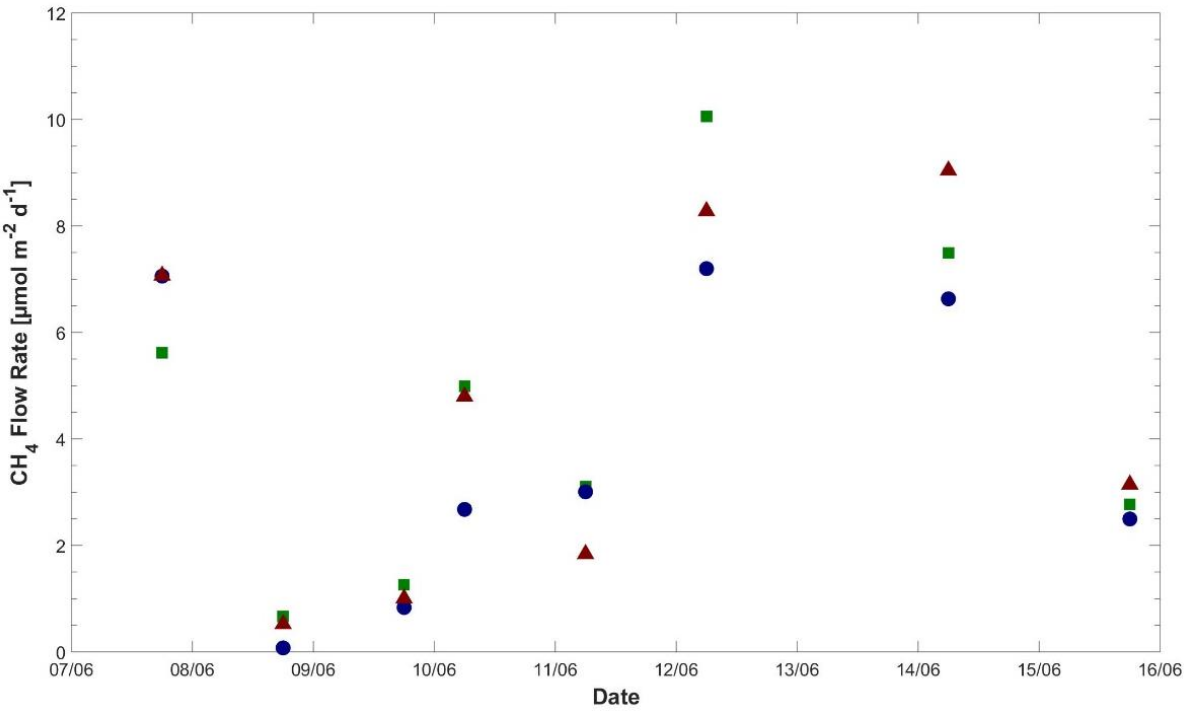

Figure 45: Mean CH_4 Flow Rates during AL510 differentiated for 0.1 m depth (blue dots), 0.5 m depth (red triangles), and 1 m depth (green squares).

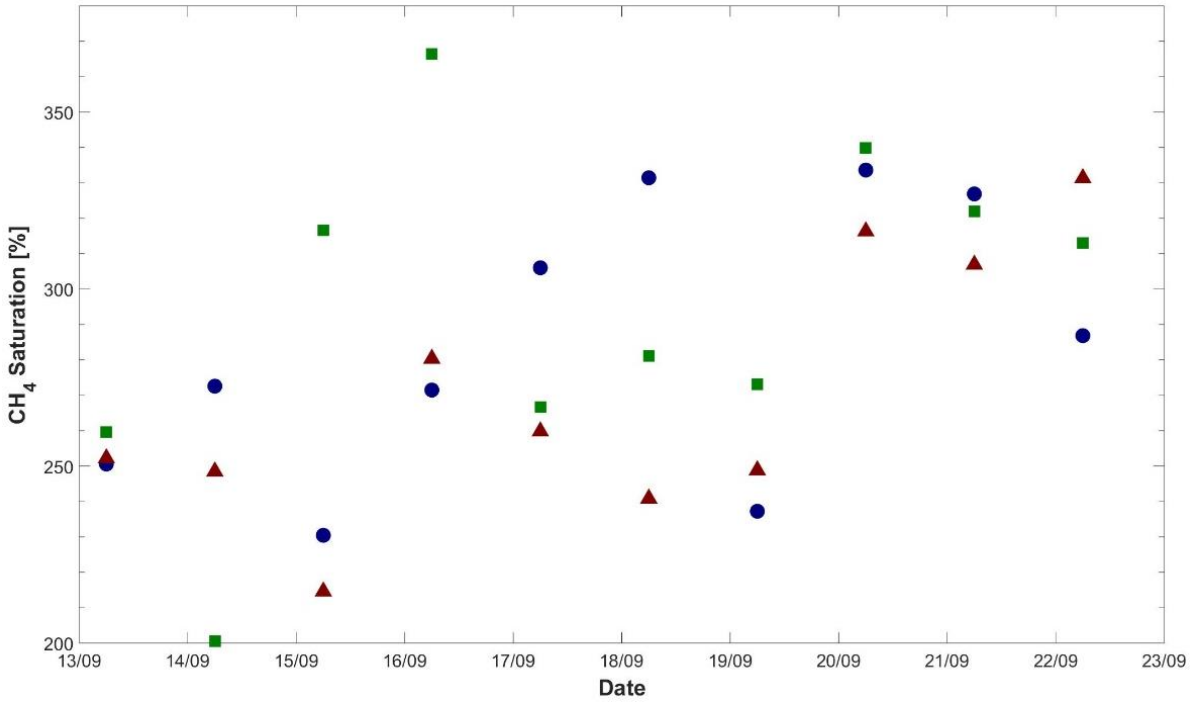

Figure 46: Mean CH_4 Saturation during AL516 differentiated for 0.1 m depth (blue dots), 0.5 m depth (red triangles), and 1 m depth (green squares).

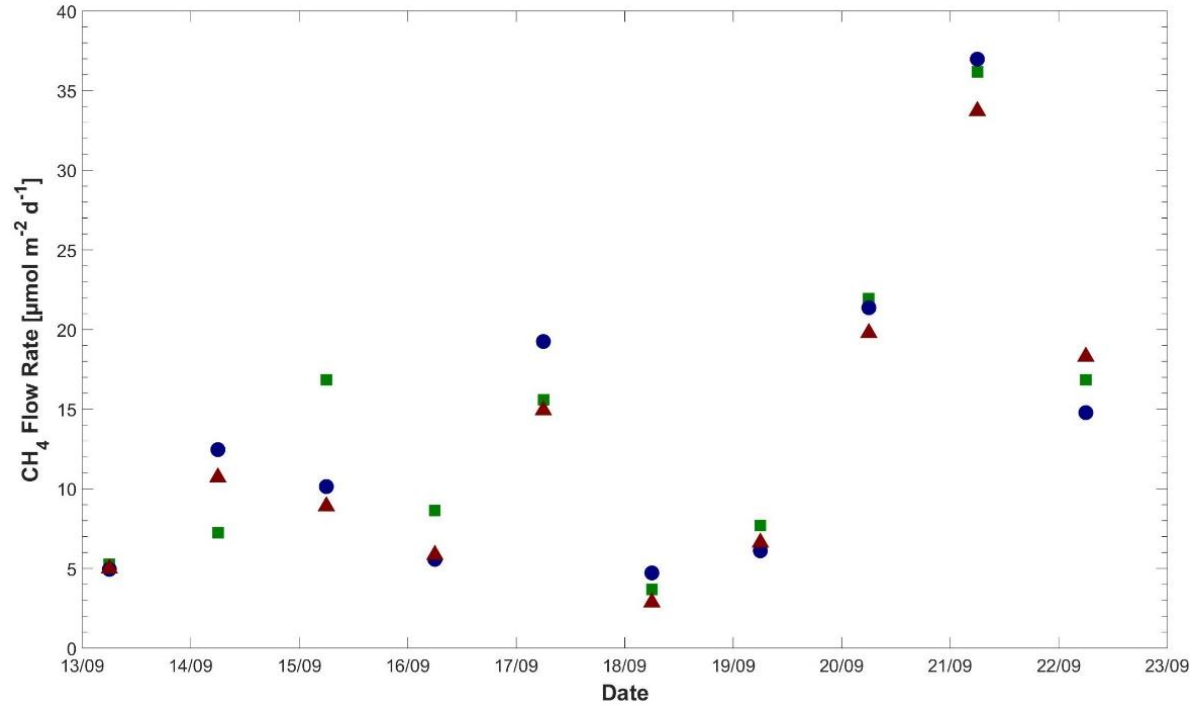

Figure 47: Mean CH_4 Flow Rate during AL516 differentiated for 0.1 m depth (blue dots), 0.5 m depth (red triangles), and 1 m depth (green squares).

5. Summary and Conclusion

The objective of this thesis to develop a PT system coupled to a GC-FID was successfully implemented. This work suggests that PT is a promising measurement technique compared to HS indicated by the good agreement of the Boknis Eck measurements and the higher precision. Moreover, PT is linked to a lower vulnerability to contaminations. However, recommended improvements for the system and measurement procedure to eliminate potential systematic errors include the implementation of a shorter column and a calibration experiment with a primary water standard. Furthermore, it is necessary to evaluate if the volume uncertainty and the gaschromatographic error relate. To estimate this, it is recommended to weigh samples before and after purging in the future. A higher precision was observed for CTD samples compared to underway and dinghy samples which might indicate air bubble contamination. In general, the whole sample collection and treatment procedures should be evaluated for possible improvement. It is recommended to repeat the comparison of discrete and continuous measurements onboard M/V Tavastland under optimized conditions and investigate the error source for the strong deviation among the different measurements.

In particular, the results from Baltic GasEx indicate that the time series station Boknis Eck is a good representation of the conditions for the Kiel Bight. The CH_4 distribution with high concentrations in the bottom water and lower but at all times oversaturated (with respect to atmospheric equilibrium) surface water concentrations fit very well to what has been observed in previous studies and at Boknis Eck. Widely observed summer season features of the study area including the building of stratification and suboxic conditions as well as the water inflow from North Sea were represented in the data.

The spatial data resolution is still insufficient for distinct conclusions about the role of surface gradients and fluxes of CH_4. The surface CH_4 distribution presented in this thesis implies that strong gradients occur in the upper 1 m of the water column. Therefore, flux densities may differ by up to approximately 50 % when calculated with the CH_4 concentration in 0.1 or 1 m respectively. This raises the question how well (continuous) UW measurements represent surface water concentrations and whether this data should be trusted for flux density calculations. However, the high error in the dinghy samples indicates that the sample collection procedure needs to be improved for reliable investigations of these gradients.

For comparable campaigns in the future it would be interesting to combine vertical profiling and continuous UW measurements to enhance the understanding of the surface CH_4 dynamics. To determine these gradients and their variability, a combined study of high-resolution surface CH_4 distribution and the related processes, such as CH_4 production and oxidation rates needs to be carried out. It would be of interest to carry out a comparable initiative during autumn and winter when the whole water column intermixes and CH_4 fluxes from the sediments can reach the atmosphere. Extremely high surface concentrations and fluxes have been observed at single observations. To understand how representative these measurements are for monthly means from one station should be estimated with more measurement campaigns of higher spatial and temporal resolution as presented in this thesis.

Acknowledgements

I would like to thank the captains and crews of R/V Alkor, R/V Littorina and M/V Tavastland for their support as well as Kastriot Qelaj and Yanan Zhao for their help with the Boknis Eck work. Many thanks to Dennis Booge for taking the samples during AL 510 & 516 and for providing the additional data of these cruises that was used for this work. I thank Anna Willstrand Wranne for her help with the ferrybox system and Tobias Steinhoff and Annette Kock for maintaining the GO-system and providing the continuous CH_4 data as well as Anna Becker for measuring the Boknis Eck and Tavastland HS samples used for comparison in this work and Daniel Bastian for his help with vial volume estimations. I would like to thank Melf Paulsen, Hanna Campen, and Riel Ingeniero for their support with the laboratory equipment as well as Tina Fiedler for the laboratory maintenance and Xiao Ma for his help regarding the data acquisition. Moreover, I thank the colleagues involved in BONUS INTEGRAL for giving me the opportunity to conduct this work. I am especially grateful for the extensive support by my supervisors Annette Kock and Hermann Bange. I highly appreciate that I could use the infrastructure and laboratory inventory of Hermann Bange and Birgit Quack at GEOMAR Helmholtz Centre for Ocean Research Kiel. Many thanks to all members of AG Bange and my colleagues at GEOMAR for the successful collaboration. Especially, I thank Annette Kock, Sunke Schmidtko, Damian Arévalo-Martínez, Sven Gindorf, Anabel von Jackowski, and Daniel Bastian and for their support, inspiration, proofreading, and the constructive discussions.

Finally, I am thankful for all the friends and colleagues I met during daily work, cruises, summer schools, and lectures creating a friendly and productive working atmosphere and inspiring me with new ideas as well as for the exhaustless support and appreciation of my family and friends. It was a great challenge and an even greater pleasure to work and grow at GEOMAR. I learned much more than I could have expected, and I am eagerly looking forward to future collaborations.

References

Abegg, F. and Anderson, A. L.: The acoustic turbid layer in muddy sediments of Eckernfoerde Bay, Western Baltic: Methane concentration, saturation and bubble characteristics, Mar. Geol., 137(1–2), 137–147, doi:10.1016/S0025-3227(96)00084-9, 1997.

Archer, D., Buffett, B. and Brovkin, V.: Ocean methane hydrates as a slow tipping point in the global carbon cycle, Proc. Natl. Acad. Sci. U. S. A., 106(49), 20596–20601, doi:10.1073/pnas.0800885105, 2009.

Arévalo-Martínez, D. L., Beyer, M., Krumbholz, M., Piller, I., Kock, A., Steinhoff, T., Körtzinger, A. and Bange, H. W.: A new method for continuous measurements of oceanic and Atmospheric N2O, CO and CO2: performance of off-axis integrated Cavity output spectroscopy (OA-ICOS) coupled to non-dispersive Infrared detection (NDIR), Ocean Sci., 9, 1071–1087, doi:doi:10.5194/os-9-1071-2013, 2013.

Atkinson, L. P. and Richards, F. A.: The occurrence and distribution of methane in the marine environment, Deep. Res. Oceanogr. Abstr., 14(6), 673–684, doi:10.1016/S0011-7471(67)80005-6, 1967.

Bange, H. W.: Gaseous Nitrogen Compounds (NO, N2O, N2, NH3) in the Ocean., in Nitrogen in the Marine Environment, CAPONE, D.G. & D.A. BRONK & M.R. MULHOLLAND & E.J. CARPENTER, Elsevier, Burlington., 2008.

Bange, H. W., Bartell, U. H., Rapsomanikis, S. and Andreae, M. O.: Methane in the Baltic and North Seas and a reassessment of the marine emissions of methane, Glob. Biogeochem. Cy., 8, 465–480, 1994.

Bange, H. W., Dahlke, S., Ramesh, R., Meyer-Reil, L. A., Rapsomanikis, S. and Andreae, M. O.: Seasonal study of methane and nitrous oxide in the coastal waters of the southern Baltic Sea, Estuar. Coast. Shelf Sci., 47(6), 807–817, doi:10.1006/ecss.1998.0397, 1998.

Bange, H. W., Bergmann, K., Hansen, H. P., Kock, A., Koppe, R., Malien, F. and Ostrau, C.: Dissolved methane during hypoxic events at the Boknis Eck time series station (Eckernförde Bay, SW Baltic Sea), Biogeosciences, 7(4), 1279–1284, doi:10.5194/bg-7-1279-2010, 2010.

Bange, H. W., Hansen, H. P., Malien, F., Laß, K., Karstensen, J., Petereit, C., Friedrichs, G. and Dale, A.: Boknis Eck Time Series Station (SW Baltic Sea): Measurements from 1957 to 2010, LOICZ-Affiliated Act., Inprint 20, 16–22, 2011.

Baral, B. S.: Methanobactin : Metal binding properties , physiological function and biosynthesis, 2017.

Becker, M., Andersen, N., Fiedler, B., Fietzek, P., Körtzinger, A., Steinhoff, T. and Friedrichs, G.: Using cavity ringdown spectroscopy for continuous monitoring of δ 13C(CO 2) and CO 2 in the surface ocean, Limnol. Oceanogr. Methods, 10(OCTOBER), 752–766, doi:10.4319/lom.2012.10.752, 2012.

Belkin, I. M.: Rapid warming of Large Marine Ecosystems, Prog. Oceanogr., 81(1–4), 207–213, doi:10.1016/j.pocean.2009.04.011, 2009.

Bižić, M., Klintzsch, T., Ionescu, D., Hindiyeh, M. Y., Günthel, M., Muro-Pastor, A. M., Eckert, W., Urich, T., Keppler, F. and Grossart, H.-P.: Aquatic and terrestrial cyanobacteria produce methane, Sci. Adv., 6(3), eaax5343, doi:10.1126/sciadv.aax5343, 2020.

Bodelier, P. L. E., Pérez, G., Veraart, A. J. and Krause, S. M. B.: Methanotroph Ecology, Environmental Distribution and Functioning, in Methanotrophs. Microbiology Fundamentals and Biotechnological Applications, edited by E. Y. Lee and A. Steinbüchel, pp. 2–38, Springer Nature Switzerland AG 2019. [online] Available from: https://doi.org/10.1007/978-3-030-23261-0, 2019.

Booge, D.: Cruise Report AL510., 2018.

Booge, D.: Cruise Report AL516., 2019.

Borges, A. V., Champenois, W., Gypens, N., Delille, B. and Harlay, J.: Massive marine methane emissions from near-shore shallow coastal areas, Sci. Rep., 6(June), 2–9, doi:10.1038/srep27908, 2016.

Borges, A. V., Speeckaert, G., Champenois, W., Scranton, M. I. and Gypens, N.: Productivity and Temperature as Drivers of Seasonal and Spatial Variations of Dissolved Methane in the Southern Bight of the North Sea, Ecosystems, 21(4), 583–599, doi:10.1007/s10021-017-0171-7, 2018.

Bowles, M. W., Samarkin, V. A., Hunter, K. S., Finke, N., Teske, A. P., Girguis, P. R. and Joye, S. B.: Remarkable Capacity for Anaerobic Oxidation of Methane at High Methane Concentration, Geophys. Res. Lett., 46(21), 12192–12201, doi:10.1029/2019GL084375, 2019.

Bussmann, I. and Suess, E.: Groundwater seepage in Eckernforde Bay (Western Baltic Sea): Effect on methane and salinity distribution of the water column, Cont. Shelf Res., 18(14–15), 1795–1806, doi:10.1016/S0278-4343(98)00058-2, 1998.

Bussmann, I., Matousu, A., Osudar, R. and Mau, S.: Assessment of the radio 3H-CH4 tracer technique to measure aerobic methane oxidation in the water column, Limnol. Oceanogr. Methods, 13(6), 312–327, doi:10.1002/lom3.10027, 2015.

Capelle, D. W., Dacey, J. W. and Tortell, P. D.: An automated, high through-put method for accurate and precise measurements of dissolved nitrous-oxide and methane concentrations in natural waters, Limnol. Oceanogr. Methods, 13(7), 345–355, doi:10.1002/lom3.10029, 2015.

Capelle, D. W., Hallam, S. J. and Tortell, P. D.: Time- series CH4 measurements from Saanich Inlet, BC, a seasonally anoxic fjord, Mar. Chem., 215(103664), doi:https://doi.org/10.1016/j.marchem.2019.103664, 2019.

Chang, J., Gu, W., Park, D., Semrau, J. D., Dispirito, A. A. and Yoon, S.: Methanobactin from Methylosinus trichosporium OB3b inhibits N2O reduction in denitrifiers, ISME J., 12(8), 2086–2089, doi:10.1038/s41396-017-0022-8, 2018.

Chappellaz, J., Barnola, J. M., Raynaud, D., Korotkevicht, Y. S. and Lorius, C.: Ice-core record of atmospheric methane over the past 160 , 000 years, Nature, 345, 127–131, 1990.

Dale, A. W., Sommer, S., Bohlen, L., Treude, T., Bertics, V. J., Bange, H. W., Pfannkuche, O., Schorp, T., Mattsdotter, M. and Wallmann, K.: Rates and regulation of nitrogen cycling in seasonally hypoxic sediments during winter (Boknis Eck, SW Baltic Sea): Sensitivity to environmental variables, Estuar. Coast. Shelf Sci., 95(1), 14–28, doi:10.1016/j.ecss.2011.05.016, 2011.

David, H. A.: Further Applications of Range to the Analysis of Variance, Oxford Univ. Press behalf Biometrika Trust, 38(3), 393–409, 1951.

Deutsch, C., Brix, H., Ito, T., Frenzel, H. and Thompson, L.: Climate-forced variability of ocean hypoxia, Science (80-.)., 333(6040), 336-339., doi:doi:10.1126/science.1202422, 2011.

Dietrich, G. and Köster, R.: Bodengestalt und Bodenbedeckung, in Meereskunde der Ostsee, Magaard, L. and Rheinheimer, G., Springer-Verlag Berlin Heidelberg., 1974.

DiSpirito, A. A., Semrau, J. D., Murrell, J. C., Gallagher, W. H., Dennison, C. and Vuilleumier, S.: Methanobactin and the Link between Copper and Bacterial Methane Oxidation, Microbiol. Mol. Biol. Rev., 80(2), 387–409, doi:10.1128/mmbr.00058-15, 2016.

Dlugokencky, E.: Monthly Averages of CH4 at Mace Head, County Galway, Ireland (MHD), NOAA Earth Syst. Res. Lab. Glob. Monit. Lab. [online] Available from: ftp://aftp.cmdl.noaa.gov/data/trace_gases/ch4/flask/surface/ch4_mhd_surface-flask_1_ccgg_month.txt (Accessed 6 July 2020a), 2020.

Dlugokencky, E.: Trends in Atmospheric Methane, NOAA/ESRL [online] Available from: https://www.esrl.noaa.gov/gmd/ccgg/trends_ch4/ (Accessed 8 February 2020b), 2020.

Donis, D., Janssen, F., Liu, B., Wenzhöfer, F., Dellwig, O., Escher, P., Spitzy, A. and Böttcher, M. E.: Biogeochemical impact of submarine ground water discharge on coastal surface sands of the southern Baltic Sea, Estuar. Coast. Shelf Sci., 189, 131–142, doi:10.1016/j.ecss.2017.03.003, 2017.

Duan, Z., Møller, N., Greenberg, J. and Weare, J. H.: The prediction of methane solubility in natural waters to high ionic strength from 0 to 250°C and from 0 to 1600 bar, Geochim. Cosmochim. Acta, 56(4), 1451–1460, doi:10.1016/0016-7037(92)90215-5, 1992.

Egger, M., Lenstra, W., Jong, D., Meysman, F. J. R., Sapart, C. J., Van Der Veen, C., Röckmann, T., Gonzalez, S. and Slomp, C. P.: Rapid sediment accumulation results in high methane effluxes from coastal sediments, PLoS One, 11(8), 1–22, doi:10.1371/journal.pone.0161609, 2016.

Emerson, S., Stump, C. and Nicholson, D.: Net biological oxygen production in the ocean: Remote in situ measurements of O2 and N2 in surface waters, Global Biogeochem. Cycles, 22(3), 1–13, doi:10.1029/2007GB003095, 2008.

Fischer, T., Kock, A., Arévalo-martínez, D. L., Dengler, M., Brandt, P. and Bange, H. W.: Gas exchange estimates in the Peruvian upwelling regime biased by multi-day near-surface stratification, , 2307–2328, 2019.

Florez-Leiva, L., Damm, E. and Farías, L.: Methane production induced by dimethylsulfide in surface water of an upwelling ecosystem, Prog. Oceanogr., 112–113, 38–48, doi:10.1016/j.pocean.2013.03.005, 2013.

Flury, S., Røy, H., Dale, A. W., Fossing, H., Tóth, Z., Spiess, V., Jensen, J. B. and Jørgensen, B. B.: Controls on subsurface methane fluxes and shallow gas formation in Baltic Sea sediment (Aarhus Bay, Denmark), Geochim. Cosmochim. Acta, 188, 297–309, doi:10.1016/j.gca.2016.05.037, 2016.

Gilek, M., Karlsson, M., Linke, S. and Smolarz, K.: Environmental Governance of the Baltic Sea: Identifying Key Challenges, Research Topics and Analytical Approaches., 2016.

Gindorf, S.: The Methane Distribution around the Macaronesian Islands in the North East Atlantic Ocean, 2020.

Gülzow, W., Rehder, G., Schneider, B., Schneider, J. and Sadkowiak, B.: A new method for continuous measurement of methane and carbon dioxide in surface waters using off-axis integrated cavity output spectroscopy (ICOS): An example from the Baltic Sea, Limnol. Oceanogr. Methods, 9(MAY), 176–184, doi:10.4319/lom.2011.9.176, 2011.

Gülzow, W., Rehder, G., Deimling, J. S. V., Seifert, T. and Tóth, Z.: One year of continuous measurements constraining methane emissions from the Baltic Sea to the atmosphere using a ship of opportunity, Biogeosciences, 10(1), 81–99, doi:10.5194/bg-10-81-2013, 2013.

Gülzow, W., Gräwe, U., Kedzior, S., Schmale, O. and Rehder, G.: Seasonal variation of methane in the water column of Arkona and Bornholm Basin, western Baltic Sea, J. Mar. Syst., 139, 332–347, doi:10.1016/j.jmarsys.2014.07.013, 2014.

Günthel, M., Donis, D., Kirillin, G., Ionescu, D., Bizic, M., McGinnis, D. F., Grossart, H. P. and Tang, K. W.: Contribution of oxic methane production to surface methane emission in lakes and its global importance, Nat. Commun., 10(1), 1–10, doi:10.1038/s41467-019-13320-0, 2019.

Gutiérrez-Loza, L., Wallin, M. B., Sahlée, E., Nilsson, E., Bange, H. W., Kock, A. and Rutgersson, A.: Measurement of air-sea methane fluxes in the baltic sea using the eddy covariance method, Front. Earth Sci., 7(May), 1–13, doi:10.3389/feart.2019.00093, 2019.

Hassler, B.: BONUS BALTSPACE deliverable: D2.2: Ambition and Realities in Baltic Sea Marine Spatial Planning and the Ecosystem Approach: Policy and Sector Coordination in Promotion of Regional Integration., , (Art 185), 69, 2017.

Hassler, B., Gee, K., Gilek, M., Luttmann, A., Morf, A., Saunders, F., Stalmokaite, I., Strand, H. and Zaucha, J.: Collective action and agency in Baltic Sea marine spatial planning: Transnational policy coordination in the promotion of regional coherence, Mar. Policy, 92(November 2017), 138–147, doi:10.1016/j.marpol.2018.03.002, 2018.

Hsu, S. A., Meindl, E. A. and Gilhousen, D. B.: Determiningthe power-law wind-profile exponent under near-neutral stability conditions at sea, J. Appl. Meteorol., 33, 757–765, 1994.

Humborg, C., Geibel, M. C., Sun, X., McCrackin, M., Mörth, C. M., Stranne, C., Jakobsson, M., Gustafsson, B., Sokolov, A., Norkko, A. and Norkko, J.: High emissions of carbon dioxide and methane from the coastal Baltic Sea at the end of a summer heat wave, Front. Mar. Sci., 6(JUL), 1–14, doi:10.3389/fmars.2019.00493, 2019.

IOW (Leibniz Institute for Baltic Sea Research Warnemünde): Profile of the Baltic Sea, [online] Available from: https://www.io-warnemuende.de/profile-of-the-baltic-sea.html (Accessed 7 February 2020), 2018.

Jähne, B., Heinz, G. and Dietrich, W.: Measurement of the diffusion coefficients of sparingly soluble gases in water, J. Geophys. Res. Ocean., 92(C10), 10767–10776, doi:10.1029/JC092iC10p10767, 1987.

Jakobs, G., Holtermann, P., Berndmeyer, C., Rehder, G., Blumenberg, M., Jost, G., Nausch, G. and Schmale, O.: Seasonal and spatial methane dynamics in the water column of the central Baltic Sea (Gotland Sea), Cont. Shelf Res., 91, 12–25, doi:10.1016/j.csr.2014.07.005, 2014.

Justus, C. G., Hargraves, W. R., Mikhail, A. and Denise Graber: Methods for Estimating Wind Speed Frequency, J. Appl. Meteorol. (, 17(3), 350–353 [online] Available from: http://www.jstor.com/stable/26178009, 1978.

Kahru, M., Elmgren, R., Kaiser, J., Wasmund, N. and Savchuk, O.: Cyanobacterial blooms in the Baltic Sea: Correlations with environmental factors, Harmful Algae, 92(August 2019), 101739, doi:10.1016/j.hal.2019.101739, 2020.

Kankaanpää, H. T. and Virtasalo, J. J.: Rapid fluctuations in the northern Baltic Sea H2S layer, J. Mar. Syst., 176, 24–37, doi:10.1016/j.jmarsys.2017.07.001, 2017.

Karl, D. M. and Tilbrook, B. D.: Production and transport of methane in oceanic particulate organic matter, Nature, 368(6473), 732–734, doi:10.1038/368732a0, 1994.

Karl, D. M., Beversdorf, L., Björkman, K. M., Church, M. J., Martinez, A. and Delong, E. F.: Aerobic production of methane in the sea, Nat. Geosci., 1(7), 473–478, doi:10.1038/ngeo234, 2008.

Karlson, B., Andersson, L. S., Kaitala, S., Kronsell, J., Mohlin, M., Seppälä, J. and Willstrand Wranne, A.: A comparison of FerryBox data vs. monitoring data from research vessels for near surface waters of the Baltic Sea and the Kattegat, J. Mar. Syst., 162, 98–111, doi:10.1016/j.jmarsys.2016.05.002, 2016.

Kirschke, S.: Three decades of global methane sources and sinks, , 28(September), doi:10.1038/ngeo1955, 2013.

Klintzsch, T., Langer, G., Nehrke, G., Wieland, A., Lenhart, K. and Keppler, F.: Methane production by three widespread marine phytoplankton species: Release rates, precursor compounds, and potential relevance for the environment, Biogeosciences, 16(20), 4129–4144, doi:10.5194/bg-16-4129-2019, 2019.

Kniebusch, M., Meier, H. E. M., Neumann, T. and Börgel, F.: Temperature Variability of the Baltic Sea Since 1850 and Attribution to Atmospheric Forcing Variables, J. Geophys. Res. Ocean., 124(6), 4168–4187, doi:10.1029/2018JC013948, 2019.

Kock, A.: Methane Measurements in Selected Ocean Areas: Eastern Tropical North Atlantic Ocean and Southwestern Labrador Sea., 2007.

Leipe, T., Tauber, F., Vallius, H., Virtasalo, J., Uścinowicz, S., Kowalski, N., Hille, S., Lindgren, S. and Myllyvirta, T.: Particulate organic carbon (POC) in surface sediments of the Baltic Sea, Geo-Marine Lett., 31(3), 175–188, doi:10.1007/s00367-010-0223-x, 2011.

Lennartz, S. T., Lehmann, A., Herrford, J., Malien, F., Hansen, H. P., Biester, H. and Bange, H. W.: Long-term trends at the Boknis Eck time series station (Baltic Sea), 1957-2013: Does climate change counteract the decline in eutrophication?, Biogeosciences, 11(22), 6323–6339, doi:10.5194/bg-11-6323-2014, 2014.

Liss, P. S. and Johnson, M. T.: Springer Earth System Sciences Ocean-Atmosphere Interactions of Gases and Particles. [online] Available from: http://www.springer.com/series/10178%0Ahttps://link.springer.com/content/pdf/10.1007%2F978-3-642-25643-1.pdf, 2014.

Liss, P. S. and Slater, P. G.: © 1974 Nature Publishing Group, 1974.

Liu, Y. and Whitman, W. B.: Metabolic, phylogenetic, and ecological diversity of the methanogenic archaea, Ann. N. Y. Acad. Sci., 1125, 171–189, doi:10.1196/annals.1419.019, 2008.

Lohrberg, A., Schmale, O., Ostrovsky, I., Niemann, H., Held, P. and Schneider von Deimling, J.: Discovery and quantification of a widespread methane ebullition event in a coastal inlet (Baltic Sea) using a novel sonar strategy, Sci. Rep., 10(1), 1–13, doi:10.1038/s41598-020-60283-0, 2020.

Lu, X., Gu, W., Zhao, L., Ul Haque, M. F., DiSpirito, A. A., Semrau, J. D. and Gu, B.: Methylmercury uptake and degradation by methanotrophs, Sci. Adv., 3(5), 1–6, doi:10.1126/sciadv.1700041, 2017.

Ma, X., Lennartz, S. T. and Bange, H. W.: A multi-year observation of nitrous oxide at the Boknis Eck Time-Series Station in the Eckernförde Bay (southwestern Baltic Sea), Biogeosciences Discuss., 1–30, doi:10.5194/bg-2019-165, 2019a.

Ma, X., Lennartz, S. T. and Bange, H. W.: A multi-year observation of nitrous oxide at the Boknis Eck Time Series Station in the Eckernförde Bay (southwestern Baltic Sea), Biogeosciences, 16(20), 4097–4111, doi:10.5194/bg-16-4097-2019, 2019b.

Ma, X., Sun, M., Lennartz, S. T. and Bange, H. W.: A decade of methane measurements at the Boknis Eck Time Series Station in Eckernförde Bay (southwestern Baltic Sea), Biogeosciences, 17, 3427–3438, doi:10.5194/bg-17-3427-2020, 2020.

Magen, C., Lapham, L. L., Pohlman, J. W., Marshall, K., Bosman, S., Casso, M. and Chanton, J. P.: A simple headspace equilibration method for measuring dissolved methane, Limnol. Oceanogr. Methods, 12(SEP), 637–650, doi:10.4319/lom.2014.12.637, 2014.

Maltby, J., Steinle, L., Löscher, C. R., Bange, H. W., Fischer, M. A., Schmidt, M. and Treude, T.: Microbial methanogenesis in the sulfate-reducing zone in sediments from Eckernförde Bay, SW Baltic Sea, Biogeosciences Discuss., 1–45, doi:10.5194/bg-2017-36, 2017.

Manzhynski, S., Siniak, N., Źrobek-Rózańska, A. and Źróbek, S.: Sustainability performance in the Baltic Sea Region, Land use policy, 57, 489–498, doi:10.1016/j.landusepol.2016.06.003, 2016.

McDougall, T. J. and Barker, P. M.: TEOS-10 and the Gibbs Seawater (GSW) Oceanographic Toolbox, [online] Available from: http://www.teos-10.org/software.htm#1, 2011.

Meier, H. E. M., Eilola, K., Almroth-Rosell, E., Schimanke, S., Kniebusch, M., Höglund, A., Pemberton, P., Liu, Y., Väli, G. and Saraiva, S.: Disentangling the impact of nutrient load and climate changes on Baltic Sea hypoxia and eutrophication since 1850, Clim. Dyn., 53(1–2), 1–22, doi:10.1007/s00382-018-4296-y, 2019.

Metcalf, W. W., Griffin, B. M., Cicchillo, R. M., Gao, J., Janga, S. C., Cooke, H. A., Circello, B. T., Evans, B. S., Martens-Habbena, W., Stahl, D. A. and Donk, W. A. van der: Synthesis of Methylphosphonic Acid by Marine Microbes: A Source for Methane in the Aerobic Ocean, Science (80-.)., 337, 1104–1107, 2012.

Mogollón, J. M., Dale, A. W., Jensen, J. B., Schlüter, M. and Regnier, P.: A method for the calculation of anaerobic oxidation of methane rates across regional scales: An example from the Belt Seas and The Sound (North Sea-Baltic Sea transition), Geo-Marine Lett., 33(4), 299–310, doi:10.1007/s00367-013-0329-z, 2013.

Mohrholz, V., Naumann, M., Nausch, G., Krüger, S. and Gräwe, U.: Fresh oxygen for the Baltic Sea - An exceptional saline inflow after a decade of stagnation, J. Mar. Syst., 148, 152–166, doi:10.1016/j.jmarsys.2015.03.005, 2015.

Müller, J. D., Schneider, B. and Rehder, G.: Long-term alkalinity trends in the Baltic Sea and their implications for CO2-induced acidification, Limnol. Oceanogr., 61(6), 1984–2002, doi:10.1002/lno.10349, 2016.

Myhre, G., Shindell, D., Bréon, F.-M., Collins, W., Fuglestvedt, J., Huang, J., Koch, D., Lamarque, J.-F., Lee, D., Mendoza, B., Nakajima, T., Robock, A., Stephens, G., Takemura, T. and Zhang, H.: Anthropogenic and Natural Radiative Forcing, in Climate Change 2013: The Physical Science Basis. Contribution of Working Group I to the Fifth Assessment Report of the Intergovernmental Panel on Climate Change, edited by T. F. Stocker, D. Qin, G.-K. Plattner, M. Tignor, S. K. Allen, J. Boschung, A. Nauels, Y. Xia, V. Bex, and P. M. (eds. . Midgley, pp. 659–740, Cambridge University Press, Cambridge, United Kingdom and New York, NY, USA., 2013.

Myllykangas, J. P., Hietanen, S. and Jilbert, T.: Legacy Effects of Eutrophication on Modern Methane Dynamics in a Boreal Estuary, Estuaries and Coasts, 43(2), 189–206, doi:10.1007/s12237-019-00677-0, 2020.

Myrberg, K., Korpinen, S. and Uusitalo, L.: Physical oceanography sets the scene for the Marine Strategy Framework Directive implementation in the Baltic Sea, Mar. Policy, 107(March 2018), 103591, doi:10.1016/j.marpol.2019.103591, 2019.

Naumann, M. and Nausch, G.: Die Ostsee atmet auf, Chemie unserer Zeit, 49(1), 76–80, doi:10.1002/ciuz.201400695, 2015.

Newman, K. R., Cormier, M. H., Weissel, J. K., Driscoll, N. W., Kastner, M., Solomon, E. A., Robertson, G., Hill, J. C., Singh, H., Camilli, R. and Eustice, R.: Active methane venting observed at giant pockmarks along the U.S. mid-Atlantic shelf break, Earth Planet. Sci. Lett., 267(1–2), 341–352, doi:10.1016/j.epsl.2007.11.053, 2008.

Niemann, H., Steinle, L., Blees, J., Bussmann, I., Treude, T., Krause, S., Elvert, M. and Lehmann, M. F.: Toxic effects of lab-grade butyl rubber stoppers on aerobic methane oxidation, Limnol. Oceanogr. Methods, 13(1), 40–52, doi:10.1002/lom3.10005, 2015.

Nightingale, P. D., Malin, G., Law, C. S., Watson, A. J., Liss, P. S., Liddicoat, M. I., Boutin, J. and Upstill-Goddard, R. C.: In situ evaluation of air-sea gas exchange parameterizations using novel conservative and volatile tracers, Global Biogeochem. Cycles, 14(1), 373–387, 2000.

Nisbet, E. G., Manning, M. R., Dlugokencky, E. J., Fisher, R. E., Lowry, D., Michel, S. E., Myhre, C. L., Platt, S. M., Allen, G., Bousquet, P., Brownlow, R., Cain, M., France, J. L., Hermansen, O., Hossaini, R., Jones, A. E., Levin, I., Manning, A. C., Myhre, G., Pyle, J. A., Vaughn, B. H., Warwick, N. J. and White, J. W. C.: Very Strong Atmospheric Methane Growth in the 4 Years 2014–2017: Implications for the Paris Agreement, Global Biogeochem. Cycles, 33(3), 318–342, doi:10.1029/2018GB006009, 2019.

Norbäck Ivarsson, L., Andrén, T., Moros, M., Andersen, T. J., Lönn, M. and Andrén, E.: Baltic sea coastal eutrophication in a thousand year perspective, Front. Environ. Sci., 7(JUN), doi:10.3389/fenvs.2019.00088, 2019.

Palacios, P. A., Snoeyenbos-West, O., Löscher, C. R., Thamdrup, B. and Rotaru, A. E.: Baltic Sea methanogens compete with acetogens for electrons from metallic iron, ISME J., 13(12), 3011–3023, doi:10.1038/s41396-019-0490-0, 2019.

Panofsky, H. and Dutton, J.: Atmospheric Turbulence., 1984.

Pawlowicz, R.: M_Map: A mapping package for MATLAB, [online] Available from: www.eoas.ubc.ca/~rich/map.html., 2020.

Rehder, G.: BONUS INTEGRAL Integrated carbon and trace gas monitoring for the Baltic Sea, [online] Available from: https://www.bonusportal.org/projects/blue_baltic_2017-2020/integral, 2020.

Rehder, G., Leifer, I., Brewer, P. G., Friederich, G. and Peltzer, E. T.: Controls on methane bubble dissolution inside and outside the hydrate stability field from open ocean field experiments and numerical modeling, Mar. Chem., 114(1–2), 19–30, doi:10.1016/j.marchem.2009.03.004, 2009.

Reindl, A. R. and Bolałek, J.: Methane flux from sediment into near-bottom water and its variability along the Hel Peninsula-Southern Baltic Sea, Cont. Shelf Res., 74, 88–93, doi:10.1016/j.csr.2013.12.006, 2014.

Repeta, D. J., Ferrón, S., Sosa, O. A., Johnson, C. G., Repeta, L. D., Acker, M., Delong, E. F. and Karl, D. M.: Marine methane paradox explained by bacterial degradation of dissolved organic matter, Nat. Geosci., 9(12), 884–887, doi:10.1038/ngeo2837, 2016.

Reusch, T. B. H., Dierking, J., Andersson, H. C., Bonsdorff, E., Carstensen, J., Casini, M., Czajkowski, M., Hasler, B., Hinsby, K., Hyytiäinen, K., Johannesson, K., Jomaa, S., Jormalainen, V., Kuosa, H., Kurland, S., Laikre, L., MacKenzie, B. R., Margonski, P., Melzner, F., Oesterwind, D., Ojaveer, H., Refsgaard, J. C., Sandström, A., Schwarz, G., Tonderski, K., Winder, M. and Zandersen, M.: The Baltic Sea as a time machine for the future coastal ocean, Sci. Adv., 4(5), doi:10.1126/sciadv.aar8195, 2018.

Royer, S.-J., Ferrón, S., Wilson, S. T. and Karl, D. M.: Production of methane and ethylene from plastic in the environment, PLoS One, 13(8), 1–13, 2018.

Saraiva, S., Markus Meier, H. E., Andersson, H., Höglund, A., Dieterich, C., Gröger, M., Hordoir, R. and Eilola, K.: Uncertainties in projections of the baltic sea ecosystem driven by an ensemble of global climate models, Front. Earth Sci., 6(January), 1–18, doi:10.3389/feart.2018.00244, 2019.

Sarmiento, J. L. and Gruber, N.: Ocean Biogeochemical Dynamics., 2006.

Schmale, O., Schneider Von Deimling, J., Gülzow, W., Nausch, G., Waniek, J. J. and Rehder, G.: Distribution of methane in the water column of the Baltic Sea, Geophys. Res. Lett., 37(12), 1–5, doi:10.1029/2010GL043115, 2010.

Schmale, O., Wäge, J., Mohrholz, V., Wasmund, N., Gräwe, U., Rehder, G., Labrenz, M. and Loick-Wilde, N.: The contribution of zooplankton to methane supersaturation in the oxygenated upper waters of the central Baltic Sea, Limnol. Oceanogr., 63(1), 412–430, doi:10.1002/lno.10640, 2018.

Schneider, B., Gülzow, W., Sadkowiak, B. and Rehder, G.: Detecting sinks and sources of CO2 and CH4 by ferrybox-based measurements in the Baltic Sea: Three case studies, J. Mar. Syst., 140(PA), 13–25, doi:10.1016/j.jmarsys.2014.03.014, 2014.

Siedler, G. and Peters, H. .: Physical properties of sea water, in Landolt-Börnstein Numerical data and functional relationships in science and technology: new series, edited by O. Madelung Gruppe, pp. 233–264, Springer, Berlin, Germany., 1986.

Stawiarski, B., Otto, S., Thiel, V., Gräwe, U., Loick-Wilde, N., Wittenborn, A. K., Schloemer, S., Wäge, J., Rehder, G., Labrenz, M., Wasmund, N. and Schmale, O.: Controls on zooplankton methane production in the central Baltic Sea, Biogeosciences, 16(1), 1–16, doi:10.5194/bg-16-1-2019, 2019.

Steinhoff, T.: Carbon and nutrient fluxes in the North Atlantic Ocean, CAU Kiel. [online] Available from: http://eldiss.uni-kiel.de/macau/receive/dissertation_diss_00005704, 2010.

Steinle, L., Maltby, J., Treude, T., Kock, A., Bange, H. W., Engbersen, N., Zopfi, J., Lehmann, M. F. and Niemann, H.: Effects of low oxygen concentrations on aerobic methane oxidation in seasonally hypoxic coastal waters, Biogeosciences, 14(6), 1631–1645, doi:10.5194/bg-14-1631-2017, 2017.

Taenzer, L., Carini, P. C., Masterson, A. M., Bourque, B., Gaube, J. H. and Leavitt, W. D.: Microbial Methane From Methylphosphonate Isotopically Records Source, Geophys. Res. Lett., 47(1), 1–9, doi:10.1029/2019GL085872, 2020.

Thamdrup, B., Dalsgaard, T. and Revsbech, N. P.: Widespread functional anoxia in the oxygen minimum zone of the Eastern South Pacific, Deep. Res. Part I Oceanogr. Res. Pap., 65, 36–45, doi:10.1016/j.dsr.2012.03.001, 2012.

Thauer, R. K., Kaster, A. K., Seedorf, H., Buckel, W. and Hedderich, R.: Methanogenic archaea: Ecologically relevant differences in energy conservation, Nat. Rev. Microbiol., 6(8), 579–591, doi:10.1038/nrmicro1931, 2008.

Thießen, O., Schmidt, M., Theilen, F., Schmitt, M. and Klein, G.: Methane formation and distribution of acoustic turbidity in organic-rich surface sediments in the Arkona Basin, Baltic Sea, Cont. Shelf Res., 26(19), 2469–2483, doi:10.1016/j.csr.2006.07.020, 2006.

Thureborn, P., Franzetti, A., Lundin, D. and Sjöling, S.: Reconstructing ecosystem functions of the active microbial community of the baltic sea oxygen depleted sediments, PeerJ, 2016(1), 1–26, doi:10.7717/peerj.1593, 2016.

Valentine, D. L.: Emerging Topics in Marine Methane Biogeochemistry, Ann. Rev. Mar. Sci., 3(1), 147–171, doi:10.1146/annurev-marine-120709-142734, 2011.

WALLENIUS SOL: M/V Tavastland, [online] Available from: https://wallenius-sol.com/en/sol-continent-line/fleet/mv-transpaper (Accessed 28 July 2020), n.d.

Wasmund, N., Busch, S., Burmeister., C. and Hansen, R.: Phytoplankton development at the coastal station "Seebrücke Heiligendamm" in 2018, Leibniz Inst. für Ostseeforsch. Warn. [online] Available from: https://www.io-warnemuende.de/algal_blooms_at_heiligendamm_2018.html (Accessed 5 August 2020), 2019.

Weber, T., Wiseman, N. A. and Kock, A.: Global ocean methane emissions dominated by shallow coastal waters, Nat. Commun., 10(4584), 1–10, doi:10.1038/s41467-019-12541-7, 2019.

Wiesenburg, D. A. and Guinasso, N. L.: Equilibrium Solubilities of Methane, Carbon Monoxide, and Hydrogen in Water and Sea Water, J. Chem. Eng. Data, 24(4), 356–360, doi:10.1021/je60083a006, 1979.

Willstrand Wranne, A.: Service Manual ferrybox Tavastland, n.d.

Wilson, S. T., Bange, H. W., Arévalo-Martínez, D. L., Barnes, J., Borges, A. V., Brown, I., Bullister, J. L., Burgos, M., Capelle, D. W., Casso, M., De La Paz, M., Farías, L., Fenwick, L., Ferrón, S., Garcia, G., Glockzin, M., Karl, D. M., Kock, A., Laperriere, S., Law, C. S., Manning, C. C., Marriner, A., Myllykangas, J. P., Pohlman, J. W., Rees, A. P., Santoro, A. E., Tortell, P. D., Upstill-Goddard, R. C., Wisegarver, D. P., Zhang, G. L. and Rehder, G.: An intercomparison of oceanic methane and nitrous oxide measurements, Biogeosciences, 15(19), 5891–5907, doi:10.5194/bg-15-5891-2018, 2018.

Winkler, L. W.: Die Bestimmung des im Wasser gelösten Sauerstoffes, , doi:doi.org/10.1002/cber.188802102122, 1888.

WWF (World Wide Fund For Nature): About the Baltic Sea, [online] Available from: https://wwf.panda.org/knowledge_hub/where_we_work/baltic/area/ (Accessed 7 February 2020), 2019.

Yan, X., Xu, X., Ji, M., Zhang, Z., Wang, M., Wu, S., Wang, G., Zhang, C. and Liu, H.: Cyanobacteria blooms: A neglected facilitator of CH4 production in eutrophic lakes, Sci. Total Environ., 651, 466–474, doi:10.1016/j.scitotenv.2018.09.197, 2019.

Zheng, Y. and Chistoserdova, L.: Multi-omics Understanding of Methanotrophs, in Methanotrophs. Microbiology Fundamentals and Biotechnological Applications, edited by E. Y. Lee and A. Steinbüchel, pp. 121–138, Springer Nature Switzerland AG 2019., 2019.

Zindler, C., Bracher, A., Marandino, C. A., Taylor, B., Torrecilla, E., Kock, A. and Bange, H. W.: Sulphur compounds, methane, and phytoplankton: interactions along a north-south transit in the western Pacific Ocean, Biogeosciences Discuss., 9(10), 15011–15049, doi:10.5194/bgd-9-15011-2012, 2012.

Zinke, L. A., Glombitza, C., Bird, J. T., Røy, H., Jørgensen, B. B., Lloyd, K. G., Amend, J. P. and Reese, B. K.: Microbial organic matter degradation potential in Baltic Sea Sediments is influenced by depositional conditions and in situ geochemistry, Appl. Environ. Microbiol., 85(4), 1–18, doi:10.1128/AEM.02164-18, 2019.

Declaration

Herewith, I declare that this thesis has been completed independently and unaided and that no other sources other than the ones given here have been used.

The submitted written version of this work is the same as the one electronically saved and submitted on CD. The written version is rating relevant.

Furthermore, I declare that this work has never been submitted at any other time and anywhere else as a final thesis.

Kiel, 13 August 2020, Sonja Gindorf